THE UNIVERSITY OF OKLAHOMA

GRADUATE COLLEGE

THE EFFECTS OF CONFINING PRESSURE ON THE MECHANICAL BEHAVIOR AND DEFORMATION MECHANISMS FOR THE OIL CREEK SANDSTONE IN LABORATORY TESTS

A THESIS

SUBMITTED TO THE GRADUATE FACULTY

in partial fulfillment of the requirements for the

degree of

MASTER OF SCIENCE

By

LOUIS ALFRED BOLDT

Norman, Oklahoma

1992

THE EFFECTS OF CONFINING PRESSURE ON THE MECHANICAL BEHAVIOR AND DEFORMATION MECHANISMS FOR THE OIL CREEK SANDSTONE IN LABORATORY TESTS

A THESIS

APPROVED FOR THE SCHOOL OF GEOLOGY AND GEOPHYSICS

BY [redacted]

ACKNOWLEDGEMENTS

I thank Dr. D.W. Stearns for introducing me to the field of rock mechanics and its underlying philosophy as a tool to the structural geologist. Also, for providing me with encouragement and creative ideas throughout this study and for teaching me the finer points of technical writing. Next, a hearty thanks to my fellow structural geology classmates who made numerous excursions to help quarry sandstone, prepare some of the samples used in this study, and for supplying me with test designs regardless of their merit. I would also like to thank to Dr. T.E. Scott for guiding me through, and discussing with me, many aspects of experimental rock deformation during the course of this study. Thanks, also, to Drs. J.L. Ahern and R.D. Elmore for their critical reviews of this manuscript which have helped to make it a better document. I would like to acknowledge both the financial and technical support of members of the OU Rock Mechanics Consortium throughout this research. I also thank U.S. Silica and Gary Perry for providing access, and allowing me to quarry the samples used in this study. Lastly, I thank my soulmate,

Margie Boldt, for always being there.

TABLE OF CONTENTS

Page

ACKNOWLEDGEMENTS iv

LIST OF TABLES viii

LIST OF FIGURES ix

ABSTRACT xiv

Chapter

I. INTRODUCTION AND PREVIOUS WORK 1

II. TESTING PROGRAM 10
Equipment 11
Testing Material 11
Triaxial Test Design 15
Indention Test Design 17

III. TEST RESULTS 22
Triaxial Compression Tests 22
Microscopic Observations of Triaxial Tests . . 39
Microscopic Observations of Hydrostatic Compression Test 44
Indention Tests 46
Microscopic Observations of Indention Tests . . 58

IV. COMPARISON OF TEST RESULTS AND NATURAL DEFORMATION BANDS 79

V. CONCLUSIONS AND RECOMMENDATIONS FOR FUTURE WORK . 83
Conclusions 83
Recommendations for Future Work 86

REFERENCES CITED 87

APPENDIX A POROSITY DETERMINATION METHOD 92

APPENDIX B ROCK SAMPLE PREPARATION 94

APPENDIX C SAMPLE COLUMN ASSEMBLY AND TESTING PROCEDURES FOR TRIAXIAL TESTS 96

APPENDIX D SAMPLE COLUMN ASSEMBLY AND TESTING PROCEDURE FOR INDENTION TESTS 99

APPENDIX E EPOXY AND SAMPLE IMPREGNATION 103

APPENDIX F MICROFRACTURE HISTOGRAM DATA 107

LIST OF TABLES

Table Page

1. Comparison of testing systems used in this study . . 14

LIST OF FIGURES

Figure Page

1. Photograph of the model #315.02 MTS® pressure vessel and load frame used in this study. 12

2. Schematic drawing of the Logan and Stearns pressure vessel and load frame (modified from Linscott (1985)). 13

3. Photograph of the unassembled components, sample and end plugs, for a triaxial compression test. On either side of the components are pieces of polyolefin shrink tubing 16

4. Photograph of an assembled sample column for a triaxial compression test with the axial (A) and radial (B) extensometers and the internal loadcell (C) attached. The entire assembly goes inside of the MTS® pressure vessel 18

5. Photograph of the unassembled components of an indention test: A) indenter, B) outside rubber seal, C) inside rubber seal, D) sample, E) lead shim, and F) base plate. 19

6. Scaled drawing of an assembled sample column for an indention test inside the Logan and Stearns pressure vessel 20

7. Illustration of deformation modes based on the macroscopic core appearance as a function of confining pressure. The symbols are defined as B = brittle behavior, T = transitional behavior, D = ductile behavior 23

8. Deformation modes of sandstones in confining pressure-porosity space. The dashed line represents the upper boundary of brittle behavior and the solid line represents the lower boundary of ductile behavior from Scott and Nielsen (1991). The symbols on the right are from this study (defined in figure 7) 25

9. Diagrammatic yield surface for soils. See text for an explanation (modified from Jones and Addis (1986)) 28

10. Stress-strain curves for Oil Creek Sandstone deformed in a triaxial compression test at a confining pressure of a) 5 MPa, b) 20 MPa, c) 40 MPa, d) 40 MPa, e) 60 MPa, f) 80 MPa, g) 100 MPa, h) 120 MPa, i) 135 MPa. . . . . 30, 31, and 32

11. Plot of axial, radial, and volumetric strain as a function of confining pressure during a hydrostatic compression test on Oil Creek Sandstone. 34

12. Yield surface in differential stress-mean pressure space for Oil Creek Sandstone. 36

13. Photomicrographs of undeformed a) Oil Creek Sandstone and b) Antlers Sandstone. The dark colored portions are epoxy filled pore spaces. 38

14. Photomicrograph of Oil Creek Sandstone deformed in a triaxial compression test in the brittle domain a) prior to and b) after slip along the fracture plane. The scale bar is parallel to the load axis. 41

15. Photomicrograph of Oil Creek Sandstone deformed in a triaxial compression test at the lower boundary of the transitional domain. a) narrow shear zone and b) broad shear zone. The scale bar is parallel to the load axis. 42

16. Photomicrographs of Oil Creek Sandstone deformed in a triaxial compression test at the upper boundary of the transitional domain. The scale bar is parallel to the load axis 44

17. Photomicrograph of Oil Creek Sandstone deformed in a triaxial compression test in the ductile domain. The scale bar is parallel to the load axis 45

18. Force-displacement record for Oil Creek Sandstone deformed in an indention test at a confining pressure of 44.8 MPa taken to 1.59 mm indention. . . 48

19. Force-displacement record for Oil Creek Sandstone deformed in an indention test at a confining pressure of 44.8 MPa taken to 3.18 mm indention. . . 49

20. Force-displacement record for Oil Creek Sandstone deformed in an indention test at a confining pressure of 44.8 MPa taken to 4.76 mm indention. . . 50

21. Force-displacement record for Oil Creek Sandstone deformed in an indention test at a confining pressure of 124.1 MPa taken to 1.59 mm indention. . 51

22. Force-displacement record for Oil Creek Sandstone deformed in an indention test at a confining pressure of 124.1 MPa taken to 3.18 mm indention. . 52

23. Force-displacement record for Oil Creek Sandstone deformed in an indention test at a confining pressure of 124.1 MPa taken to 4.76 mm indention. . 53

24. Macroscopic appearance of Oil Creek Sandstone deformed in an indention test at a confining pressure of 44.8 MPa a) photograph of an actual sample and b) schematic drawing of the deformed region. Arcuate lineations are saw marks 56

25. Macroscopic appearance of Oil Creek Sandstone deformed in an indention test at a confining pressure of 124.1 MPa a) photograph of an actual sample and b) schematic drawing of the deformed region. Arcuate lineations are saw marks 58

26. Damage contour map for Oil Creek Sandstone deformed in an indention (1.59 mm) test at a confining pressure of 44.8 MPa. See text for explanation of contour values. The boundary between damaged and undamaged regions is denoted by the letter B 61

27. Photomicrograph mosaic of the region underneath the edge of the indenter in figure 26. 62

28. Damage contour map for Oil Creek Sandstone deformed in an indention (3.18 mm) test at a confining pressure of 44.8 MPa. See text for explanation of contour values. The boundary between damaged and undamaged regions is denoted by the letter B. The hatchured regions are not analyzed 63

29. Photomicrograph mosaic of the region underneath the edge of the indenter in figure 28. 64

30. Damage contour map for Oil Creek Sandstone deformed in an indention (4.76 mm) test at a confining pressure of 44.8 MPa. See text for explanation of contour values. The boundary between damaged and undamaged regions is denoted by the letter B. The hatchured region is not analyzed 65

31. Photomicrograph mosaic of the region underneath the edge of the indenter in figure 30. 66

32. Photomicrograph of the highly compacted, triangular region in figure 24: a) plane light b) polarized light. 68

33. Photomicrograph of the border of the compacted region in figure 24: a) above and b) below this region 69

34. Significant microfracture orientations and their spatial relationship with the indenter. See text for explanation of their significance. The solid lines are interpreted maximum principal stress trajectories 70

35. Photomicrograph mosaic of the region underneath the edge of the indenter (same position as in Figure 28) in Oil Creek Sandstone deformed in an indention (1.59 mm) test at a confining pressure of 124.1 MPa 73

36. Photomicrograph mosaic of the region underneath the edge of the indenter (same position as in Figure 30) in the Oil Creek Sandstone deformed in an indention (3.18 mm) test at a confining pressure of 124.1 MPa. 74

37. Damage contour map for Oil Creek Sandstone deformed in an indention (4.76 mm) test at a confining pressure of 124.1 MPa. See text for explanation of contour values. The boundary between damaged and undamaged regions is denoted by the letter B. The hatchured region is not analyzed 75

38. Photomicrograph mosaic of the region underneath the edge of the indenter in figure 37. 76

39. Photomicrograph illustrating heterogeneous distribution of strain in an indention test. Points A, B, and C are the centers of 0.5 mm diameter circles. 77

40. Photomicrographs of deformation bands in naturally deformed Oil Creek Sandstone 80

ABSTRACT

Laboratory rock testing procedures are used to study the effect of confining pressure on the mechanical behavior and deformation mechanisms for the Oil Creek Sandstone: a lightly cemented (quartz), high porosity (≈35%) quartz sandstone. Triaxial compression tests are run on room dry samples, at 25^0C, and a constant strain rate of 1.34×10^{-5}sec^{-1}, at confining pressures of 5, 20, 40, 60, 80, 100, 120, and 135 MPa. Stress-strain curves for the sandstone are derived from triaxial test data. Indention tests are run on room dry samples, at 25^0C, an approximate displacement rate of 1.76×10^{-4} mm(sec)$^{-1}$, and at confining pressures of 44.8 MPa (low) and 124.1 MPa (high). Indention test samples are utilized to study mechanisms by which this sandstone deforms.

Triaxial compression tests illustrate that: 1) the confining pressure at which the boundaries between brittle, transitional, and ductile behavior occurs is higher than for the lower porosity samples tested by Scott and Nielsen (1991), 2) the entire yield surface for Oil Creek Sandstone is delineated over confining pressures encountered in the shallow crust, and 3) porosity is a dominant factor controlling the

yield strength of sandstones.

Microscopic observations of both triaxial and indention test samples reflect several types of grain fracturing. Brittle behavior is characterized by grain-contact microfractures that parallel the load axis. Slip along a shear fracture plane is required to produce an extreme reduction in grain size. Transitional behavior is divided into two categories. Category 1, associated with the lower boundary of transitional behavior, is similar to brittle behavior (an abundance of grain-contact microfractures parallel to the load axis with only a small percentage of fine particles). In category 2, associated with the upper boundary of transitional behavior, grain-contact microfractures parallel to the load axis are present, but fewer in number and there is a substantial increase in the percentage of fine particles. The increase in fine particles, however, is not a function of slip as is the case in the brittle domain. Ductile behavior is characterized by grain contact microfractures that do not show a preferred orientation.

Indention tests illustrate two modes of grain fracturing. Mode 1 is simply grain-contact microfractures. Mode 2, on the other hand, is another type of grain fracturing that polygonizes the grain into randomly oriented, small fragments. In low confining pressure tests, there is a spatial relationship between the indenter, the amount of indention,

and growth and development of a zone of mode 2 grain fracturing.

Some of the textures developed, and genesis of the textures, in triaxial and indention tests are similar to natural deformation bands. The texture associated with the brittle domain, after visible slip along a shear fracture occurs, is somewhat similar to natural deformation bands. However, in natural deformation bands, this same texture is produced with only minuscule displacement. The texture of category 2 in transitional behavior is also similar to natural deformation bands and, like natural deformation bands, extreme granulation occurs without visible slip. In low pressure indention tests, the texture and development of mode 2 grain fracturing is also similar to natural deformation bands.

THE EFFECTS OF CONFINING PRESSURE ON THE MECHANICAL BEHAVIOR AND DEFORMATION MECHANISMS FOR THE OIL CREEK SANDSTONE IN LABORATORY TESTS

CHAPTER I

INTRODUCTION AND PREVIOUS WORK

In an effort to further understand the manner in which high porosity (>25%) sandstones deform, in terms of their mechanical properties as well as the mechanisms by which they deform, laboratory rock deformation tests were performed on Oil Creek Sandstone. The tests are run over a suite of confining pressures to determine its effect on the behavior of this sandstone.

In the shallow crust (< 20 km), the predominate deformation mechanism in structurally deformed sedimentary rocks is cataclastic flow (Stearns, 1968). This deformation mechanism involves one or more of the following processes at the micro-, meso-, and macroscopic scales: fracture, rigid-body rotation, and rigid-body translation. The dominant meso- and macroscopic mechanisms, in sandstones deformed by

cataclastic flow are fractures (Stearns, 1967 and 1968), deformation bands (Aydin, 1978; Pittman, 1981; Jamison and Stearns, 1982; Underhill and Woodcock, 1987), or a combination of both (Cook and Stearns, 1975; Stearns and Jamison, 1977; Young, 1982; Hillman, 1986). A fracture represents at least a momentary loss of cohesion across a somewhat planar surface (Griggs and Handin, 1960). The term "deformation band", first coined by Aydin (1978), is a quasi-planar zone composed of comminuted grains of the host sandstone across which there has been discernible (milli- to centimeters) shear offset (Aydin, 1978; Jamison and Stearns, 1982). Because there is shear offset, these features are also termed "microfaults" (Jamison and Stearns, 1982). Aydin (1978) notes that there is not a discrete surface of discontinuity associated with deformation bands. This classification is not a matter of semantics. There are several very fundamental differences between these two mechanisms of cataclastic flow. Microscopically, there is a sharp contrast between shear fractures and deformation bands. Grain fracturing occurs within several grain diameters away from both natural shear fractures (Friedman, 1969; Engelder, 1974) and those created in the laboratory (Handin and Hager, 1957; Borg et al.,1960; Friedman, 1963; Dunn et al., 1973). With deformation bands, on the other hand, there is virtually no increase in the amount of microfracturing bordering the band (Aydin, 1978; Pittman, 1981; Jamison and Stearns, 1987;

Young, 1982; Hillman, 1986; Freeman, 1991). In addition, Aydin (1978), Jamison (1979), Underhill and Woodcock (1987), and Freeman (1991) all observe a two part division to a deformation band; an inner and an outer zone. The studies by Aydin (1978) and Underhill and Woodcock (1987) document that the inner zone is comprised of comminuted sand grains and the outer zone is a region of host porosity reduction without grain comminution (i.e., rigid body rotation and translation of grains). These workers delineated the outer zone utilizing SEM analysis. Jamison (1979) and Freeman (1991), on the other hand, define their outer zone, using standard optical microscopy, as a region of porosity reduction but it can contain a few comminuted sand grains. Their inner zone is essentially the same as other workers. Mechanical destruction of most grains within the deformation band is so extensive that the original grain boundaries are indiscernible (Aydin, 1978; Jamison, 1979; Pittman, 1981; Underhill and Woodcock, 1987; Freeman, 1991).

Another difference between shear fractures and deformation bands is in their outcrop pattern related to local structure. Fractures associated with faulted and/or folded sandstones form distinct patterns that can be related to local structures by the typical geometry of two shear fractures and the associated extension fracture. The fracture pattern is fixed with respect to the local maximum, intermediate, and

least principal stresses following a Coulomb geometry (Stearns, 1967 and 1968; Stearns and Friedman, 1972).

Deformation bands, however, do not usually follow these ordered patterns. Only in areas of low, plane strain, do deformation bands seem to follow a Coulomb geometry (Stearns, 1972; Engelder, 1974). In areas of low, three-dimensional strain, deformation bands form in an orthorhombic pattern (Aydin, 1978; Aydin and Reches, 1982) characteristic of three-dimensional strain in many materials (Reches, 1978; Reches and Dietrich, 1983). In areas of high, three-dimensional strain, on the other hand, there is no apparent band pattern (Jamison, 1979; Jamison and Stearns, 1982; Young, 1982). At times, deformation bands, unlike fractures, follow sedimentary structures such as cross bedding and at others, the bands cut across sedimentary structures as do fractures. Occasionally, deformation bands will form in a distinct main shear-Riedel shear pattern (Jamison, 1979).

While there is no universal theory that explains the formation of meso- and macroscopic fractures, there is a wealth of experimental (Handin and Hager, 1957; Borg et al., 1960; Handin et al., 1963) and field data (Stearns, 1967 and 1968) that empirically supports the Coulomb shear fracture criterion (Stearns et al., 1981). At the microscopic scale in sandstones, the formation of a through going fracture is always preceded by microfracturing of individual grains (Borg

et al., 1960; Friedman, 1963; Scholtz, 1968). Gallagher et al. (1974) document that these microfractures form as a result of stress concentrations developed at grain contacts and are extension (or tension) fractures that follow local maximum principal stress trajectories, with high stress differences, within grains.

The mechanical genesis of deformation bands is understood to a lesser degree than that of fractures. Studies by Aydin (1978), Jamison (1979), and Underhill and Woodcock (1987) suggest that deformation band genesis obeys a work-hardening flow law. The evidence supporting this hypothesis comes from their microscopic observations of deformation bands. The outer zone of porosity reduction is the first stage in band development. This is followed by the onset of grain comminution which requires more energy to produce the comminuted grains within the inner zone. The last stage of band genesis is continued slip by cataclastic flow within the band. During the last phase, the resistance to slip (τ/σ) increases because of the increase in surface area caused by the comminution process which reduces σ while τ remains constant. This eventually leads to the abandonment of the deformation band. This is the reason why band displacement rarely exceeds a few centimeters and why new bands form adjacent to the old bands producing an anastomosing texture (Aydin, 1978; Jamison, 1979; Underhill and Woodcock, 1987).

One of the more perplexing aspects of deformation band formation is the manner in which individual sand grains breakdown. Studies that incorporate microscopic observations of deformation bands all document that the mechanical destruction of grains within a band is so pervasive that the original grain outlines are indiscernible (Aydin, 1978; Jamison, 1979; Young, 1982; Underhill and Woodcock, 1987; Freeman, 1991). Aydin (1978), based on his microscopic observations, generates a hypothesis regarding the manner in which grains breakdown. The first stage involves the development of grain-contact microfractures which creates angular fragments of the original grain. During the next stage, corners of these fragments are broken off as they are rotated and translated to produce a further reduction in grain size and sorting. Underhill and Woodcock (1987) also document a similar process of grain breakdown. This hypothesis however, is not all inclusive. Jamison (1978) and Freeman (1991) both document several cases where the displacement along a deformation band is minuscule, yet, there is extensive grain comminution. Therefore, all grain comminution within a band cannot be explained by the fracturing of fragments as they are rotated and translated.

Jamison (1979) does not mention any significant evidence of point-contact microfractures in deformation bands in the Wingate Sandstone. He does, however, observe a slight increase

in the amount and degree of undulose extinction in grains that comprise the boundary of the comminuted zone. This may indicate that crystal plastic mechanisms are operating during deformation band genesis. Jamison also observes that there is no change in the amount of undulose extinction in the center of the deformation bands which may indicate that the grains separate along boundaries of differential crystal plastic flow within grains.

The overall purpose of this research is to study, through laboratory testing, the mechanical behavior of Oil Creek Sandstone as a function of confining pressure. In particular, one of the main objectives is to study the manner in which individual grains, under confining pressure, breakdown when subjected to differential stress.

Numerous triaxial compression test studies on sedimentary rocks delineate three domains of deformation: brittle, transitional, and ductile (Handin and Hager, 1957; Griggs and Handin, 1960; Handin et al., 1963; Byerlee, 1968; Bernabe and Brace, 1990; Scott and Nielsen, 1991). Some of these studies are devoted to details of cataclastic flow as a deformation mechanism at the microscopic scale (Borg et al., 1960; Friedman, 1963; Dunn et al., 1973; Gallagher et al., 1974). Fewer studies, however, make systematic microscopic observations of sandstones deformed in triaxial compression tests (Scott, 1989; Bernabe and Brace, 1990). The majority of

published microscopic observations pertain to the brittle domain (Handin and Hager, 1957; Hoshino and Koide, 1970; Dunn et al., 1973). Some studies cover brittle and ductile domains (Borg et al., 1960; Friedman, 1963) but not the transitional domain. Several recent studies pertain to mechanisms associated with hydrostatic compaction tests (Zhang et al., 1990a and 1990b). In triaxial deformation tests in brittle and transitional domains, microscopic observations document a relationship between microfractures and mesoscopic shear fractures that is identical to shear fractures and microfractures in nature. That is, near the fracture there is an increase in the frequency of microfractures and the statistical orientation of the microfractures is consistent with the local maximum principal stress trajectory that produced the shear fracture.

Therefore, there is considerable evidence from both field and laboratory studies that shear fractures and deformation bands are distinctly different features. Further study of these differences and the mechanical genesis of deformation bands is another purpose of this study. This will be accomplished by performing rock deformation tests on Oil Creek Sandstone: a porous sandstone known to contain deformation bands where naturally deformed.

There are three types of testing procedures employed in this study. All three procedures involve subjecting a test

sample, at least initially, to a uniform, confining pressure. Because this is the only step in one of the procedures, it is called a hydrostatic compression test. In the other two testing procedures, samples, after reaching a uniform confining pressure, are then subsequently subjected to differential loads by advancing a piston onto the sample. The difference between these two procedures is the amount of test sample that is being loaded. When the test sample and the loading piston are the same diameter, the test procedure is known as a triaxial compression test. When the diameter of the sample exceeds the diameter of the loading piston, the test procedure is known as an indention test. This term is derived from the loading conditions. That is, since the diameter of the piston is smaller than the sample diameter, the piston must indent the sample surface as it is advanced. In addition, this loading condition produces deformation that is restricted to only a small region of the sample underneath the piston.

CHAPTER II

TESTING PROGRAM

As pointed out by Stearns and Friedman (1972), rock deformed in nature is always constrained laterally, and in some instances vertically, by undeformed rock. This is not the case in triaxial tests where the deformed rock is only constrained laterally by a weak jacketing material and a compressible confining fluid. In a triaxial test taken to shear failure, a fracture (i.e., a loss of cohesion or a discontinuity) rapidly propagates across the entire sample and further displacement along the fracture is relatively unconstrained. In an indention test, on the other hand, the area of the sample being loaded is always less than the total area of sample. Any deformation produced during the experiment, therefore, is constrained laterally by undeformed rock. The indention test does not represent a very geologically meaningful boundary condition, but because the deformation is constrained, certain aspects regarding the mechanics of this system might be more geologically meaningful than in triaxial compression tests. Lawn and Wilshaw (1975)

provide a comprehensive review of principles involved in, and applications of, indention tests.

The purpose of triaxial compression tests is to study mechanical properties of Oil Creek Sandstone as a function of confining pressure. The purpose of indention tests is to study mechanisms by which Oil Creek Sandstone deforms.

Equipment

Equipment dictates that indention tests be performed dry. Therefore, triaxial compression tests are also performed dry in order to compare results from the two systems. Triaxial compression tests are carried out in a commercial, model #315.02, MTS® pressure vessel and load frame (Figure 1). Indention tests are carried out in a one-of-a-kind pressure vessel and load frame designed by Logan and Stearns (Figure 2) and described in detail by Linscott (1985). In addition to slight design differences, there are also differences between the systems used for triaxial tests and indention tests in specifications, controls, and data acquisition systems (Table 1).

Testing Material

The sandstone used in this study is Oil Creek Sandstone, the basal member of the Oil Creek Formation, (Middle Ordovician Simpson Group) which is a high porosity, friable quartz sandstone. The samples are from U.S. Silica's Plant #39 just north of Mill Creek, Oklahoma.

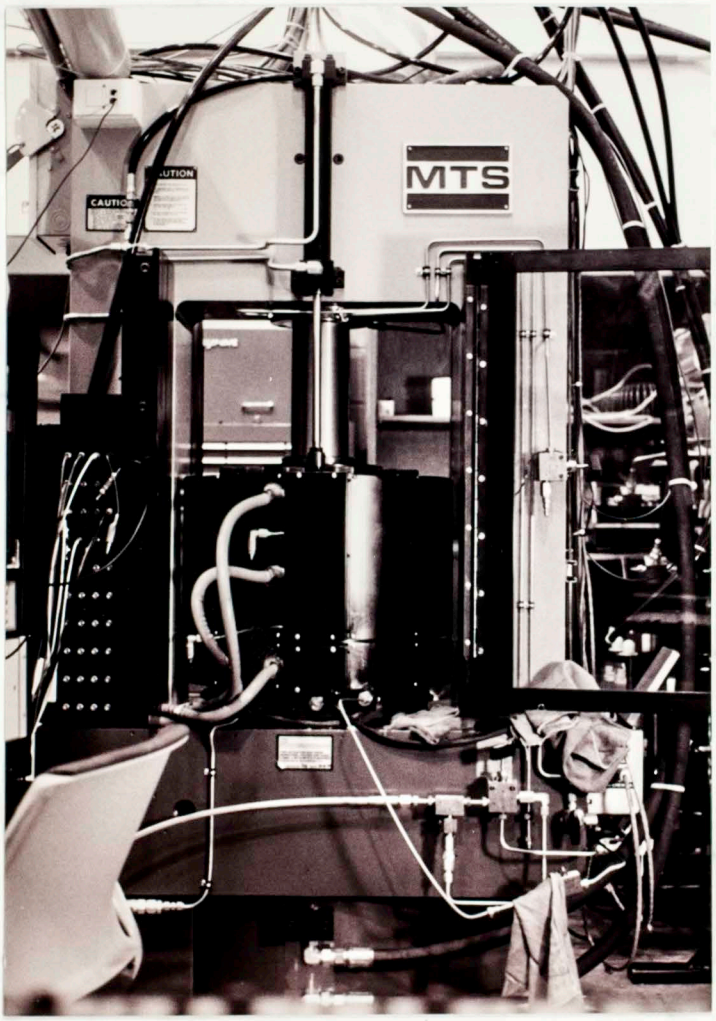

Figure 1. Photograph of the model #315.02 MTS® pressure vessel and load frame used in this study.

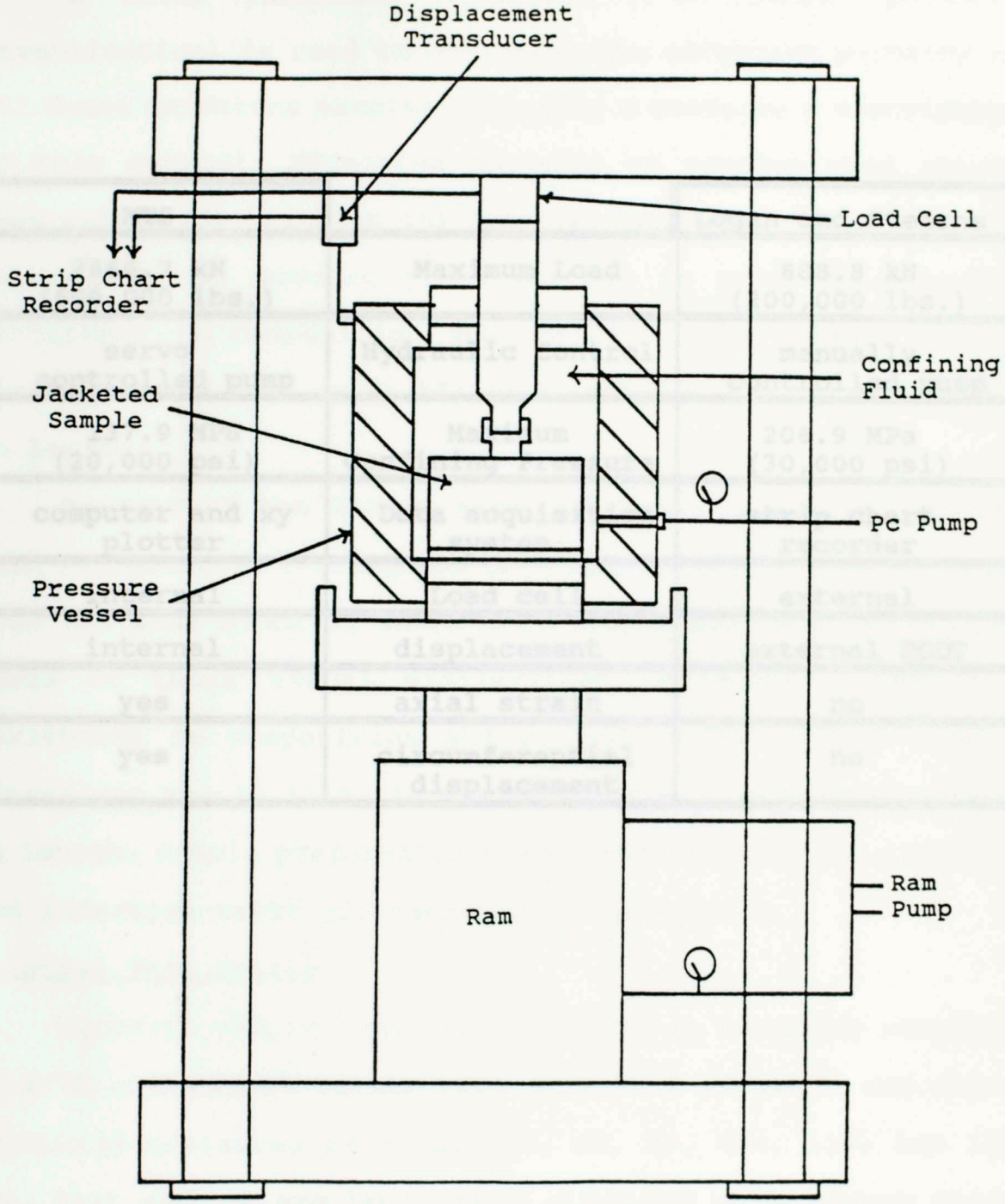

Figure 2. Schematic drawing of the Logan and Stearns pressure vessel and load frame (modified from Linscott (1985)).

MTS		Logan and Stearns
2666.7 kN (600,000 lbs.)	Maximum Load	888.8 kN (200,000 lbs.)
servo controlled pump	Hydraulic Control	manually controlled pump
137.9 MPa (20,000 psi)	Maximum Confining Pressure	206.9 MPa (30,000 psi)
computer and xy plotter	Data acquisition system	strip chart recorder
internal	Load cell	external
internal	displacement	external DCDT
yes	axial strain	no
yes	circumferential displacement	no

Table 1. Comparison of testing systems used in this study.

A water immersion technique (T.E. Scott, personal communication) is used to determine the effective porosity of Oil Creek Sandstone samples (Appendix B contains a description of this method). Effective porosity of samples used ranges from 33% to 35%. Samples for triaxial tests are taken from the same block and bedding plane horizon in order to minimize variations in composition and porosity. The nominal sample dimensions are 3.91 cm (1.5") in diameter and 8.255 cm (3.25") in length.

Because of the larger size and large number of samples used in indention testing for this study, samples can not come from the same block of sandstone. Blocks are selected on the basis of their visual similarities in order to minimize variations in composition and porosity. The nominal sample dimensions are 10.16 cm (4.0") in diameter and 8.89 cm (3.5") in length. Sample preparation procedures for both the triaxial and indention tests are reported in Appendix C.

Triaxial Test Design

Triaxial compression tests are run on room dry samples, at 25°C, a constant strain rate of $1.34 \times 10^{-5} sec^{-1}$, and under confining pressures of 5, 20, 40, 60, 80, 100, 120, and 135 MPa. Test samples are jacketed to steel end plugs before being aligned with the piston in the pressure vessel (Figure 3). Step by step procedures used in triaxial testing appear in Appendix D.

Figure 3. Photograph of the unassembled components, sample and end plugs, for a triaxial compression test. On either side of the components are pieces of polyolefin shrink tubing.

An internal load cell and axial and circumferential extensometers are employed in triaxial testing (Figure 4). The internal loadcell permits a direct measurement of load being applied to the sample column. The axial extensometer measures the axial shortening, or strain (ε_A), during an experiment. The circumferential extensometer, on the other hand, measures changes in the circumference which are used to calculate radial strain (ε_R).

Indention Test Design

Indention tests are run on room dry samples, at 25°C, an approximate displacement rate of 1.76×10^{-4} mm(sec)$^{-1}$, and under confining pressures of 44.8 MPa (low) and 124.1 MPa (high). The indenter is a right-circular cylinder of high strength, steel 2.54 cm (1.0") in diameter. Because the sample diameter greatly exceeds the diameter of the indenter, the deformation is restricted to a small region beneath the indenter and is, therefore, constrained by undeformed sandstone.

The sample is sealed from the confining fluid using two layers of polyolefin shrink tubing and a neoprene rubber patch. The outside neoprene rubber patch (Figure 5) is sealed both to the indenter and to the inside polyolefin jacket. The inside jacket is also sealed at the steel base plate (Figure 6). The outer polyolefin jacket prevents confining fluid from puncturing the inside jacket at the contact between the sample and steel base plate. The inside rubber patch rests on top of

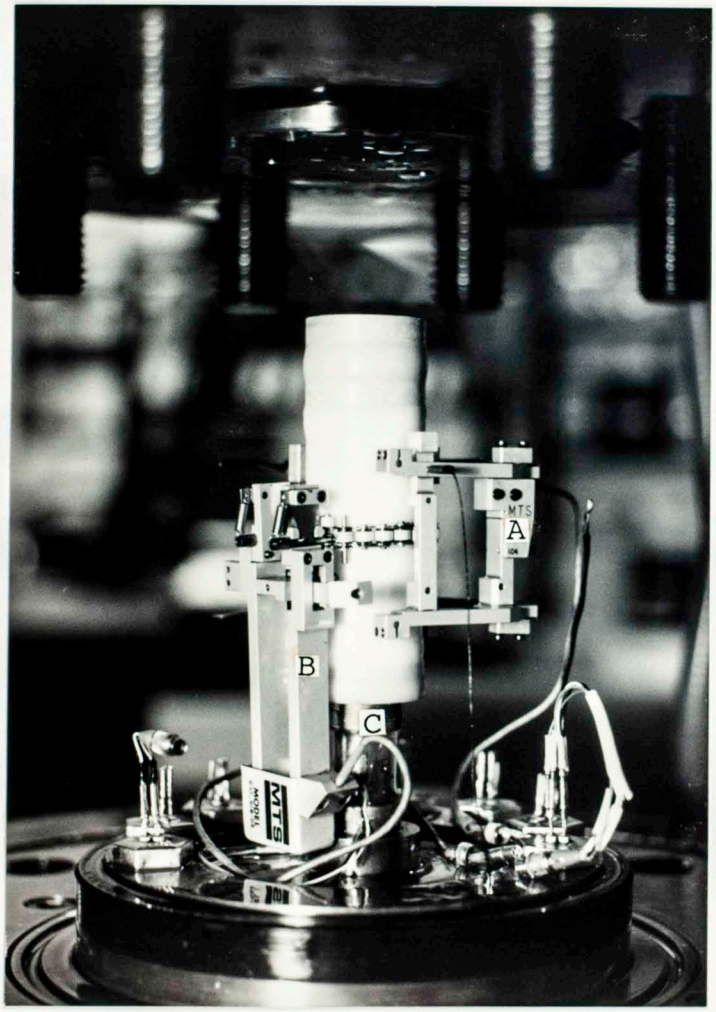

Figure 4. Photograph of an assembled sample column for a triaxial compression test with the axial (A) and radial (B) extensometers and the internal loadcell (C) attached. The entire assembly goes inside of the MTS® pressure vessel.

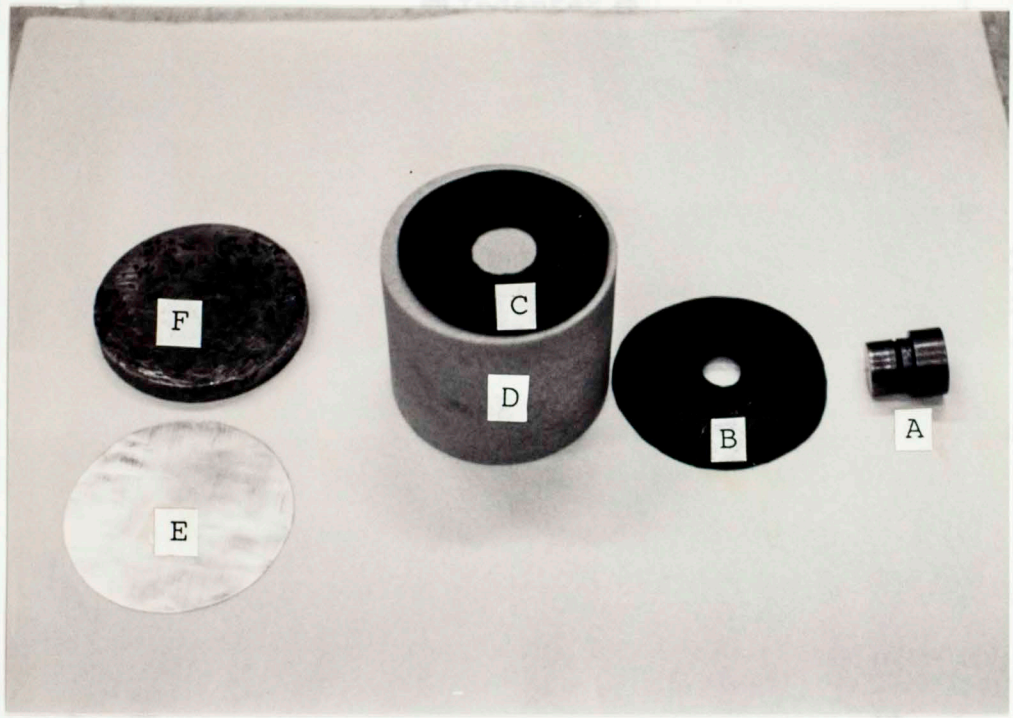

Figure 5. Photograph of the unassembled components of an indention test: A) indenter, B) outside rubber seal, C) inside rubber seal, D) sample, E) lead shim, and F) base plate.

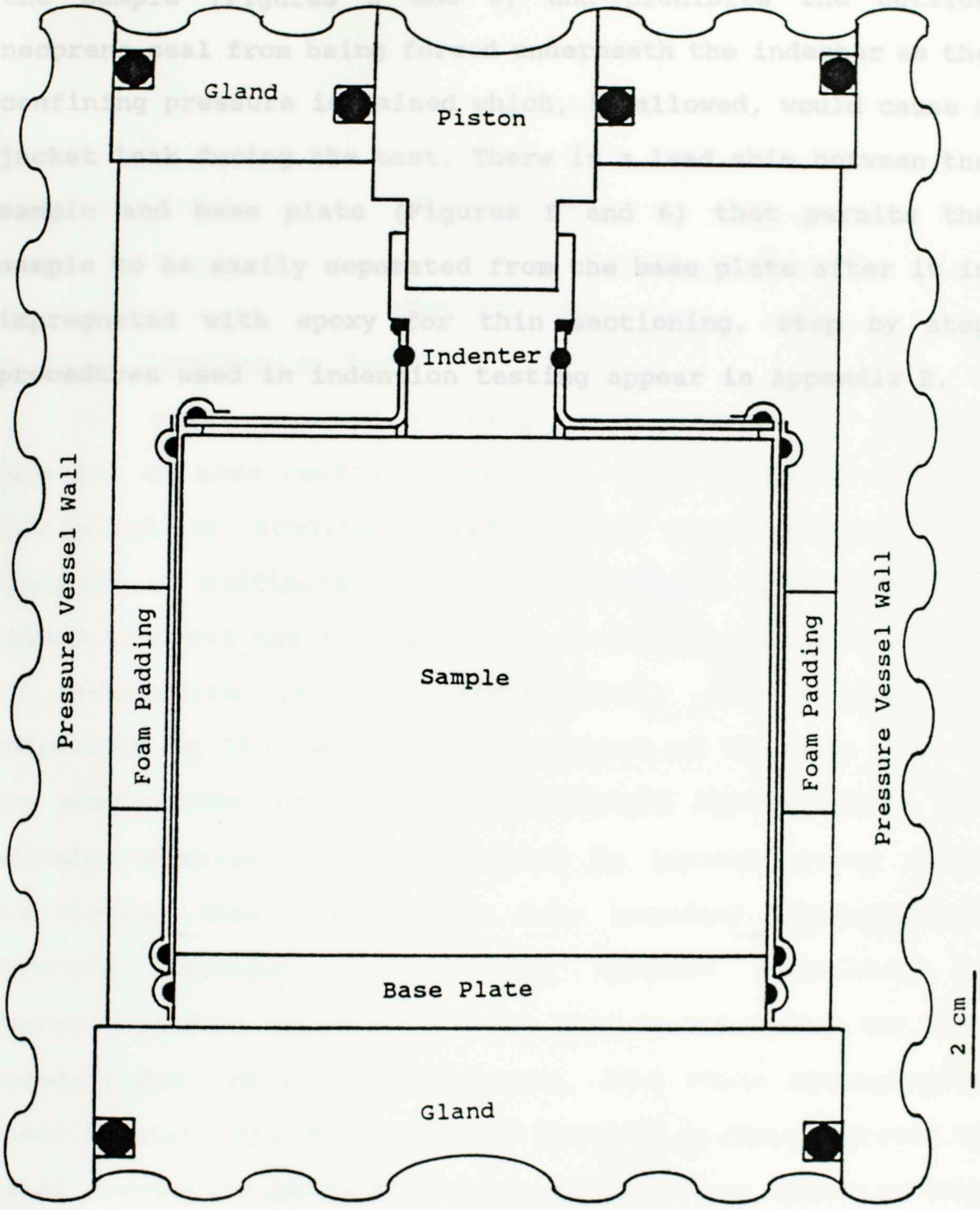

Figure 6. Scaled drawing of an assembled sample column for an indention test inside the Logan and Stearns pressure vessel.

the sample (Figures 5 and 6) and prohibits the outside neoprene seal from being forced underneath the indenter as the confining pressure is raised which, if allowed, would cause a jacket leak during the test. There is a lead shim between the sample and base plate (Figures 5 and 6) that permits the sample to be easily separated from the base plate after it is impregnated with epoxy for thin sectioning. Step by step procedures used in indention testing appear in Appendix E.

CHAPTER III

TEST RESULTS

Triaxial Compression Tests

All rocks undergo a change from brittle to ductile behavior at some confining pressure. This change is usually determined by studying stress-strain curve shapes as a function of confining pressure. However, in this study the method of Scott and Nielsen (1991) is followed where the mode of deformation (brittle, transitional, and ductile) is determined by the macroscopic appearance of the core and not the characteristics of the stress-strain curve (Figure 7). Brittle behavior is characterized by through going shear fracture(s) that offsets the core boundary. Transitional behavior (between brittle and ductile behavior) is characterized by cataclastic zones that do not offset the core boundary and are wider, in general, than those accompanying shear fracture(s). Purely ductile behavior is characterized by axial shortening accomplished by crushed zones approximately perpendicular to the long axis of the sample. Scott and Nielsen (1991) report significant barreling of samples

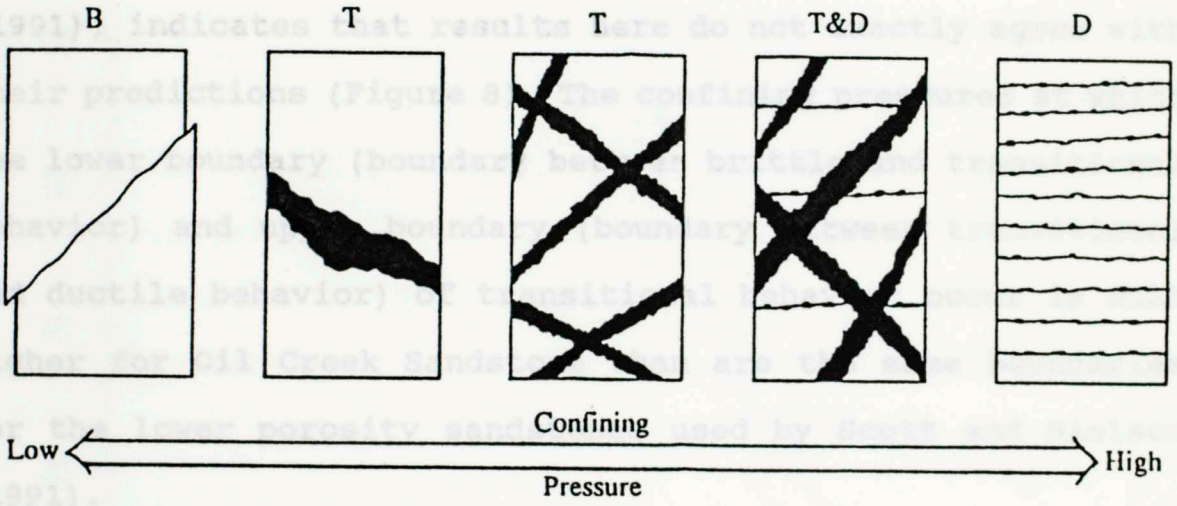

Figure 7. Illustration of deformation modes based on the macroscopic core appearance as a function of confining pressure. The symbols are defined as B=brittle behavior, T=transitional behavior, D=ductile behavior.

associated with transitional and ductile behavior taken to 7% and 8% axial shortening. This characteristic is not observed in cores in this study that were shortened only 3% to 4%. Some deformed samples display characteristics of both transitional and ductile behavior (Figure 7).

Plotting the behavior mode of Oil Creek Sandstone on a confining pressure versus porosity (initial) graph, an expanded version of the method used by Scott and Nielsen (1991), indicates that results here do not exactly agree with their predictions (Figure 8). The confining pressures at which the lower boundary (boundary between brittle and transitional behavior) and upper boundary (boundary between transitional and ductile behavior) of transitional behavior occur is much higher for Oil Creek Sandstone than are the same boundaries for the lower porosity sandstones used by Scott and Nielsen (1991).

This discrepancy could be explained by differences in test conditions and/or mineral composition. The tests reported here are run under room dry conditions. Even though a thorough mineralogic analysis was not performed, microscopic observations indicate that the predominate cement type is quartz which is in agreement with the petrographic analysis of Pittman (1981). Tests in Scott and Nielsen (1991), on the other hand, are run under drained conditions (i.e., constant pore pressure). The mineral composition of the specific

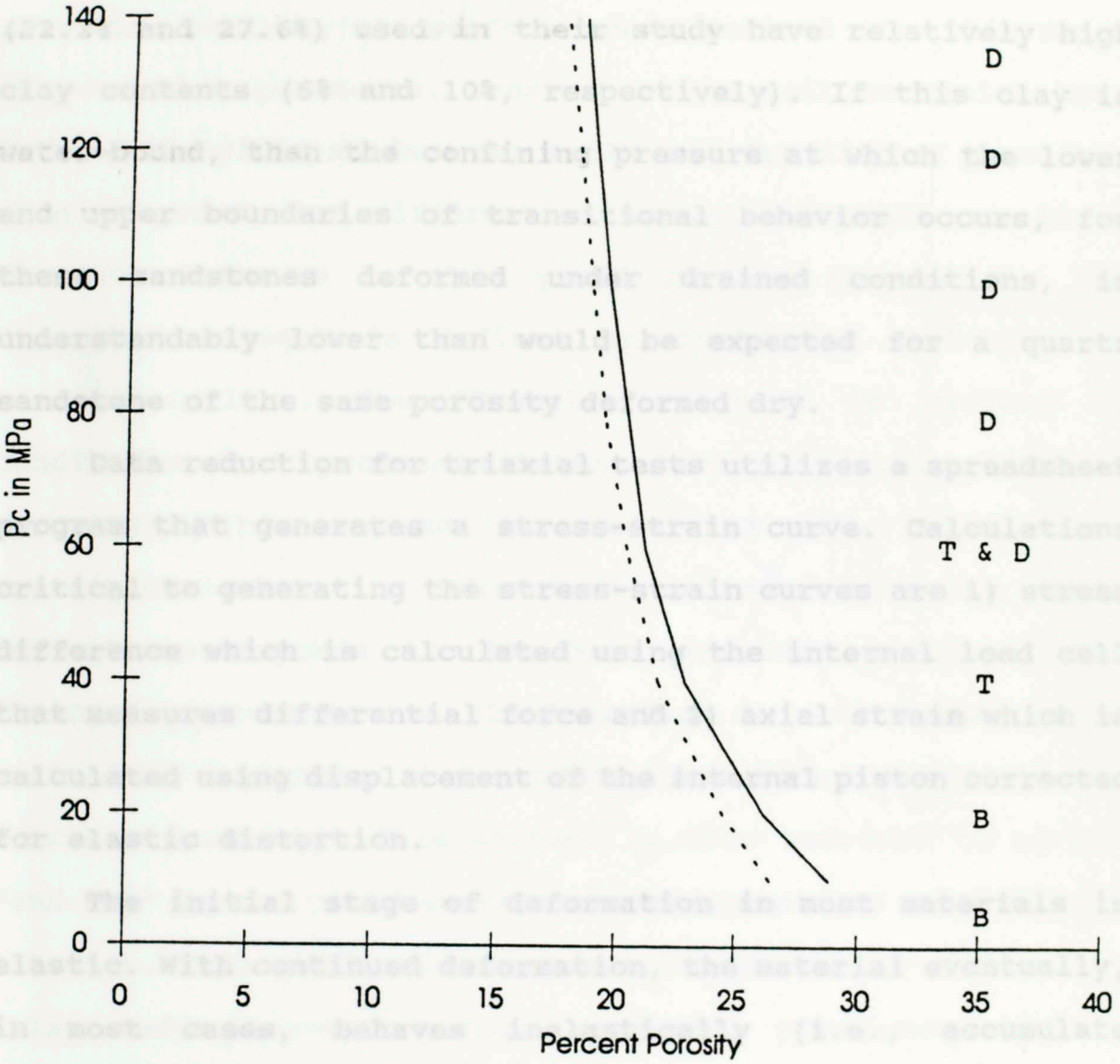

Figure 8. Deformation modes of sandstones in confining pressure-porosity space. The dashed line represents the upper boundary of brittle behavior the solid line represents the lower boundary of ductile behavior from Scott and Nielsen (1991). The symbols on the right are from this study (defined in Figure 7).

sandstones discussed in Scott and Nielsen (1991) are actually reported in Scott (1989). The two high porosity sandstones (22.2% and 27.6%) used in their study have relatively high clay contents (6% and 10%, respectively). If this clay is water-bound, then the confining pressure at which the lower and upper boundaries of transitional behavior occurs, for these sandstones deformed under drained conditions, is understandably lower than would be expected for a quartz sandstone of the same porosity deformed dry.

Data reduction for triaxial tests utilizes a spreadsheet program that generates a stress-strain curve. Calculations critical to generating the stress-strain curves are 1) stress difference which is calculated using the internal load cell that measures differential force and 2) axial strain which is calculated using displacement of the internal piston corrected for elastic distortion.

The initial stage of deformation in most materials is elastic. With continued deformation, the material eventually, in most cases, behaves inelastically (i.e., accumulate permanent strain). The onset of inelastic behavior is known as the "yield point". A yield surface is defined by determining the yield points over a suite of confining pressures.

For most sedimentary rocks over the range of confining pressures encountered in the shallow crust, brittle and occasionally transitional behavior are the dominate behavior

modes and ductile behavior is rarely observed. In unconsolidated sediments, or soils, however, this is not the case; the entire yield surface can be defined over this range of confining pressures. Researchers in soil mechanics have defined the yield surface for soils as a function of porosity, mean pressure, and differential stress and there are three distinct segments to this yield surface (Figure 9). The "tension" segment is defined by conditions that produce tensile failure. The "Hvorslev" segment is defined by conditions that produce dilatant behavior (i.e., increase porosity). This segment is associated with brittle and transitional behavior. For most sedimentary rocks, this segment corresponds to the Mohr fracture envelope. The "Roscoe" segment of the yield surface in soil mechanics is defined by conditions that produce compactive behavior (i.e., decrease porosity). This segment is also referred to as the "end cap" to the yield surface and is associated with ductile behavior. This yield surface nomenclature will be utilized in this study because at high confining pressures, lightly cemented, high porosity sandstones are closer in mechanical behavior to soils than they are to normally consolidated rocks.

In this study, the stress-strain curves for samples which exhibit brittle behavior (Figures 10a and 10b) are characterized by stress drops, on the order of 20 MPa,

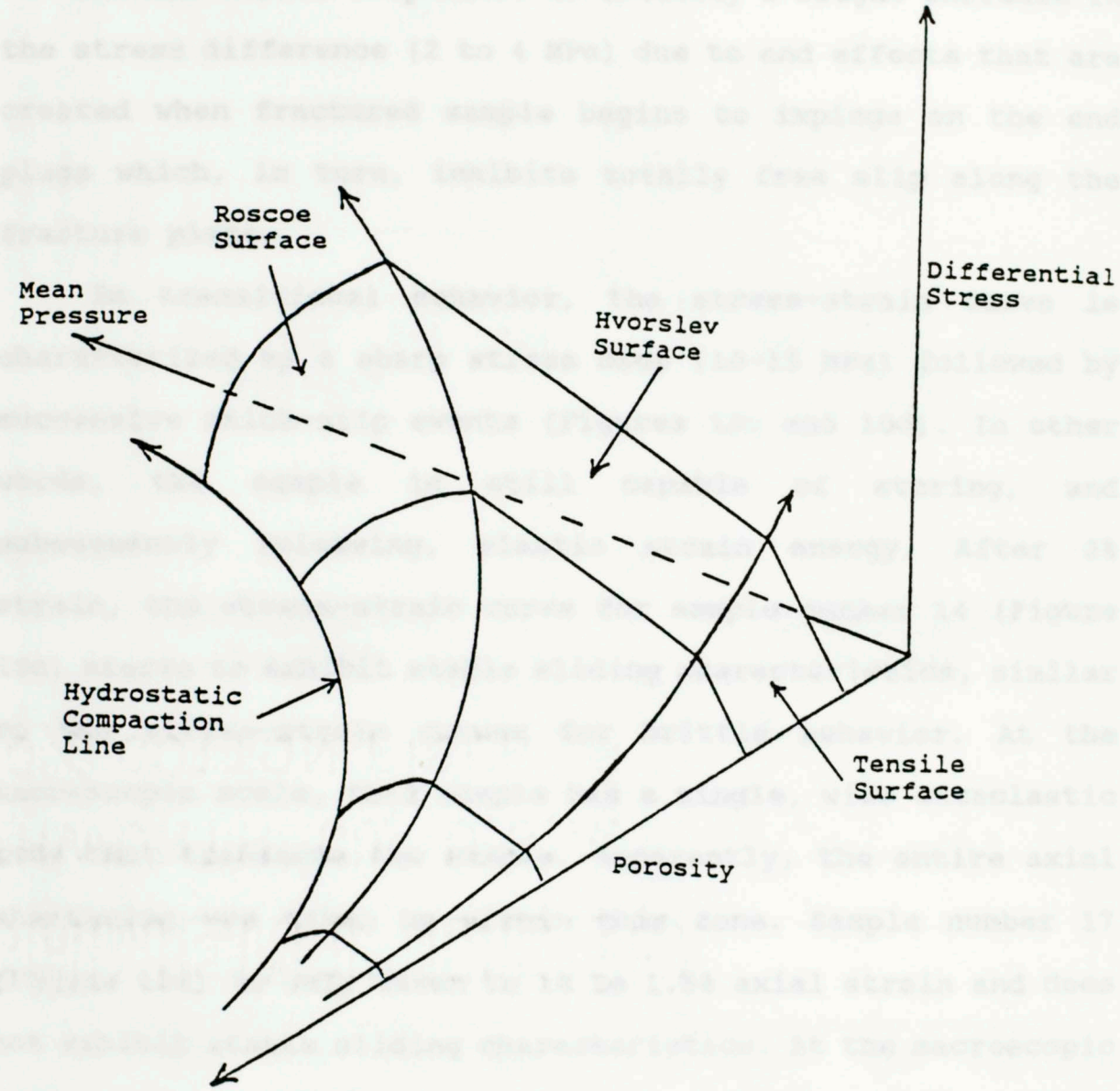

Figure 9. Diagrammatic yield surface for soils. See text for an explanation (modified from Jones and Addis ((1986)).

followed by stable sliding (i.e., a relatively flat stress-strain curve) along the fracture plane. In both tests after the initial stress drop there is actually a slight increase in the stress difference (2 to 4 MPa) due to end effects that are created when fractured sample begins to impinge on the end plugs which, in turn, inhibits totally free slip along the fracture plane.

In transitional behavior, the stress-strain curve is characterized by a sharp stress drop (10-15 MPa) followed by successive stick-slip events (Figures 10c and 10d). In other words, the sample is still capable of storing, and subsequently releasing, elastic strain energy. After 2% strain, the stress-strain curve for sample number 14 (Figure 10c) starts to exhibit stable sliding characteristics, similar to the stress-strain curves for brittle behavior. At the macroscopic scale, this sample has a single, wide cataclastic zone that transects the sample. Apparently, the entire axial shortening was taken up within this zone. Sample number 17 (Figure 10d) is only taken to 1% to 1.5% axial strain and does not exhibit stable sliding characteristics. At the macroscopic scale, this sample has several narrow, cross-cutting cataclastic zones across which the axial shortening was being distributed.

The stress-strain curve at a confining pressure that produces both transitional and ductile behavior (Figure 10e)

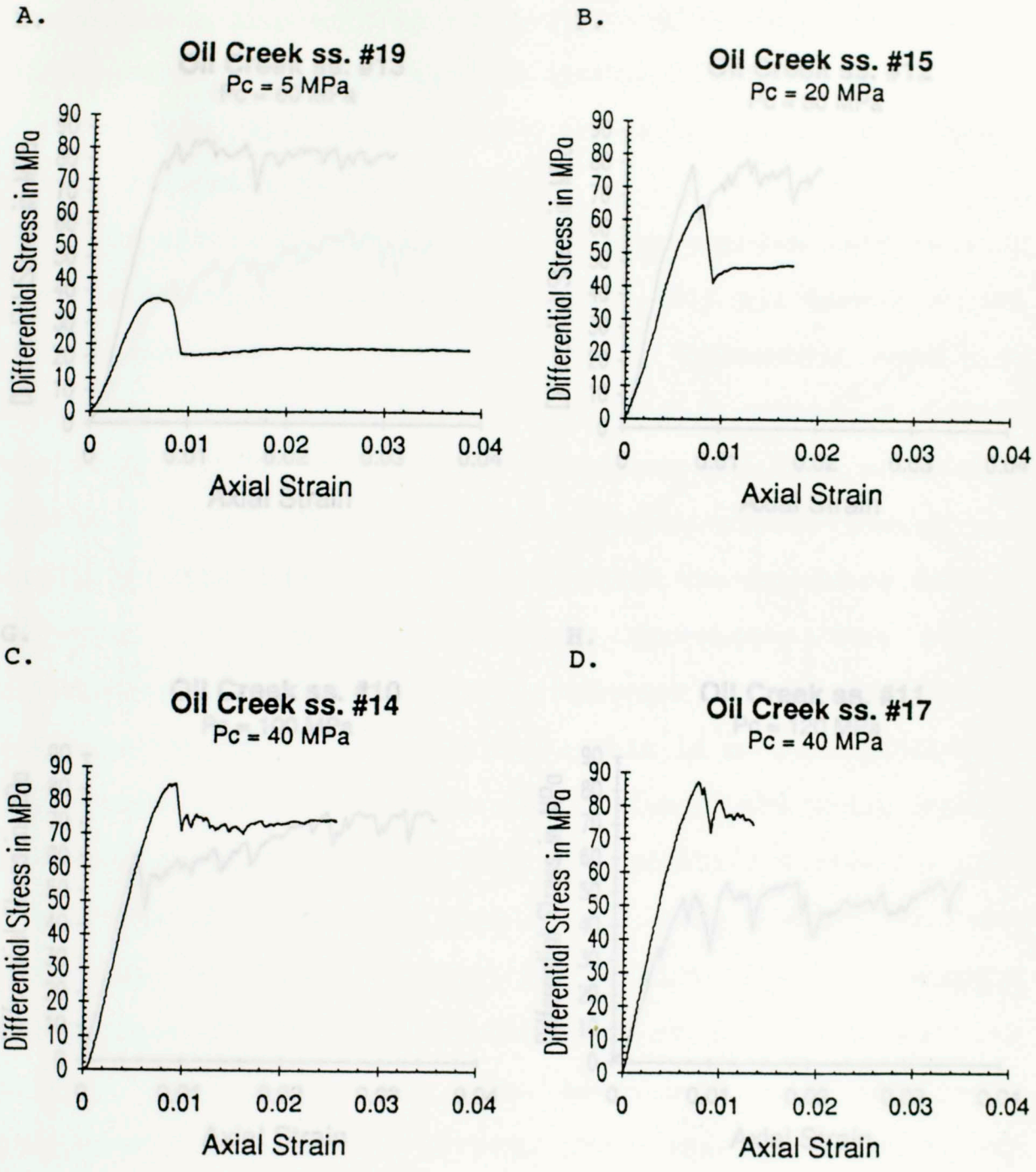

Figure 10. Stress-strain curves for Oil Creek Sandstone deformed in a triaxial compression test at a confining pressure of a) 5 MPa, b) 20 MPa, c) 40 MPa, d) 40 MPa.

E.

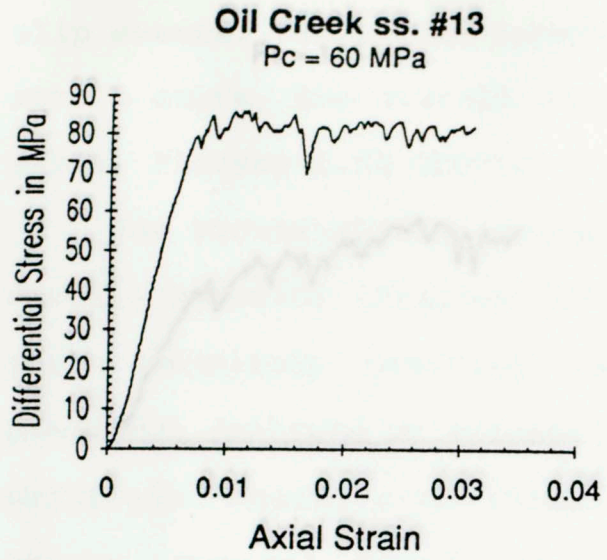

F.

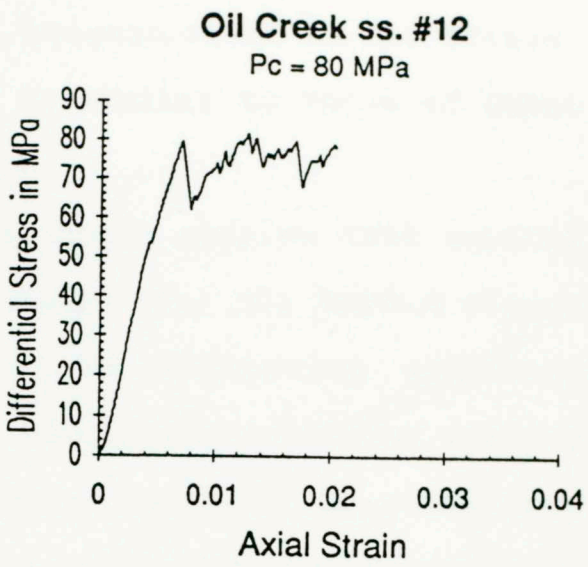

G.

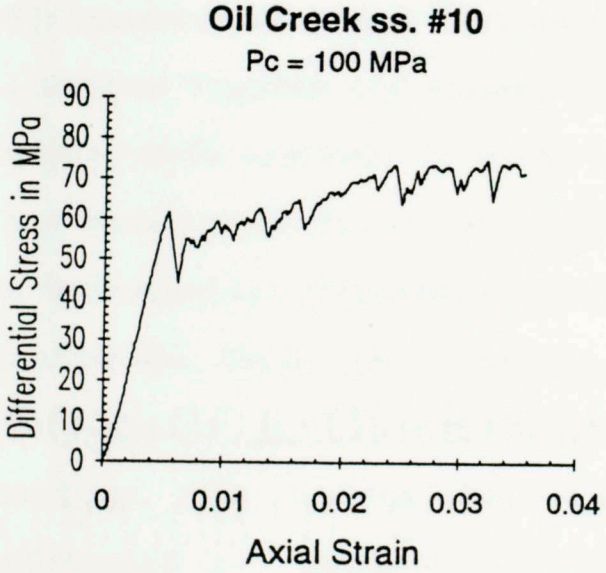

H.

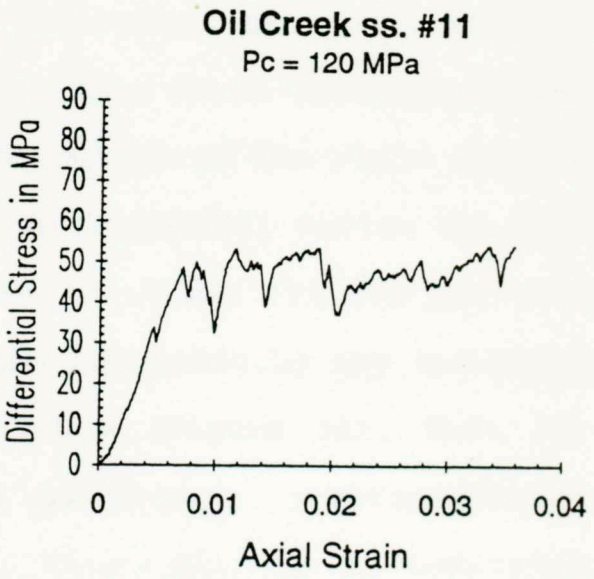

Figure 10. Stress-strain curves for Oil Creek Sandstone deformed in a triaxial compression test at a confining pressure of e) 60 MPa, f) 80 MPa, g) 100 MPa, h) 120 MPa.

I.

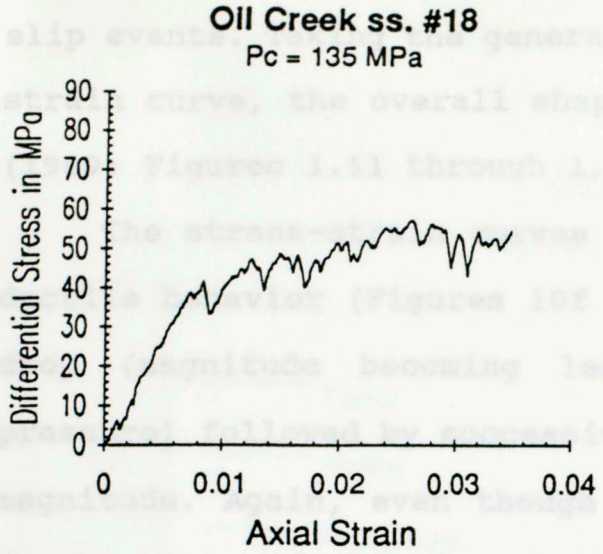

Figure 10. Stress-strain curves for Oil Creek Sandstone deformed in a triaxial compression test at a confining pressure of i) 135 MPa.

has a stress drop of 2 to 4 MPa followed by successive stick-slip events. Taking the general, average trend of the stress-strain curve, the overall shape is similar to those of Scott (1989: Figures 1.11 through 1.13).

The stress-strain curves for those samples that exhibit ductile behavior (Figures 10f through 10i) all have a stress drop (magnitude becoming less with increasing confining pressure) followed by successive stick-slip events of varying magnitude. Again, even though there are numerous stick-slip events, general trends of these stress-strain curves are similar to those of Scott (1989). Within the domain of ductile behavior, as confining pressure increases, the stress difference at which inelastic behavior occurs is reduced (compare Figures 10f through 10i). This is an indication that these tests are well into the cap portion of the yield surface for this sandstone. In an effort to completely define the cap, a hydrostatic compression test to 137.9 MPa (20,000 psi) was performed. This test, however, did not indicate any inelastic deformation at the macroscopic scale (Figure 11). That is, neither the sample nor the electronic instrumentation indicated any permanent strain. Therefore, it is concluded that hydrostatic compaction of Oil Creek Sandstone occurs above 138 MPa. Below 40 MPa confining pressure (Figure 11), radial strain values are incorrect because the jacket, and hence circumferential extensometer, is being forced into pores

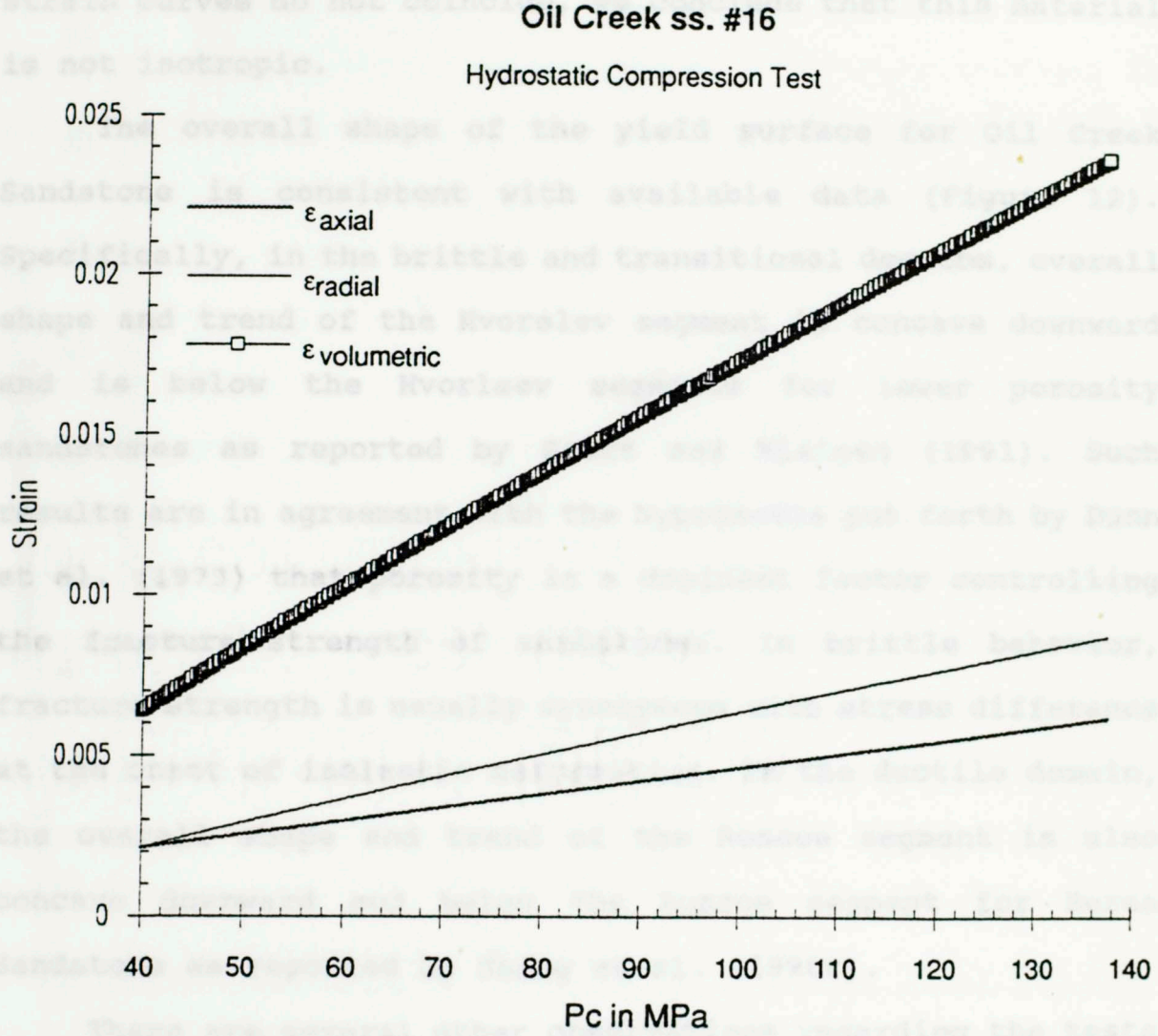

Figure 11. Plot of axial, radial, and volumetric strain as a function of confining pressure during a hydrostatic compression test on Oil Creek Sandstone.

on the wall of the sample. Therefore, radial strain values at, and beyond, 40 MPa confining pressure are adjusted to provide a more accurate assessment. Because the axial and radial strain curves do not coincide, we conclude that this material is not isotropic.

The overall shape of the yield surface for Oil Creek Sandstone is consistent with available data (Figure 12). Specifically, in the brittle and transitional domains, overall shape and trend of the Hvorslev segment is concave downward and is below the Hvorlsev segments for lower porosity sandstones as reported by Scott and Nielsen (1991). Such results are in agreement with the hypothesis put forth by Dunn et al. (1973) that porosity is a dominant factor controlling the fracture strength of sandstones. In brittle behavior, fracture strength is usually synonymous with stress difference at the onset of inelastic deformation. In the ductile domain, the overall shape and trend of the Roscoe segment is also concave downward and below the Roscoe segment for Berea Sandstone as reported by Zhang et al. (1990c).

There are several other observations regarding the tests here and those in previous studies. Transitional behavior in the test rock is exhibited over a range of confining pressures that is broader than that for lower porosity sandstones, which follows the trend observed by Scott and Nielsen (1991). One difference between tests in this study and those of previous

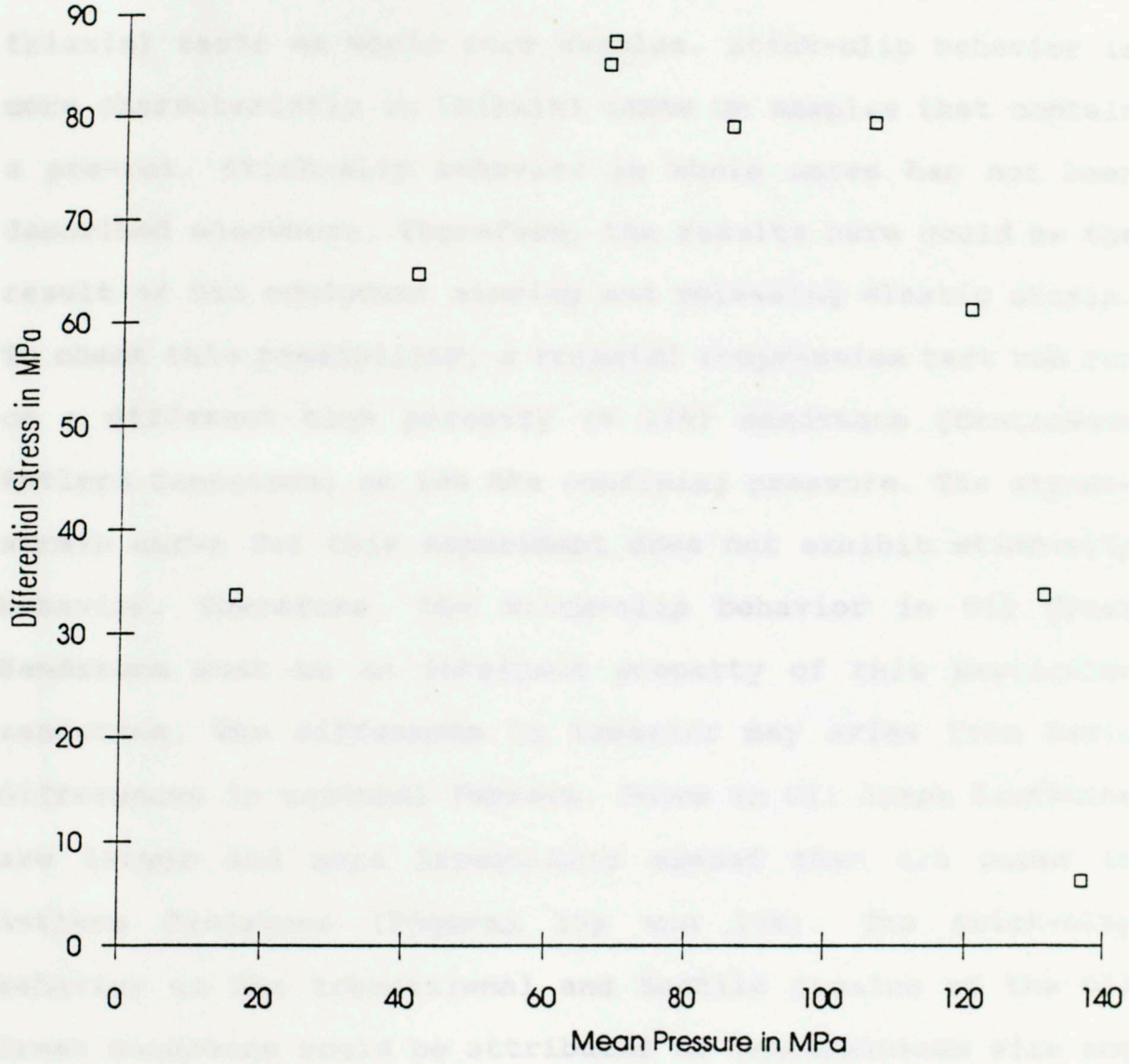

Figure 12. Yield surface in differential stress-mean pressure space for Oil Creek Sandstone.

workers is that tests here are run at confining pressures which put the test rock into the end cap region.

Stick-slip behavior for samples in the transitional and ductile domains (Figures 10c through 10i) is very unusual in triaxial tests on whole core samples. Stick-slip behavior is more characteristic in triaxial tests on samples that contain a pre-cut. Stick-slip behavior in whole cores has not been described elsewhere. Therefore, the results here could be the result of the equipment storing and releasing elastic strain. To check this possibility, a triaxial compression test was run on a different high porosity (≈ 37%) sandstone (Cretaceous Antlers Sandstone) at 100 MPa confining pressure. The stress-strain curve for this experiment does not exhibit stick-slip behavior. Therefore, the stick-slip behavior in Oil Creek Sandstone must be an intrinsic property of this particular sandstone. The difference in behavior may arise from basic differences in textural fabrics. Pores in Oil Creek Sandstone are larger and more irregularly spaced than are pores in Antlers Sandstone (Figures 13a and 13b). The stick-slip behavior in the transitional and ductile domains of the Oil Creek Sandstone could be attributed to inhomogeneous size and distribution of pores that, in turn, produce heterogeneous pore collapse (T.E. Scott, personal communication). An alternative explanation for this stick-slip behavior involves grain shape. Oil Creek Sandstone is composed of well rounded

A.

B.

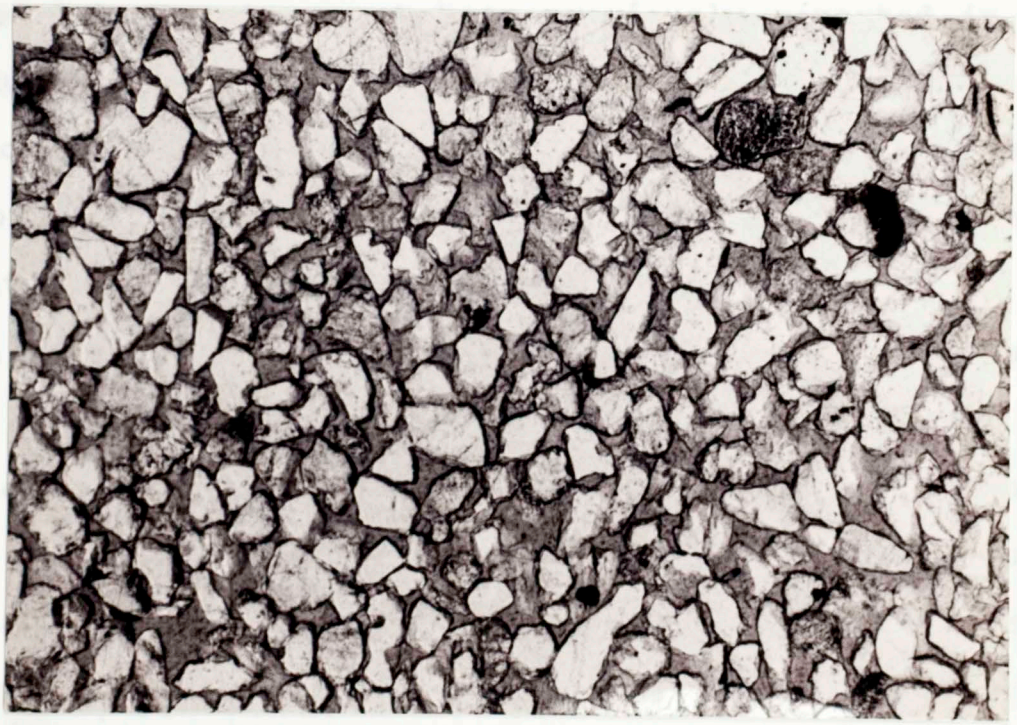

1 mm

Figure 13. Photomicrographs of undeformed a) Oil Creek Sandstone and b) Antlers Sandstone. The dark colored portions are epoxy filled pore spaces.

sand grains while the sand grains in Antlers Sandstone are angular (Figure 13a and 13b). Angular grains tend to have long grain contacts that when loaded will create a uniform stress distribution throughout the sample. Well rounded grains, on the other hand, tend to have point contacts that when loaded produce localized stress concentrations in sample. These localized stress concentrations create heterogeneous grain breakdown which produces the stick-slip behavior in the stress-strain curves (G. Wong, personal communication).

Microscopic Observations of Triaxial Tests

Systematic microscopic observations regarding the three modes of behavior have not been previously reported in the literature. Neither were disciplined microscopic studies of the deformation modes a major emphasis in this study. However, a cursory microscopic investigation was performed and these observations suggest certain conclusions.

In the brittle domain, breakdown of individual sand grains seems to be a two-stage process. Stage one is characterized by grain-contact microfracturing that produces large, angular fragments of original grains. Microfractures are related to high stress concentrations developed at grain contacts and they follow maximum principal stress trajectories due to point contact loading as illustrated by Gallagher et al. (1974). These microfractures have a statistically preferred orientation parallel to the loading direction

(Figure 14a). Microfractures are all within two to three grain diameters of the shear fracture and are developed before much slip has accumulated on the shear fracture. The second stage of the breakdown process occurs as slip along the shear fracture increases. Here, grain breakdown is related to the spalling off of corners as fragments are rotated and translated. In turn, this produces an increase in the percentage of small particles thus eventually creating a gouge along the shear fracture (Figure 14b).

Because transitional behavior in Oil Creek Sandstone is exhibited over a broad range of confining pressures, it is divided into two categories for microscopic study: category 1) transitional behavior associated with the boundary between brittle and transitional behavior and category 2) transitional behavior associated with the boundary between transitional and ductile behavior. Microscopic observations in category 1 samples (Figure 15) are similar to those in the brittle domain. The cataclastic zones contain a high percentage of grain-contact microfractures that, in general, have a preferred orientation parallel to the loading direction. The main difference from brittle behavior is that in category 1 the cataclastic zones have variable widths and can display cross-cutting relationships at both the micro- and macroscopic scales. Microscopic observations from category 2 samples (Figure 16) are quite different from those in category 1.

A.

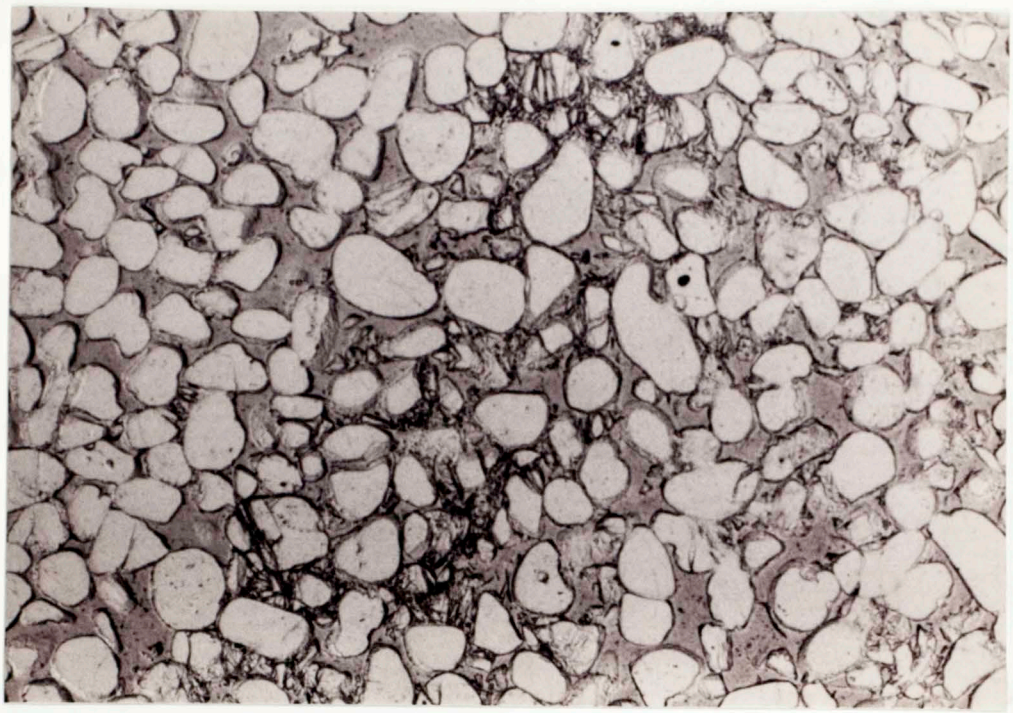

B.

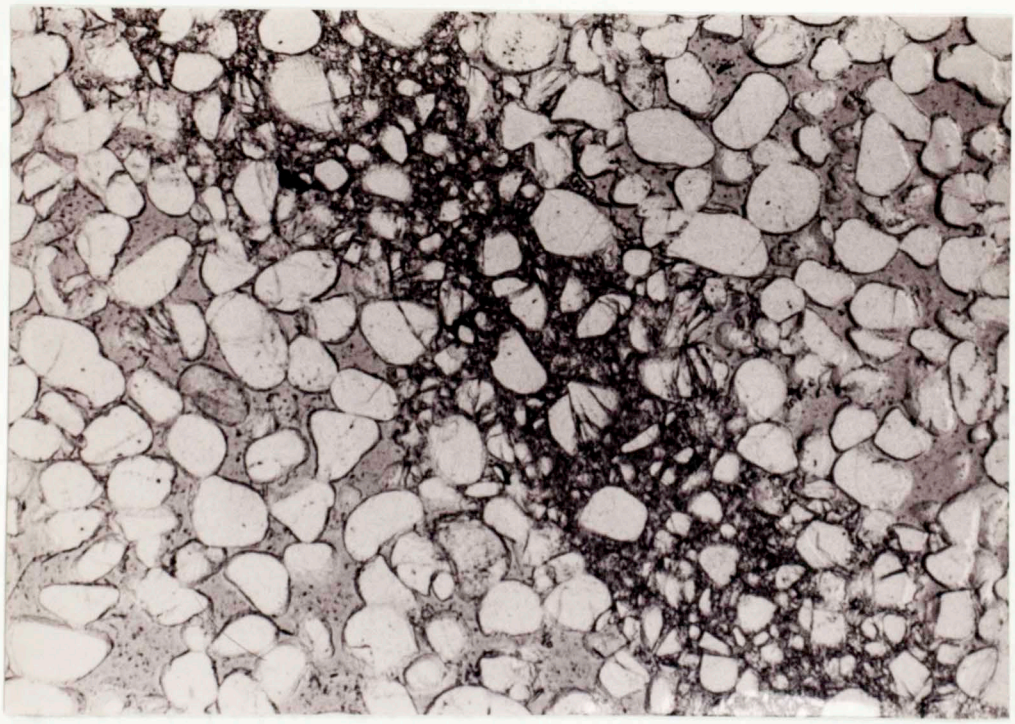

1 mm

Figure 14. Photomicrograph of Oil Creek Sandstone deformed in a triaxial compression test in the brittle domain a) prior to and b) after slip along the fracture plane. The scale bar is parallel to the load axis.

A.

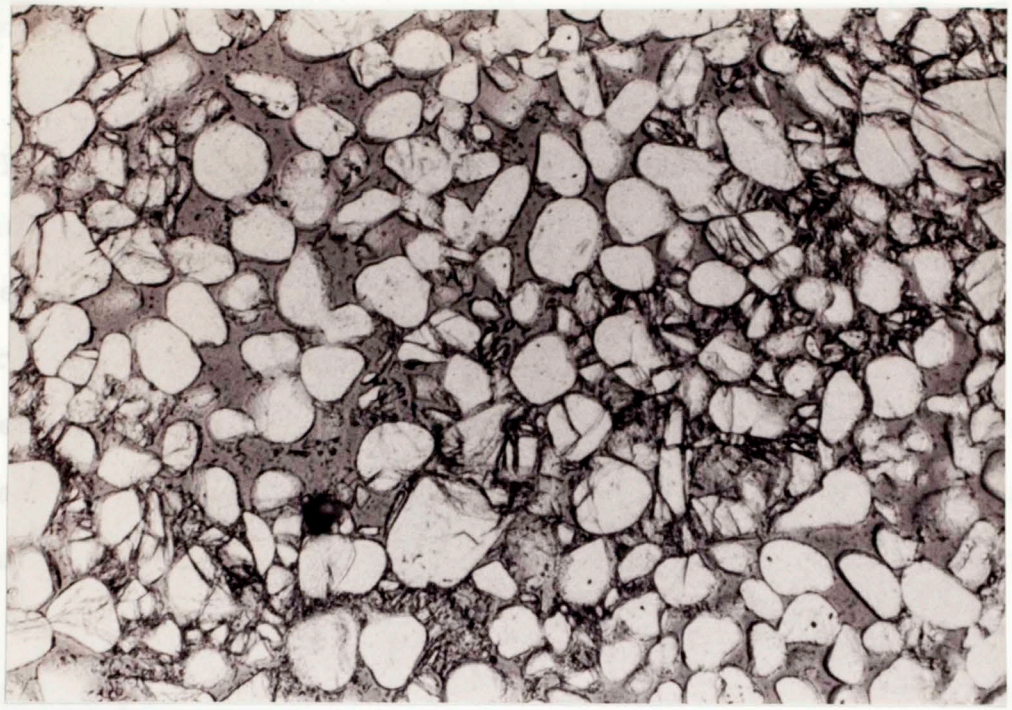

B.

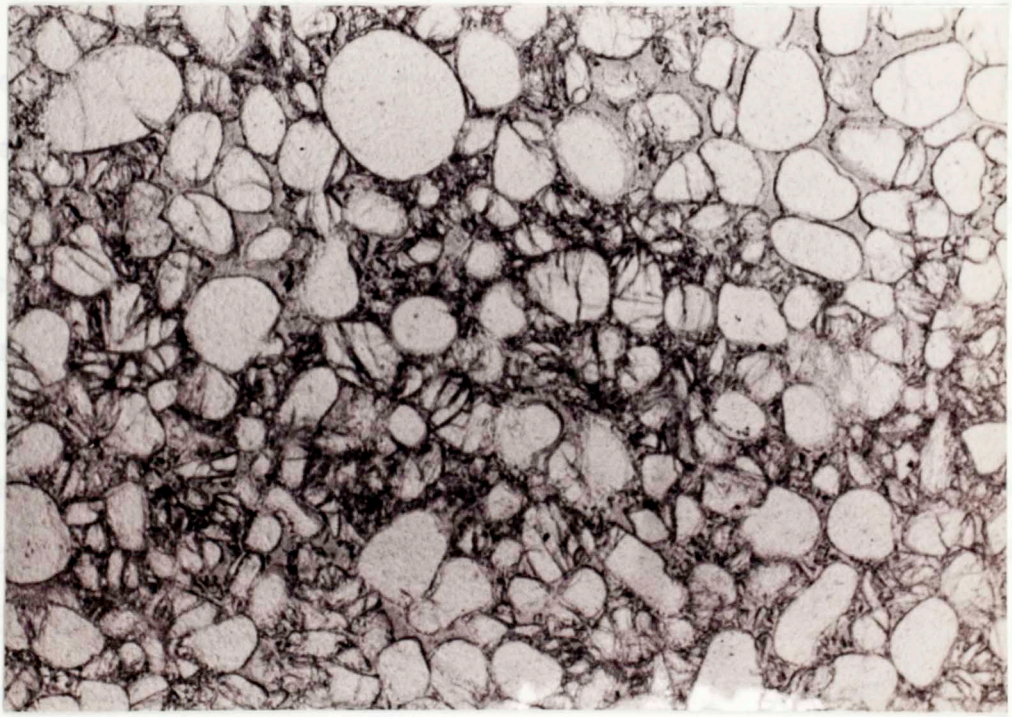

1 mm

Figure 15. Photomicrograph of Oil Creek Sandstone deformed in a triaxial compression test at the lower boundary of the transitional domain. a) narrow shear zone and b) broad shear zone. The scale bar is parallel to the load axis.

Oriented grain-contact microfractures still exist but the number of grain-contact microfractures is much lower in category 2 (compare Figure 15 to Figure 16). In addition, there is a significant increase in the percentage of small particles (compare Figure 15 to Figure 16). This increase in the percentage of small particles is not an artifact of displacement along the cataclastic zone. Original grain outlines are preserved in grains containing grain-contact microfractures, i.e., fragments have not been rotated (Figure 16).

Microscopic observations in the ductile domain (Figure 17) are consistent with those of Bernabe and Brace (1990: Fig. 7), where deformation is characterized by grain-contact microfractures but they no longer have a statistically preferred orientation. This could be attributed to the loss of pore space, thereby increasing the number of high-stress-difference, grain contacts in and out of the plane of the thin section. In addition, there is a relatively low percentage of small particles, or gouge, in the ductile domain when compared to category 2 in the transitional domain (compare Figure 16 to Figure 17).

Microscopic Observations of Hydrostatic Compression Test

The sample deformed in the hydrostatic compression test does not exhibit any inelastic deformation at the macroscopic scale. Studies by Zhang et al. (1990a, 1990b) indicate that

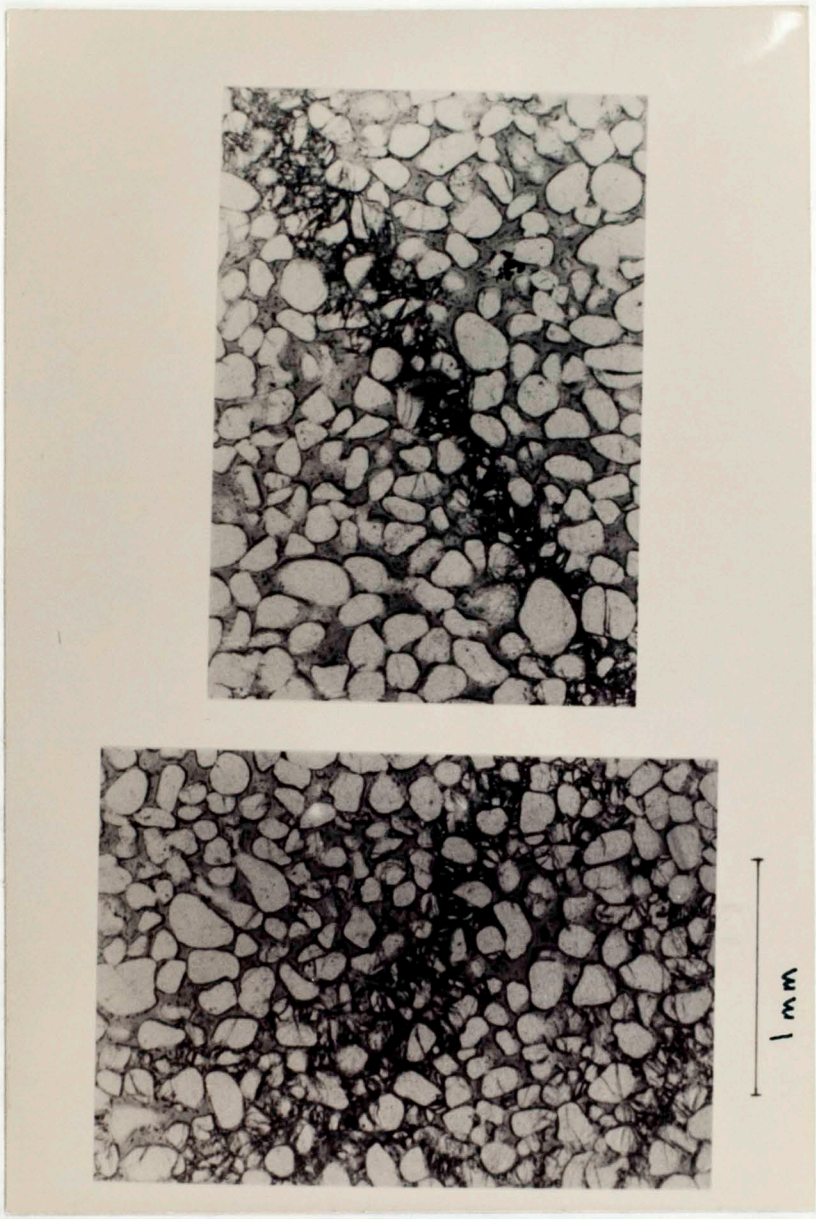

Figure 16. Photomicrographs of Oil Creek Sandstone deformed in a triaxial compression test at the upper boundary of the transitional domain. The scale bar is parallel to the load axis.

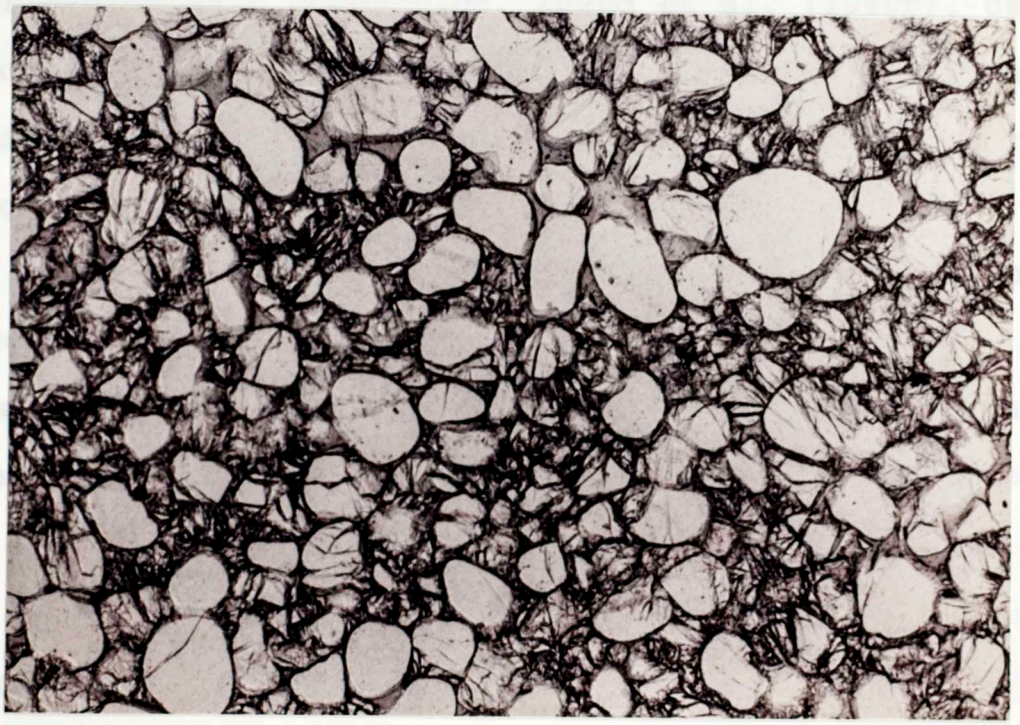

Figure 17. Photomicrograph of Oil Creek Sandstone deformed in a triaxial compression test in the ductile domain. The scale bar is parallel to the load axis.

the onset of pure hydrostatic compaction is accompanied by pervasive grain crushing (1990a: Figure 4). Microscopic observations of the hydrostatic compression test on Oil Creek Sandstone do not indicate total grain crushing. The sample does, however, contain isolated grain-contact microfractures that appear to be related to the hydrostatic compression test. That is, they are not inherited. The presence of these microfractures may indicate that the sample is close to the onset of hydrostatic compaction. Zhang et al. (1990b), using acoustic emission, delineate two stages in hydrostatic compaction. In stage 1, the grains rotate and translate. Grain crushing, on the other hand, is associated with stage 2. It may be, then, that grain-contact fracturing can actually occur in stage 1. Assuming this to be the case, results here are interpreted to indicated that pure hydrostatic compaction of Oil Creek Sandstone should occur at a confining pressure between 137.9 MPa and 145 MPa.

Indention Tests

Because mechanical behavior as a function of confining pressure for Oil Creek Sandstone is delineated in triaxial compression tests, indention tests are performed at only two confining pressures; 44.8 MPa (low) and 124.1 MPa (high). At each confining pressure, tests are run to varying amounts of indention: 1.59 mm, 3.28 mm, and 4.76 mm. Sample indention

begins at the first force drop, or inflection point, on the force-displacement record (prior to this point most of the distortion is elastic). Therefore, the amount of indention is measured from this point.

In indention tests, stress-strain curves cannot be calculated from force displacement records because the entire sample is not being loaded. Therefore, observations of, and interpretations from, indention tests are related to force-displacement records, not stress-strain curves. Data for each experiment is recorded on a conventional strip-chart recorder then digitized to generate force-displacement records (Figures 18 through 23).

There are several similarities between all force-displacement relationships that are independent of confining pressure. First, the overall trend of the records indicates that each increment of indention requires an increase in applied load (compare Figures 18 through 23). This should be expected because deformation in these tests is constrained. Such is also the case in indention tests reported by Suarez-Rivera et al. (1990). Another similarity is that with force drop magnitudes greater than 5 kN, there is always an audible grinding or crushing sound outside the pressure vessel.

The inflection point on the force-displacement records for low confining pressure tests (Figures 18 through 20) occurs at an applied load between 60 and 80 kN. In addition,

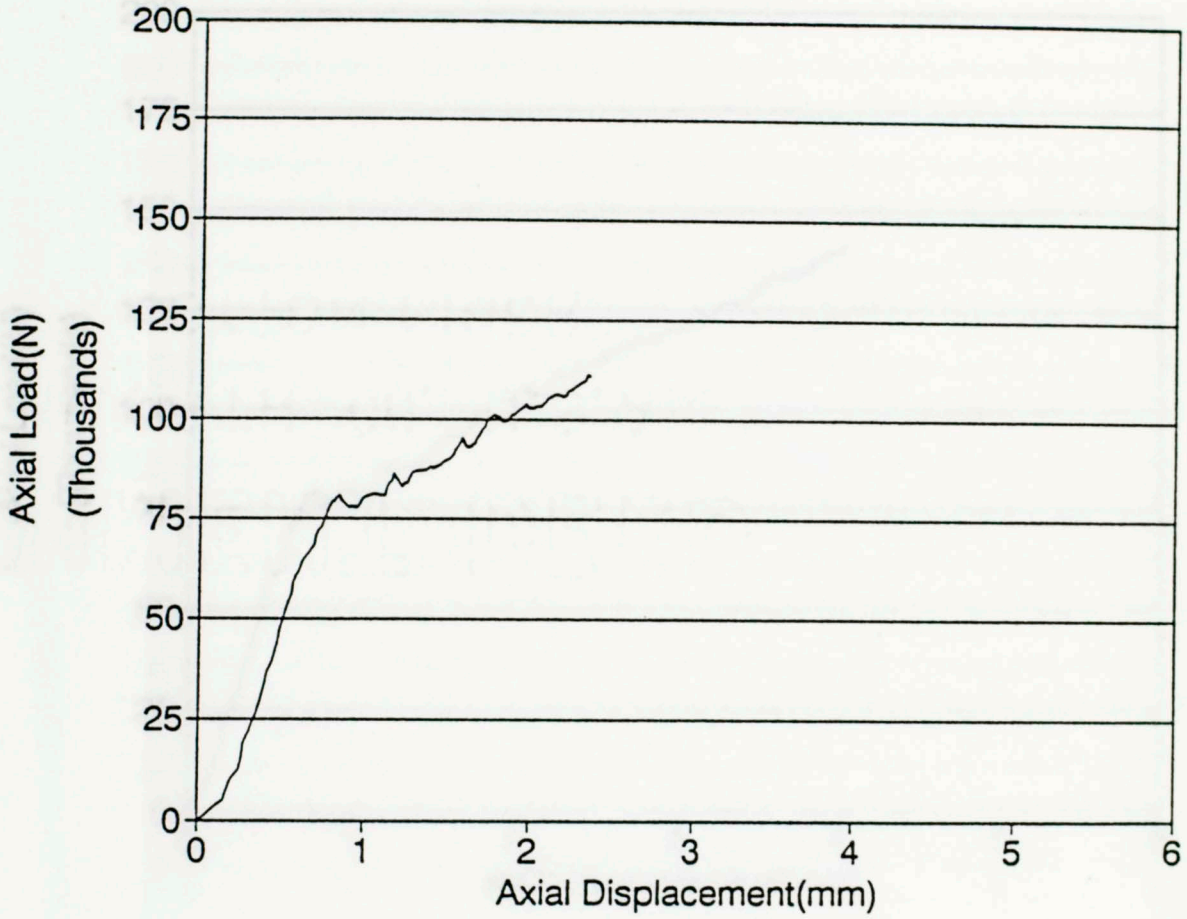

Figure 18. Force-displacement record for Oil Creek Sandstone deformed in an indention test at a confining pressure of 44.8 MPa taken to 1.59 mm indention.

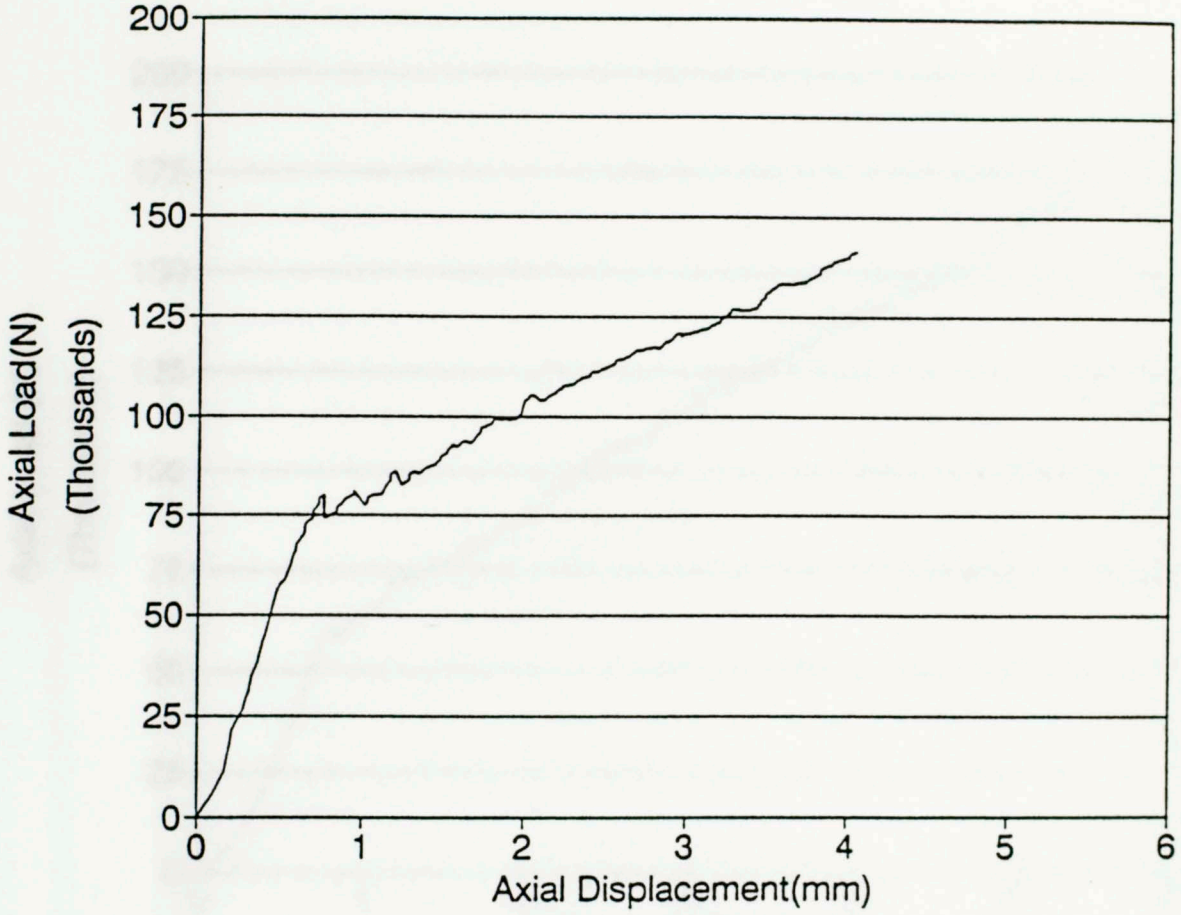

Figure 19. Force-displacement record for Oil Creek Sandstone deformed in an indention test at a confining pressure of 44.8 MPa taken to 3.18 mm indention.

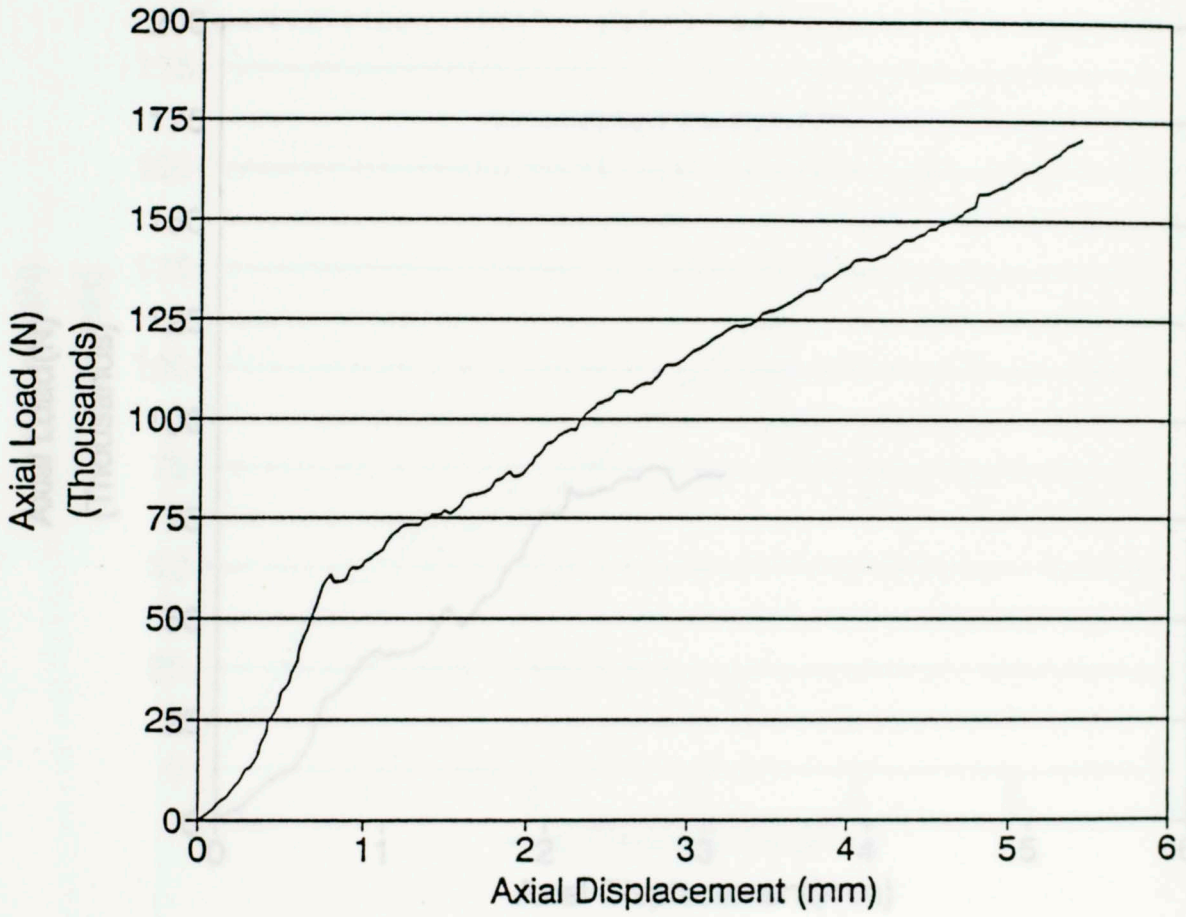

Figure 20. Force-displacement record for Oil Creek Sandstone deformed in an indention test at a confining pressure of 44.8 MPa taken to 4.76 mm indention.

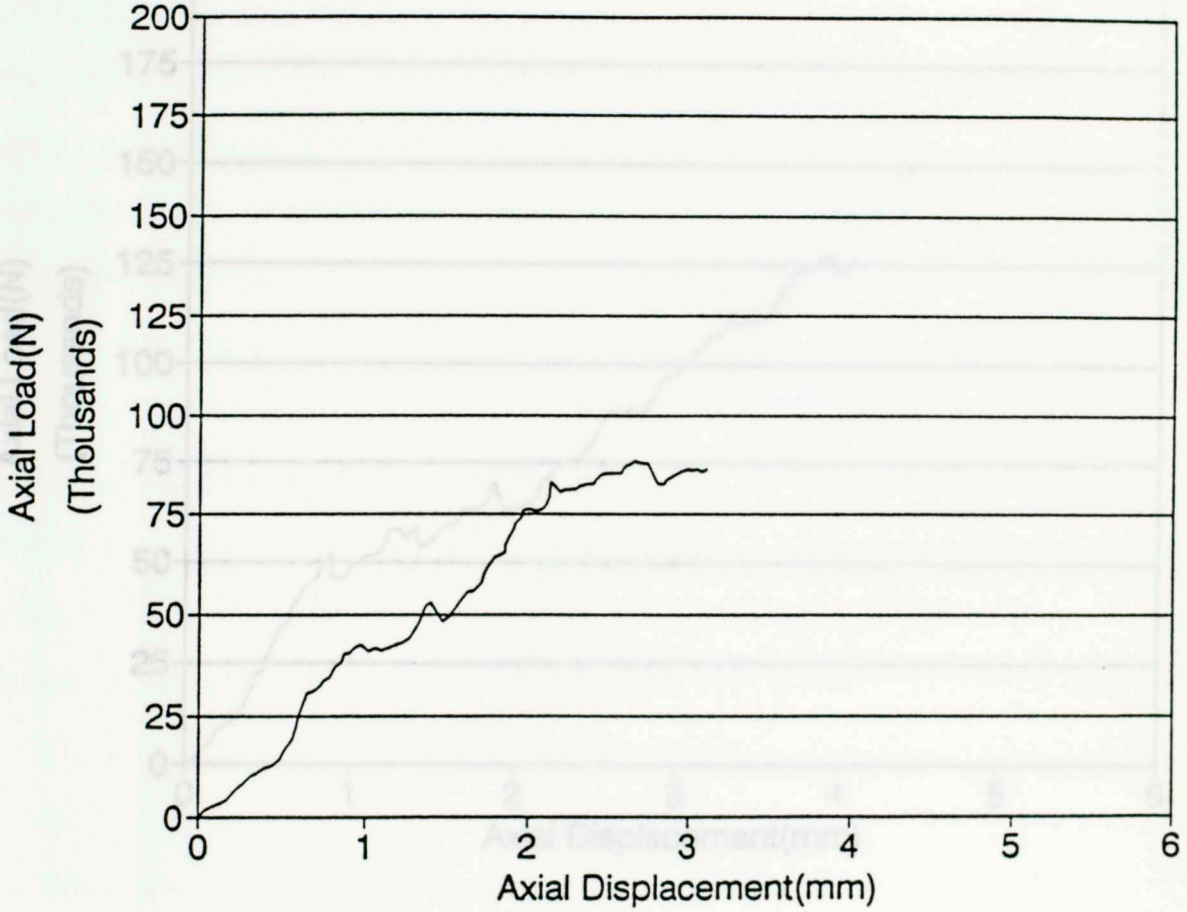

Figure 21. Force-displacement record for Oil Creek Sandstone deformed in an indention test at a confining pressure of 124.1 MPa taken to 1.59 mm indention.

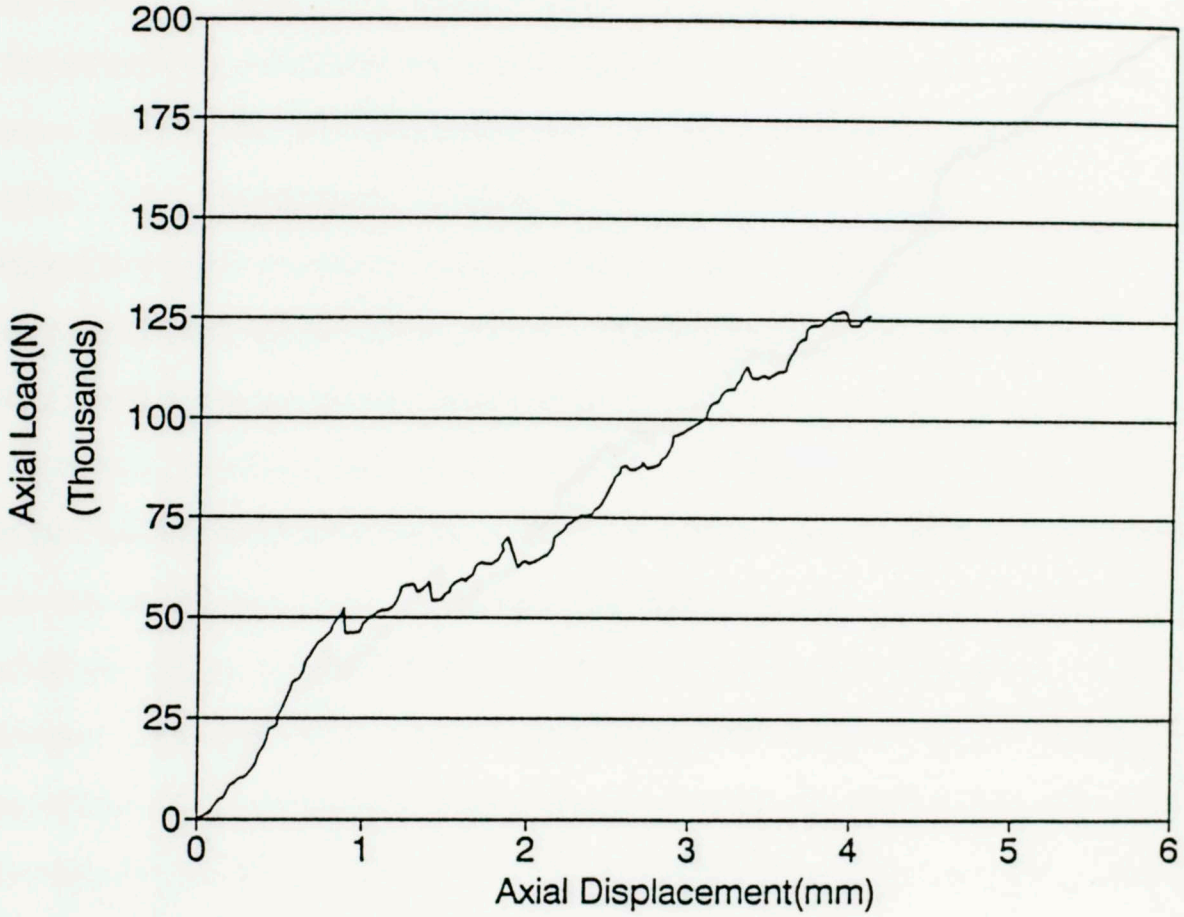

Figure 22. Force-displacement record for Oil Creek Sandstone deformed in an indention test at a confining pressure of 124.1 MPa taken to 3.18 mm indention.

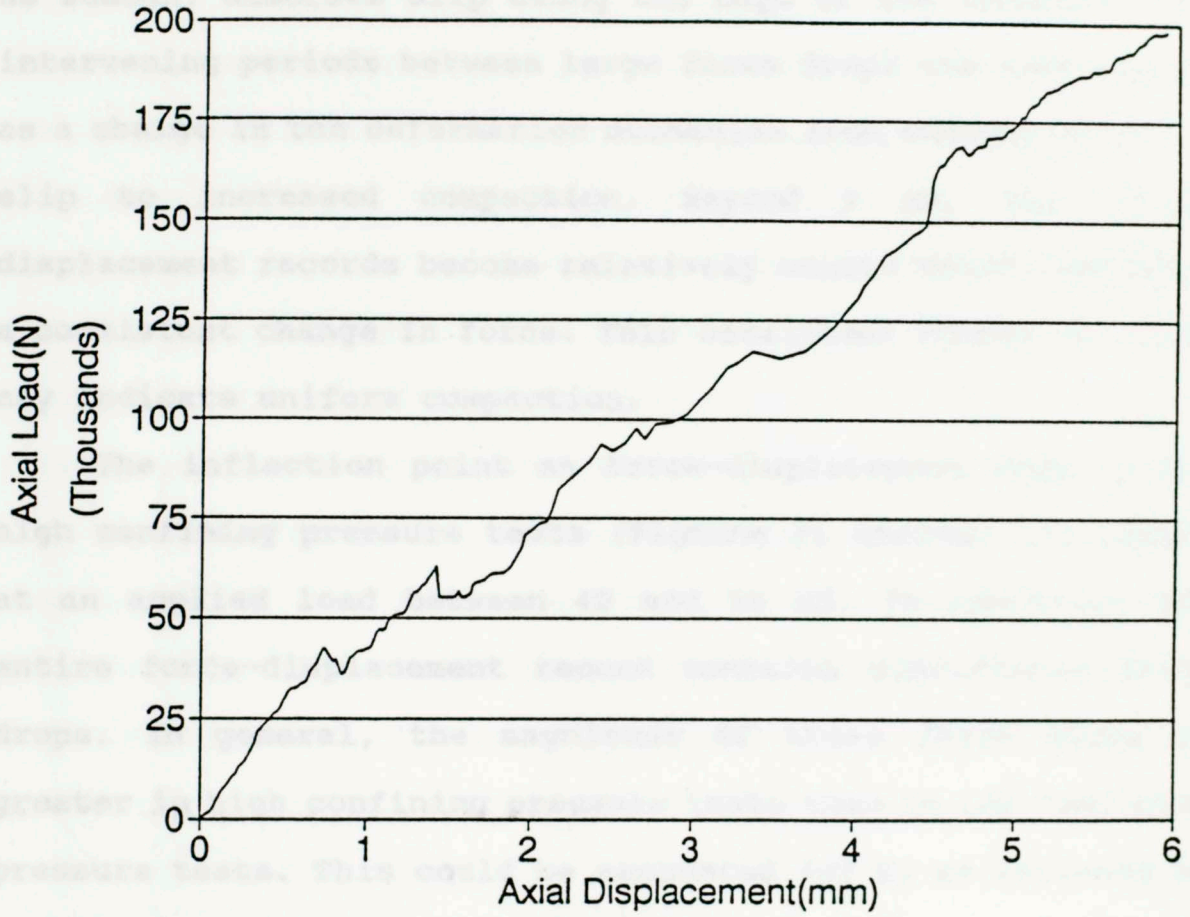

Figure 23. Force-displacement record for Oil Creek Sandstone deformed in an indention test at a confining pressure of 124.1 MPa taken to 4.76 mm indention.

the initial portion of the record up to 1.5 mm to 2.0 mm indention is characterized by frequent force drops with intermittent periods where force drops are severely reduced or non-existent. The periodic, larger force drops are interpreted as sudden, discrete slip along the edge of the indenter. The intervening periods between large force drops are interpreted as a change in the deformation mechanism from sudden, discrete slip to increased compaction. Beyond 2 mm, the force-displacement records become relatively smooth which indicates a consistent change in force. This consistent change in force may indicate uniform compaction.

The inflection point on force-displacement records for high confining pressure tests (Figures 21 through 23) occurs at an applied load between 40 and 50 kN. In addition, the entire force-displacement record contains significant force drops. In general, the magnitude of these force drops is greater in high confining pressure tests than in low confining pressure tests. This could be accounted for by an increase in resistance to slip (i.e., mostly friction) between grains at the higher confining pressure. Beyond 2 mm indention, large force drops with intervening periods of reduced force drops become less frequent. Again, the intervening periods are interpreted as a change in deformation mechanism, possibly a more uniform compaction.

Stress-strain curves for tests at 40 and 120 MPa (Figures

10c, 10d, and 10h) are also characterized by frequent stress drops. The primary difference between triaxial compression and corresponding indention tests is that in indention tests there is an audible grinding or crushing sound associated with force drops that do not occur in triaxial compression tests. In addition, the stress-strain curve at 120 MPa (Figure 10h) does not have portions where stress drops are suppressed to the same extent as are force drops in the indention tests. These observations lead to the possible conclusion that stress drops in triaxial compression tests and force drops in the indention tests are due to different processes. This conclusion is further indicated by microscopic observations reported later.

Deformation in low confining pressure indention tests is restricted to the region directly underneath the indenter (Figure 24). This pattern is consistent with the pattern reported by Suarez-Rivera et al. (1990). The deformed region under the indenter contains two sub-regions. There is a central, somewhat triangular region (shaded region in Figure 24) that develops between 1.59 and 3.18 mm of indention. At the microscopic scale, this region is characterized by a nearly complete loss of porosity and sand grains are severely broken and crushed. In the damaged region outside the triangle, the sandstone is also compacted and crushed but to a lesser extent than within the triangle.

In high pressure indention tests, macroscopic deformation

A.

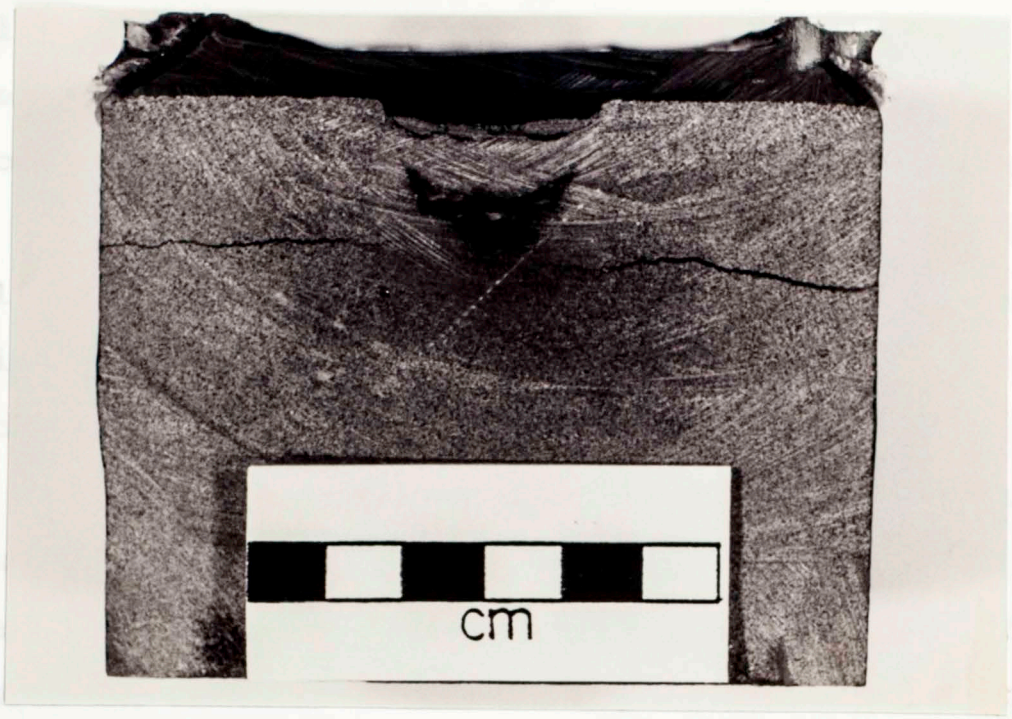

B.

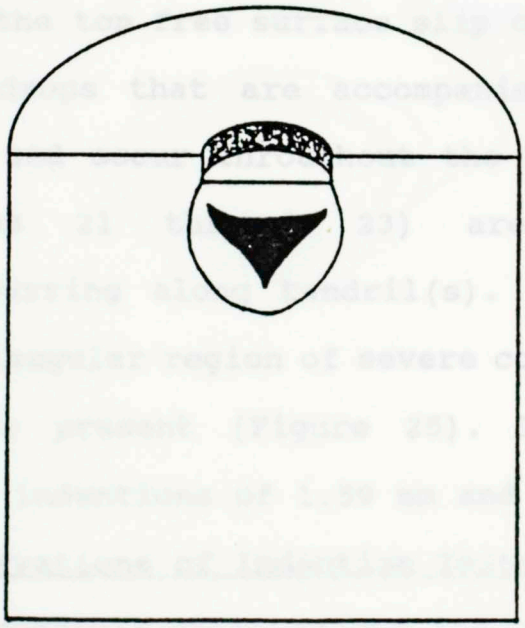

Figure 24. Macroscopic appearance of Oil Creek Sandstone deformed in an indention test at a confining pressure of 44.8 MPa a) photograph of an actual sample and b) schematic drawing of the deformed region. Arcuate lineations are saw marks.

initially extends beyond the region directly underneath the indenter (Figure 25) which indicates that indenter displacement is being distributed over a broader region than in low confining pressure tests. The deformed region expands laterally, away from the indenter, with increasing amounts of indention up to approximately 4.50 mm. At this stage, indenter displacement again becomes distributed over a narrow region as in low confining pressure, indention tests. Why this happens is a matter of conjecture. The expanded deformation region contains features, here called "tendrils", that extend from underneath the indenter toward the top of the sample. When a tendril reaches the top free surface slip can occur along the tendril. Force drops that are accompanied by grinding or crushing sounds and occur throughout the force-displacement records (Figures 21 through 23) are interpreted as displacement occurring along tendril(s). At high confining pressure, the triangular region of severe compaction and grain crushing is also present (Figure 25). This region again develops between indentions of 1.59 mm and 3.18 mm.

Microscopic Observations of Indention Tests

Cursory microscopic observations indicate that two modes of grain fracturing occur in these indention tests. Mode 1 grain fracturing is by simple grain-contact microfractures. Mode 2 grain fracturing, however, is grain crushing where the fractures do not emanate solely from grain contacts, but

A.

B.

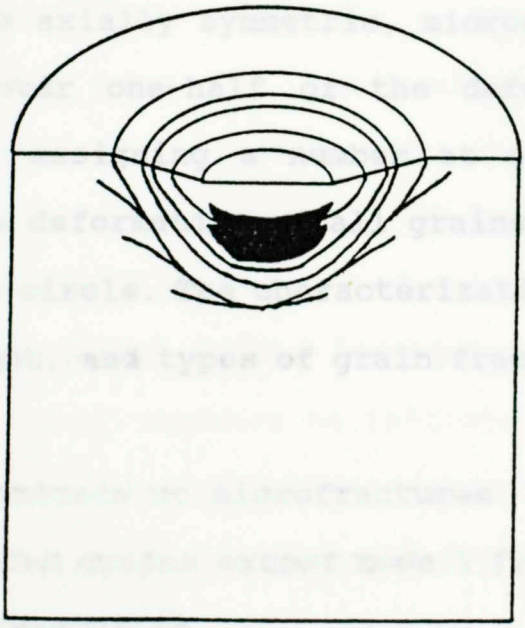

Figure 25. Macroscopic appearance of Oil Creek Sandstone deformed in an indention test at a confining pressure of 124.1 MPa a) photograph of an actual sample and b) schematic drawing of the deformed region. Arcuate lineations are saw marks.

rather polygonize the grain into randomly oriented, small segments. It is also noted that the rate of change between mode 1 and mode 2 grain fracturing is greatest within 2 mm of either side of the indenter edge. This observation prompted the use of a grid pattern to make systematic microscopic observations. Within 2 mm of the indenter edge, grid spacing is 0.5 mm on a side and extends 8 mm below the bottom of the indenter. Grid spacing for the rest of the thin section is 1 mm on a side. Within smaller grids, the area analyzed is a circle 0.25 mm in diameter while within larger grids, observations are made in 0.5 mm diameter circles. Because the indention test is axially symmetric, microscopic analysis is only performed over one-half of the deformed region. The analysis entails assigning a number at each location that characterizes the deformation of all grains inside of, and in contact with, the circle. The characterization number is based on presence, amount, and types of grain fracturing observed as follows:

0 = grains contain no microfractures.

1 = unfractured grains exceed mode 1 fractured grains and no mode 2 grain fracturing.

2 = mode 1 fractured grains exceed unfractured grains and no mode 2 grain fracturing.

3 = only mode 1 grain fractures are present.

4 = mode 1 grain fractures exceed mode 2 grain fractures

but some unfractured grains are present.

5 = all grains are fractured and mode 1 grain fractures exceed mode 2 grain fractures.

6 = mode 2 grain fractures exceed mode 1 grain fractures but some unfractured grains are present.

7 = all grains are fractured and mode 2 grain fractures exceed mode 1 grain fractures.

Even though this system is subjective, there is a certain level of consistency since analysis is done by the same operator. After analyzing each thin section, observation circle numbers are contoured by hand to generate damage contour maps.

Damage contour maps for low confining pressure tests (Figures 26, 28, and 30) illustrate the change in grain scale deformation with increasing amounts of indention. At 1.59 mm of indention (Figures 26 and 27), a change from mode 1 to mode 2 grain fracturing occurs as the indenter edge is approached. Mode 2 grain fracturing appears to initiate at the edge of the indenter and extends vertically into the deformed region. With increasing indention to 3.18 mm and 4.76 mm the zone of mode 2 grain fracturing continuously widens, extends deeper into the sample, and the trend of the zone diverges from vertical (Figures 28 through 31). Two other features seem to accompany increasing indention: 1) unfractured, or slightly fractured, grains begin to be incorporated into the zone of mode 2 grain

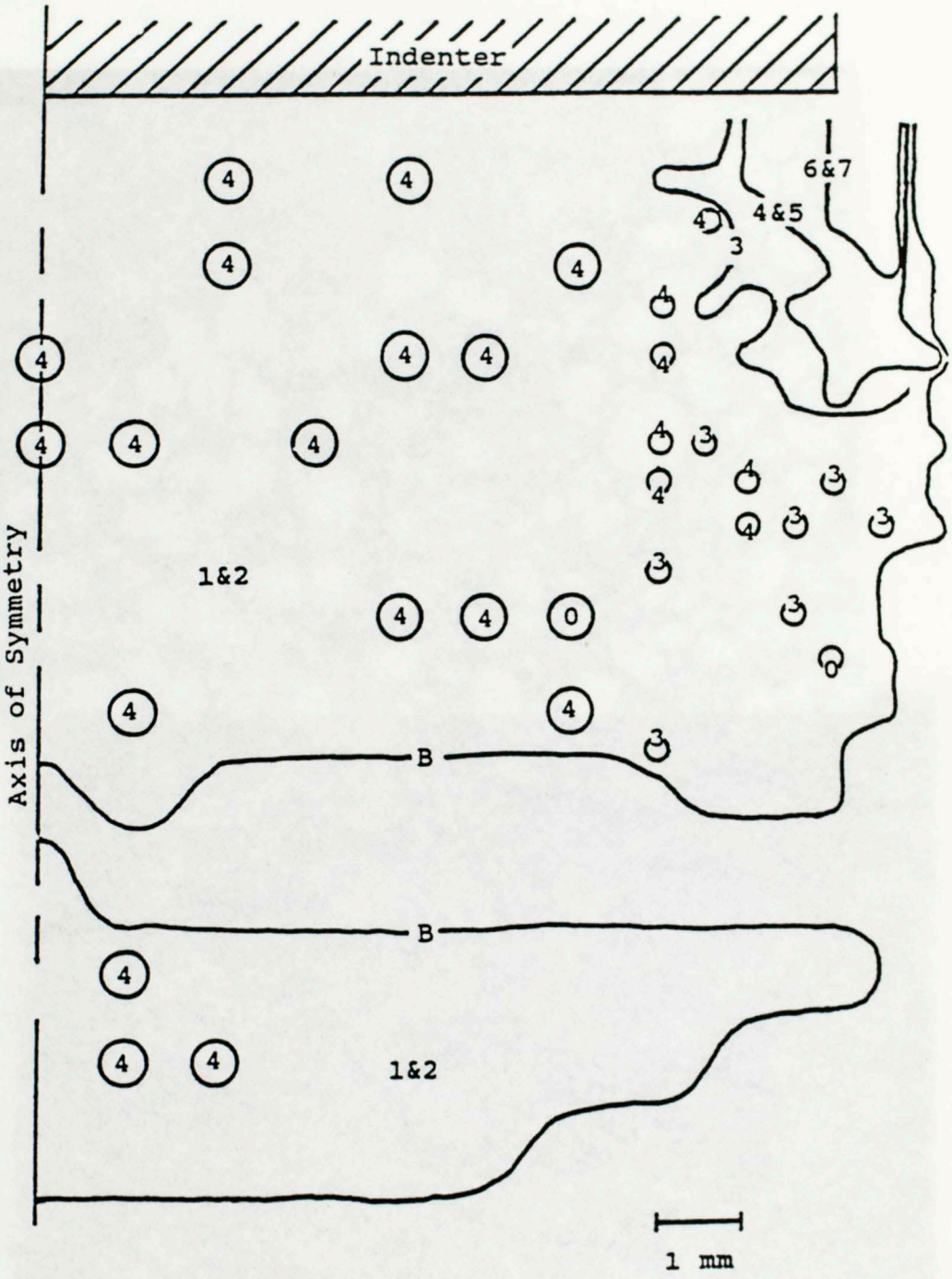

Figure 26. Damage contour map for Oil Creek Sandstone deformed in an indention (1.59 mm) test at a confining pressure of 44.8 MPa. See text for explanation of contour values. The boundary between damaged and undamaged regions is denoted by the letter B.

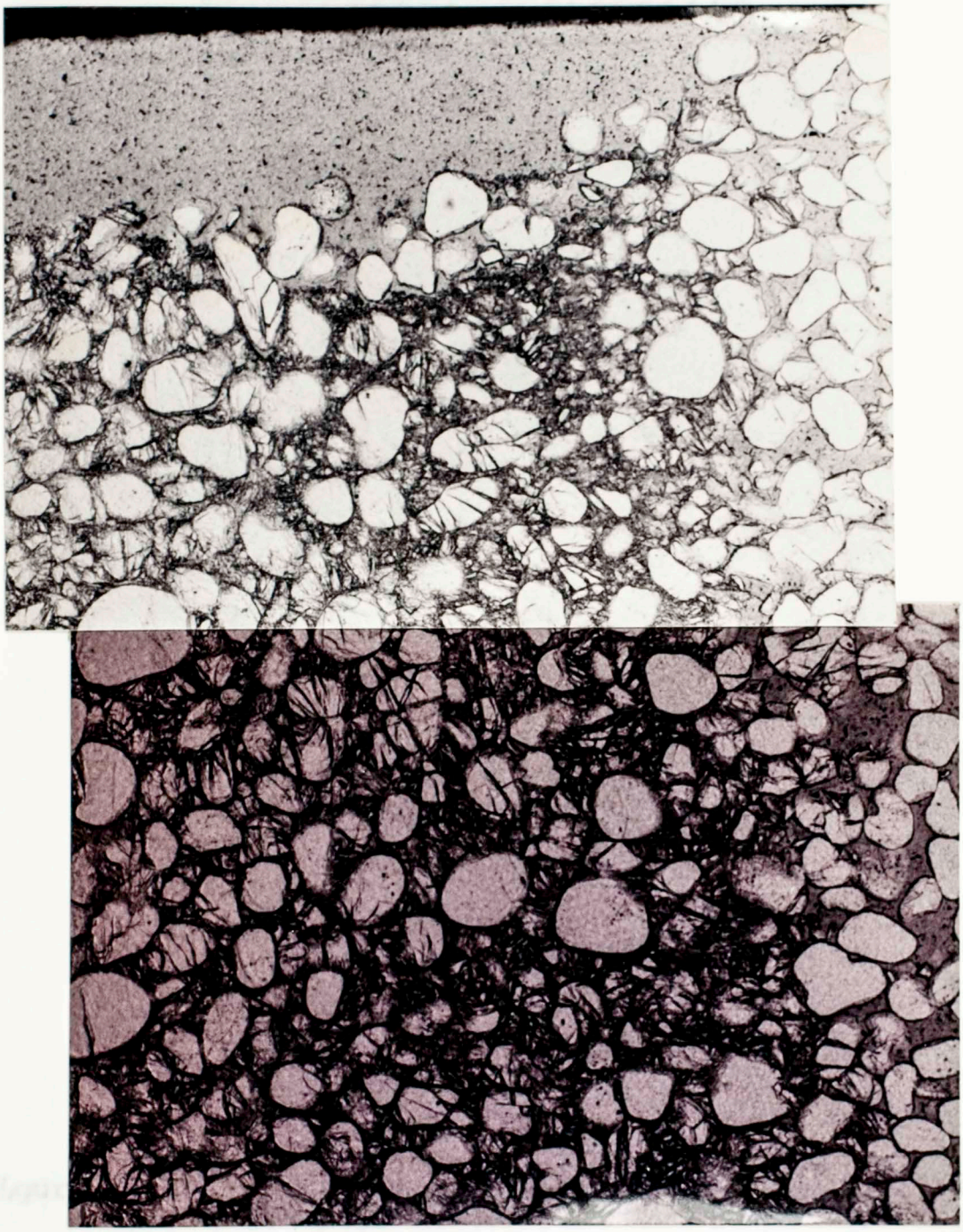

Figure 27. Photomicrograph mosaic of the region underneath the edge of the indenter in figure 26.

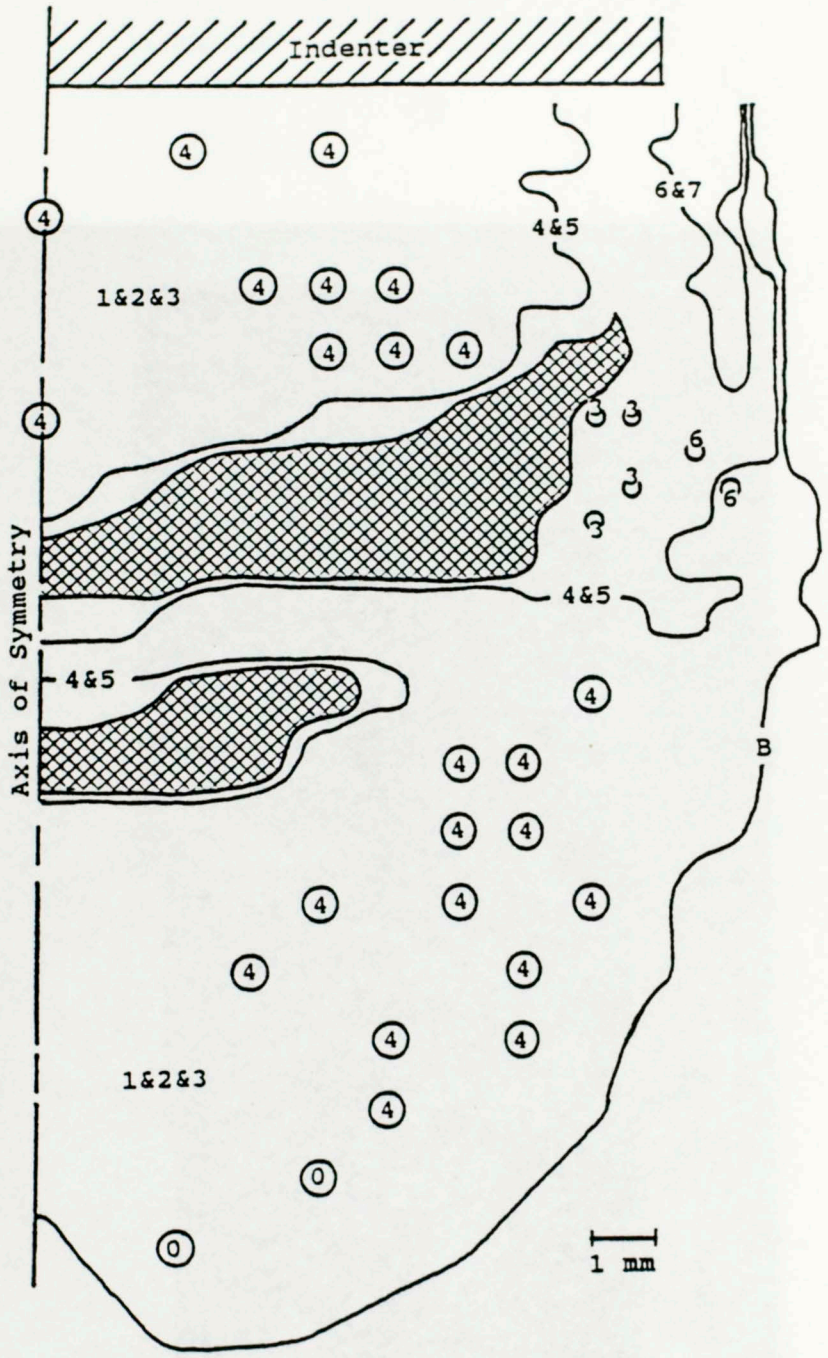

Figure 28. Damage contour map for Oil Creek Sandstone deformed in an indention (3.18 mm) test at a confining pressure of 44.8 MPa. See text for explanation of contour values. The boundary between damaged and undamaged regions is denoted by the letter B. The hatchured regions are not analyzed.

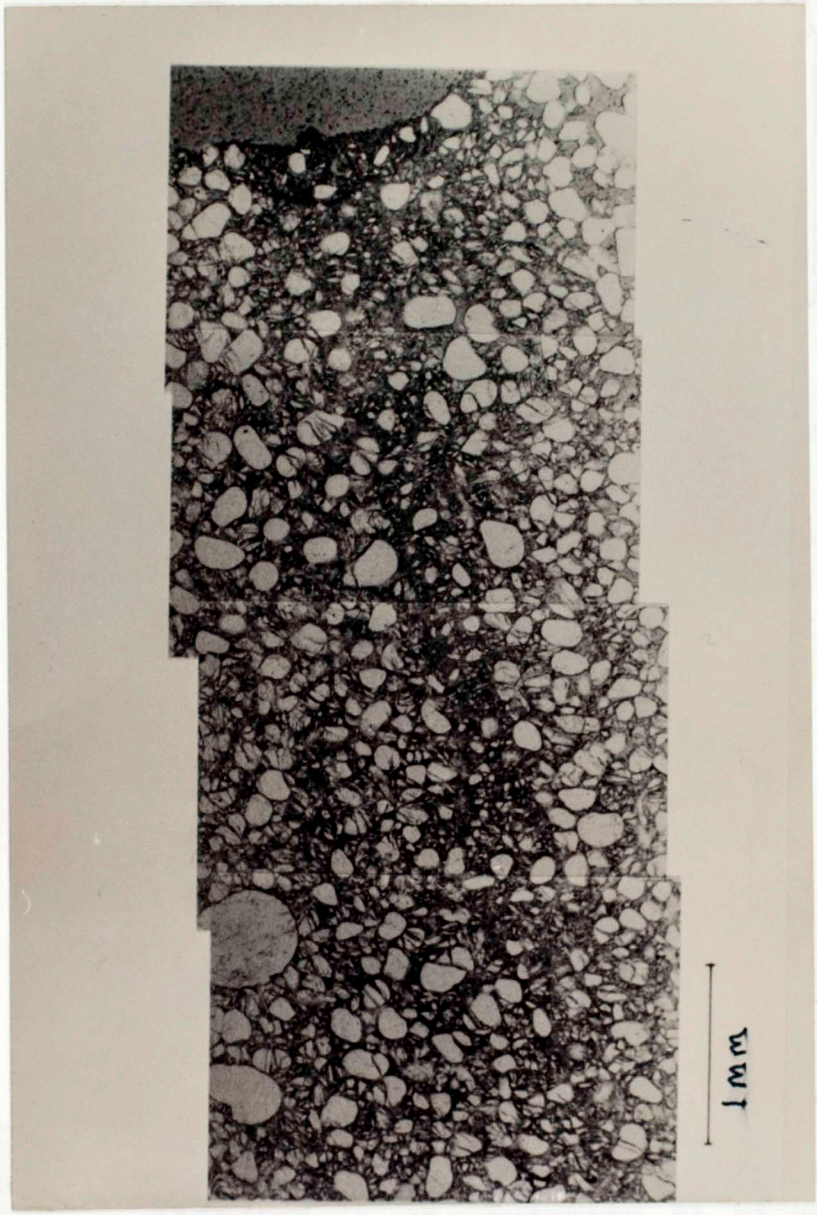

Figure 29. Photomicrograph mosaic of the region underneath the edge of the indenter in figure 28.

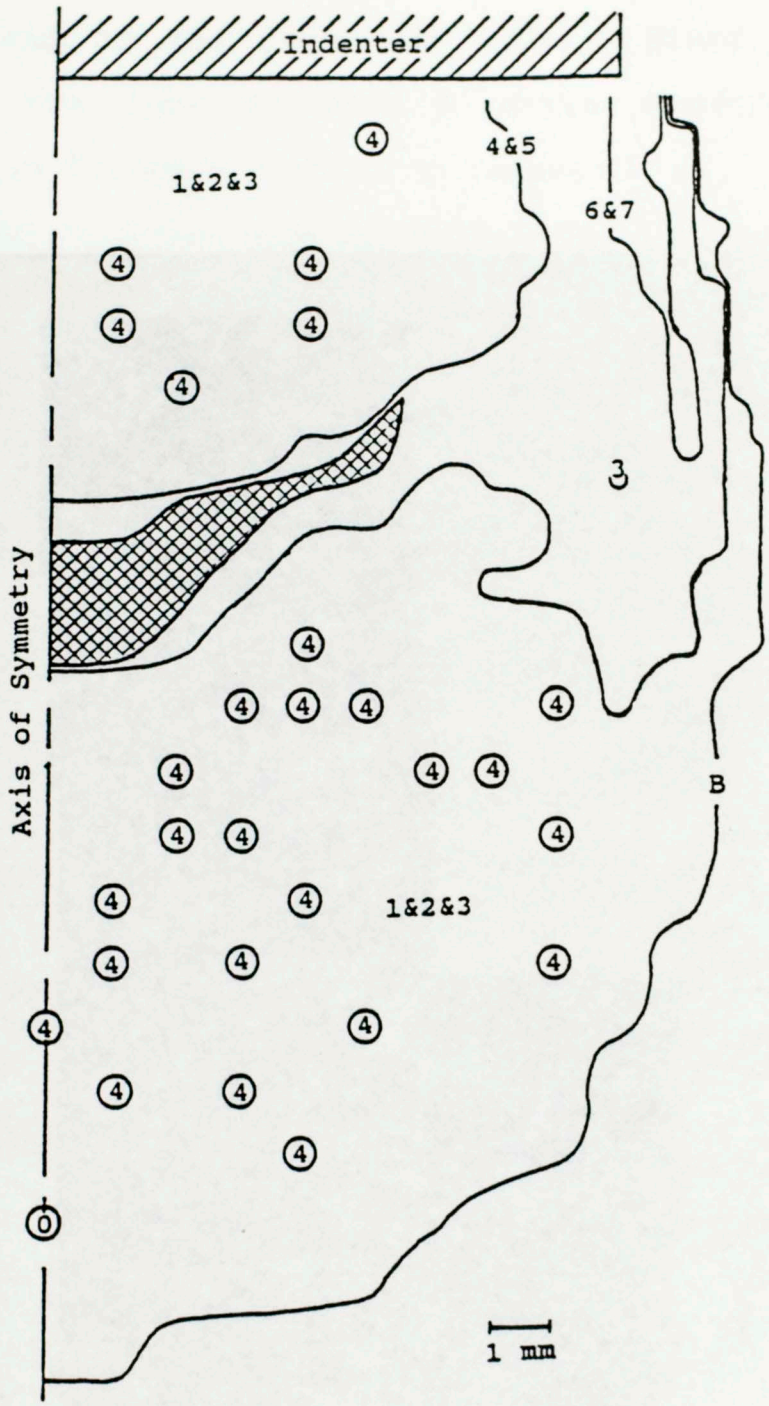

Figure 30. Damage contour map for Oil Creek Sandstone deformed in an indention (4.76 mm) test at a confining pressure of 44.8 MPa. See text for explanation of contour values. The boundary between damaged and undamaged regions is denoted by the letter B. The hatchured region is not analyzed.

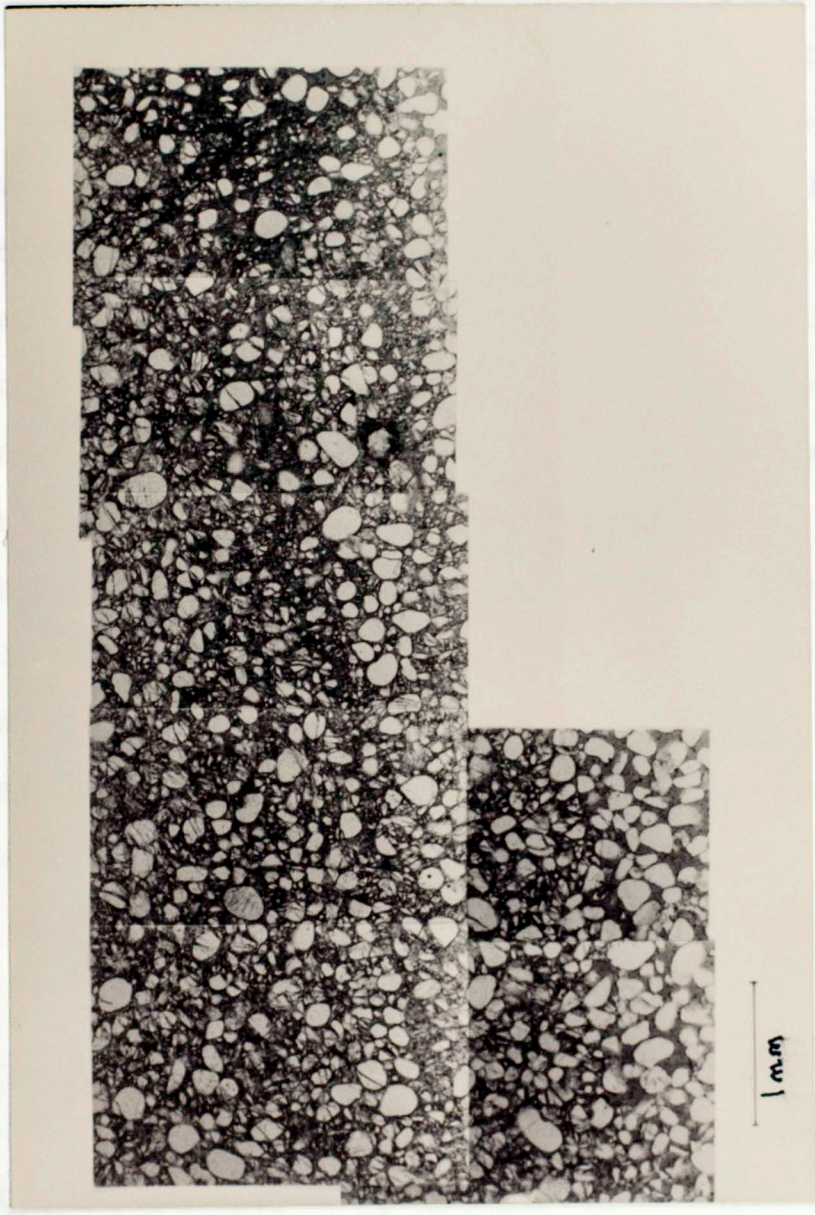

Figure 31. Photomicrograph mosaic of the region underneath the edge of the indenter in figure 30.

fracturing and 2) the region of mode 1 grain fracturing surrounding the zone of mode 2 grain fracturing grows asymmetrically (compare Figures 26 through 31).

A complete and thorough analysis of the highly compacted, triangular region beneath the indenter, is not possible because of grain plucking during the thin sectioning process. However, examination of the unplucked grains in this region indicates that porosity is nearly eliminated (compare Figures 13a and 32a). Grains within this region exhibit both modes of grain fracturing (Figure 32b), but mode 2 appears to dominate. As the highly compacted region is approached from above or below, there is a gradual change from predominantly mode 1 to predominantly mode 2 grain fracturing (Figure 33). Additionally, there is a gradual reduction in porosity and an increase in the percentage of small particles.

Several other microscopic observations regarding the low confining pressure tests are:

1) a sharp boundary exists between deformed and undeformed regions (Figures 27, 29, and 31).

2) mapping grain-contact microfractures provides a method for mapping maximum principal stress trajectories underneath the indenter. In the test to 3.18 mm of indention, microfracture histograms of frequency versus orientation (located in Appendix F) indicate that microfractures follow the maximum principal stress trajectories expected for an

A.

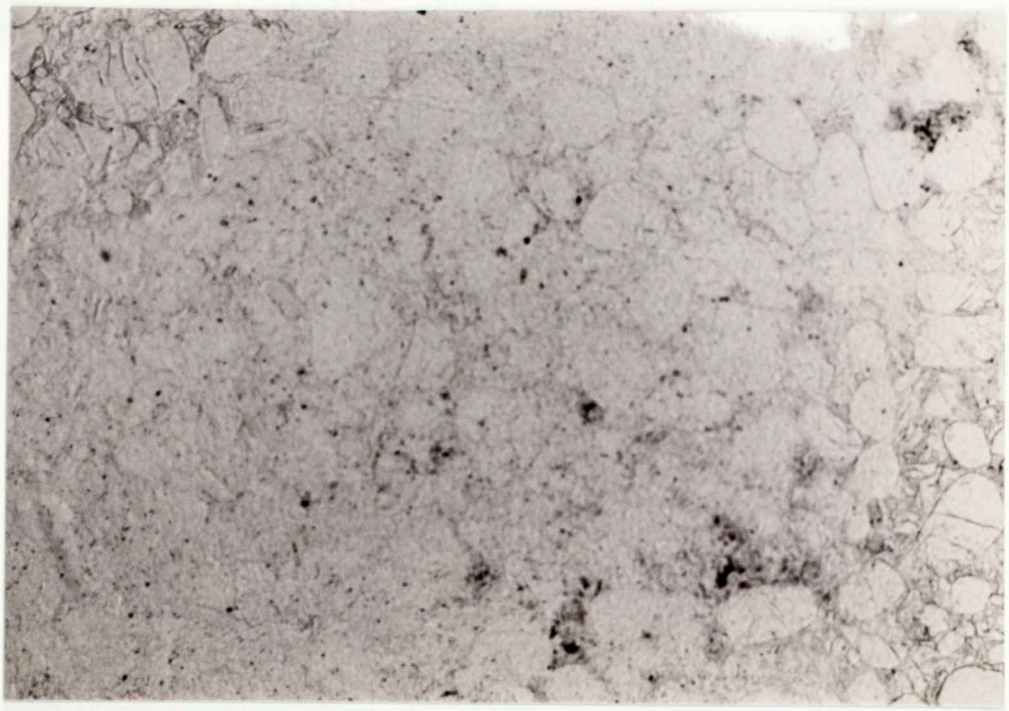

B.

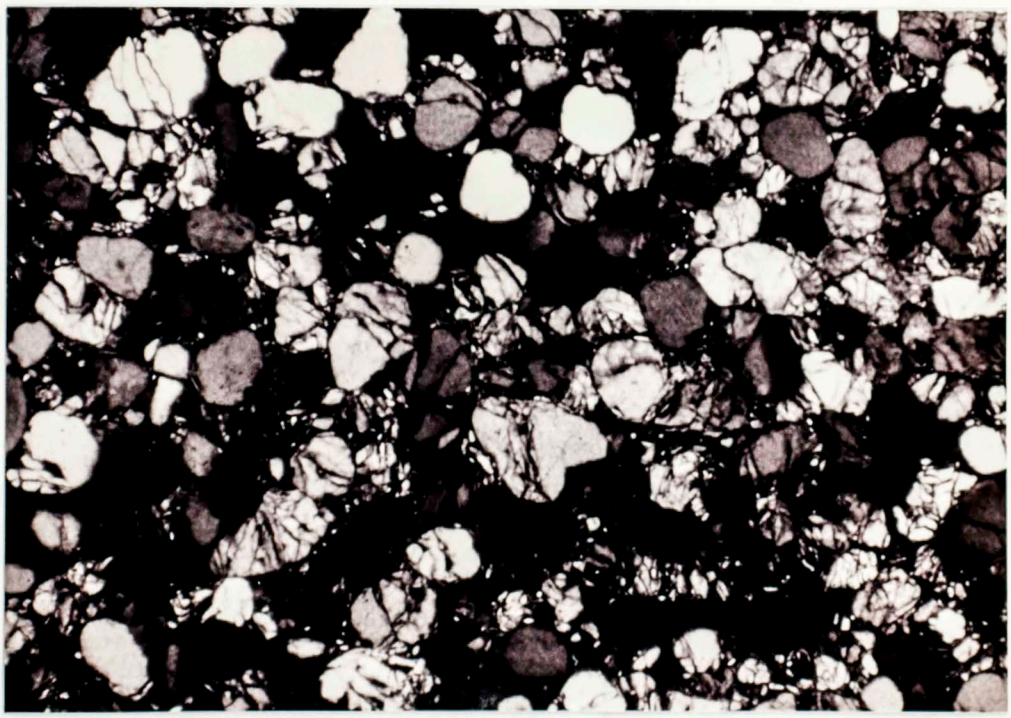

1 mm

Figure 32. Photomicrograph of the highly compacted, triangular region in figure 24: a) plane light b) polarized light.

A.

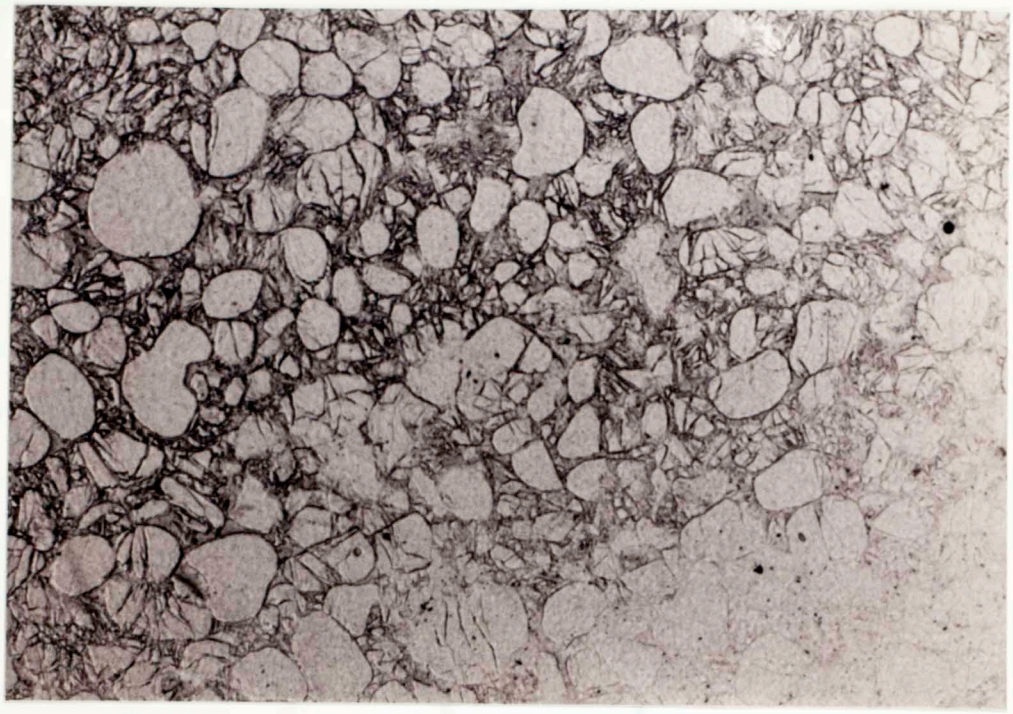

B.

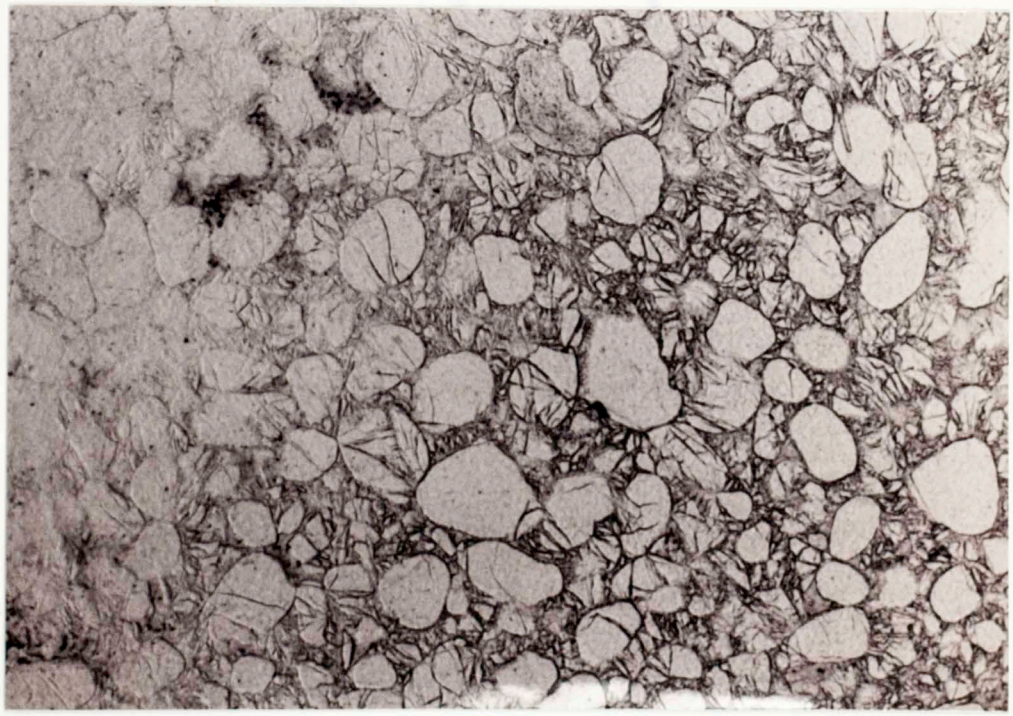

1 mm

Figure 33. Photomicrograph of the border of the compacted region in figure 25: a) above and b) below this region.

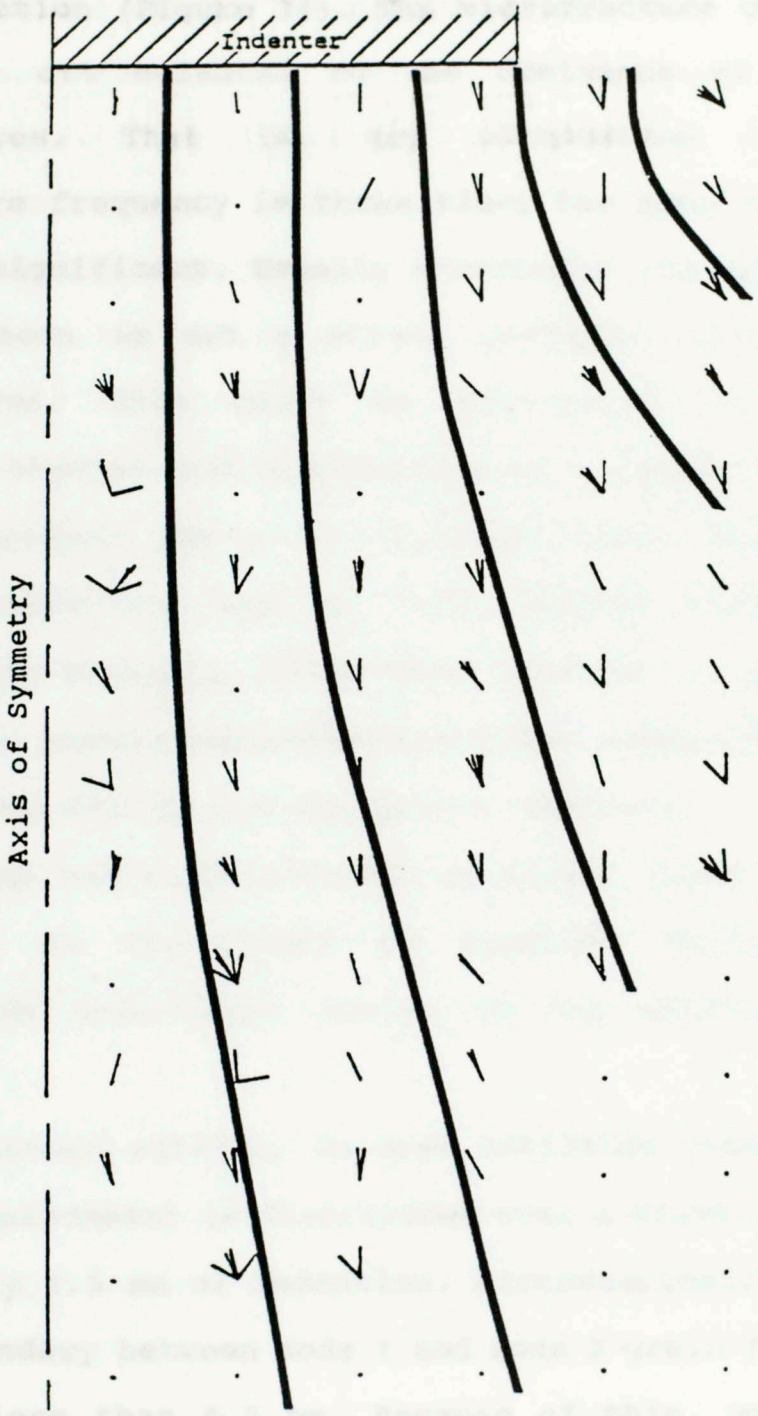

Figure 34. Significant microfracture orientations and their spatial relationship with the indenter. See text for explanation of their significance. The solid lines are interpreted maximum principal stress trajectories.

elastic solution (Figure 34). The microfracture orientations (Figure 34) are selected on the dominance of the given microfractures. That is, any orientation cell whose microfracture frequency is three times the mean frequency is considered significant. Usually underneath the center of the indenter, there is not a strong preferred orientation to microfractures. This could be attributed to: 1) post-fracturing rotation and translation of fragments from their original position and/or 2) microfractures developing in several orientations due to large stress differences at numerous grain contacts. These data, however, do not preclude stress fields associated with rheologies, other than elastic, if such stress fields are similar in response.

3) Though not quantitatively measured, there seems to be an increase in the amount of undulose extinction when comparing the undeformed region to the highly compacted region.

As indicated earlier, in high confining pressure tests, indenter displacement is distributed over a broad region up to approximately 4.5 mm of indention. Microscopically, there is no sharp boundary between mode 1 and mode 2 grain fractures at indentions less than 4.5 mm. Because of this, and the grid arrangement, damage contour maps for tests to 1.59 mm and 3.18 mm of indention do not realistically illustrate the grain scale damage. In the 1.59 mm indention test, mode 1 is the

dominate mode of grain fracturing. Near the edge of the indenter, there is a small increase in the amount of mode 2 grain fracturing, but it is not concentrated (Figure 35). Increasing indention to 3.18 mm, indicates a small increase in amount, and aerial extent, of mode 2 grain fracturing but mode 1 still dominates (Figure 36). At 4.76 mm indention, a well defined zone of mode 2 grain fracturing develops adjacent to the edge of the indenter (Figures 37 and 38). The trend of this zone is near vertical. Unbroken, or slightly broken, grains seem to have been incorporated into the zone of mode 2 grain fracturing (compare Figures 35, 36, and 38).

The highly compacted region in high confining pressure tests has virtually identical characteristics to this same region in low confining pressure tests. Here too, there appears to be an increase in undulose extinction when comparing the undeformed region and highly compacted regions.

The last microscopic observation regarding these indention tests is independent of confining pressure. This observation is that strain within the deformed region is heterogeneously distributed over small domains (Figure 39). Because of this, the exact positioning of a small sampling circle within the deformed region greatly effects the numerical value assigned to it. Because of rapid, but random, changes in damage, contour maps in some areas may be difficult to understand (Figures 26, 28, 30, and 37).

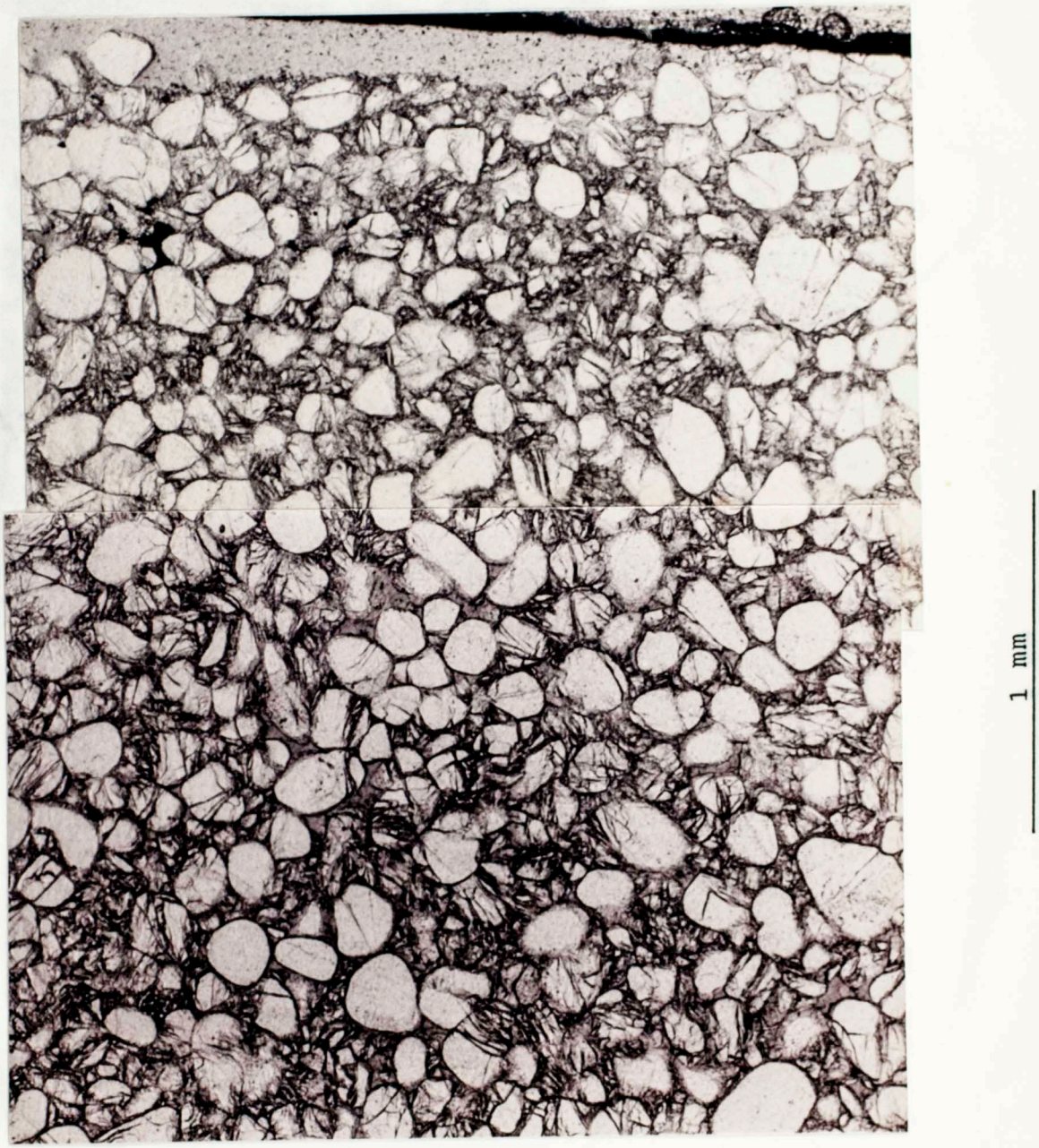

Figure 35. Photomicrograph mosaic of the region underneath the edge of the indenter (same position as in Figure 28) in Oil Creek Sandstone deformed in an indention (1.59 mm) test at a confining pressure of 124.1 MPa.

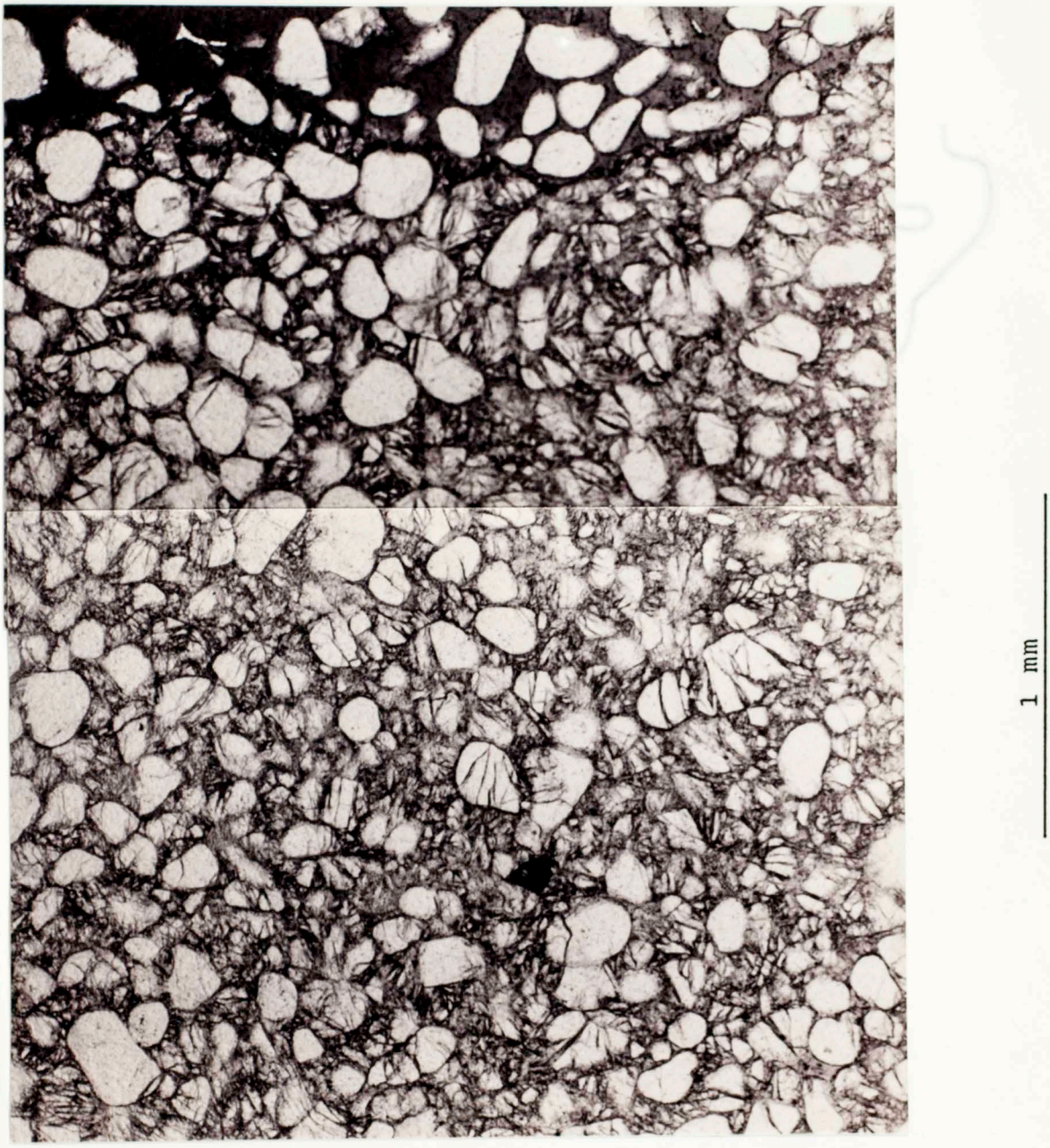

Figure 36. Photomicrograph mosaic of the region underneath the edge of the indenter (same position as in Figure 30) in Oil Creek Sandstone deformed in an indention (3.18 mm) test at a confining pressure of 124.1 MPa.

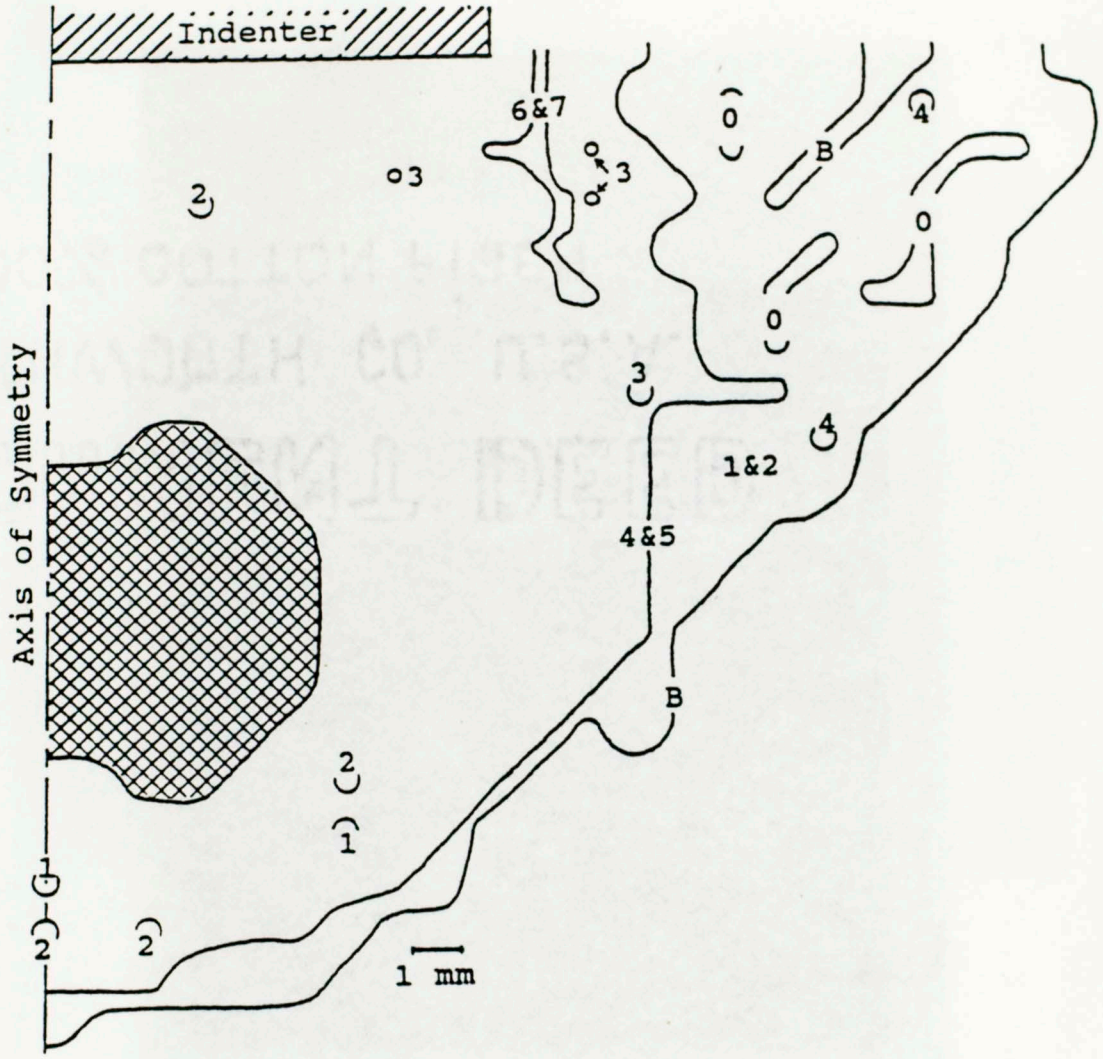

Figure 37. Damage contour map for Oil Creek Sandstone deformed in an indention (4.76 mm) test at a confining pressure of 124.1 MPa. See text for explanation of contour values. The boundary between damaged and undamaged regions is denoted by the letter B. The hatchured region is not analyzed.

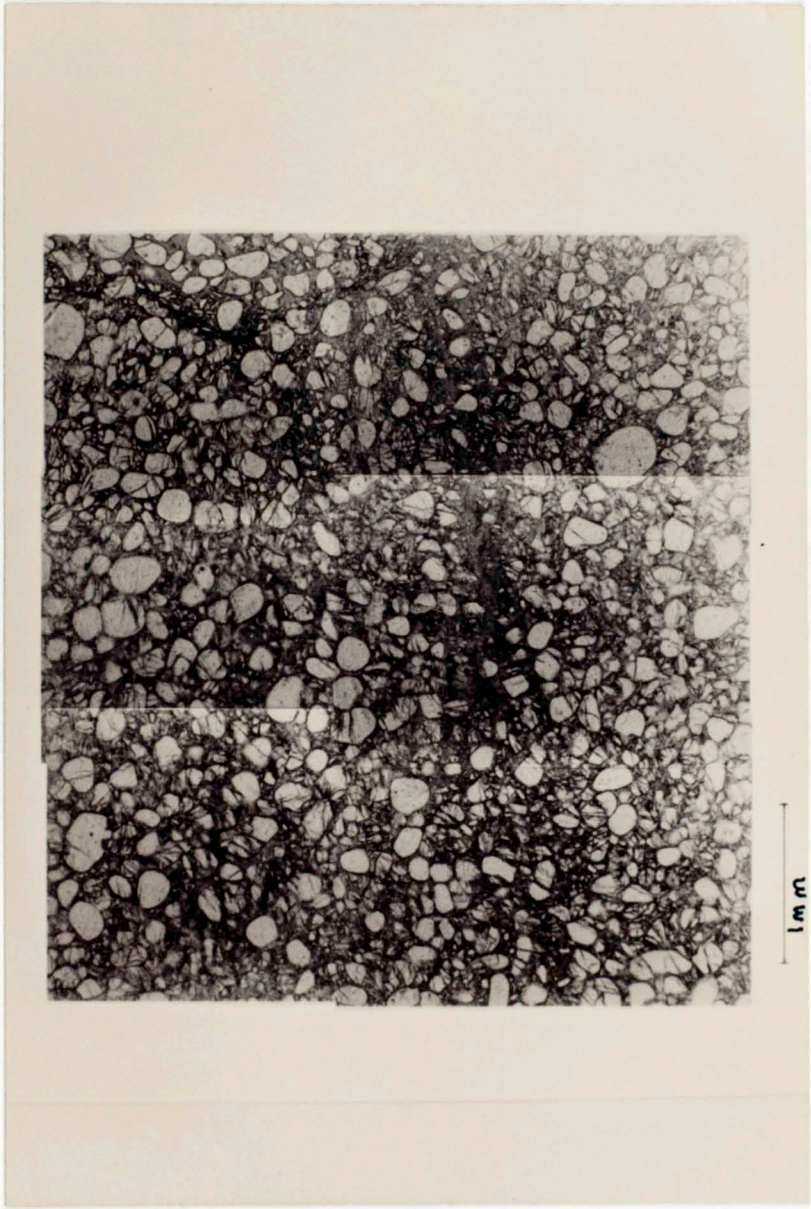

Figure 38. Photomicrograph mosaic of the region underneath the edge of the indenter in figure 37.

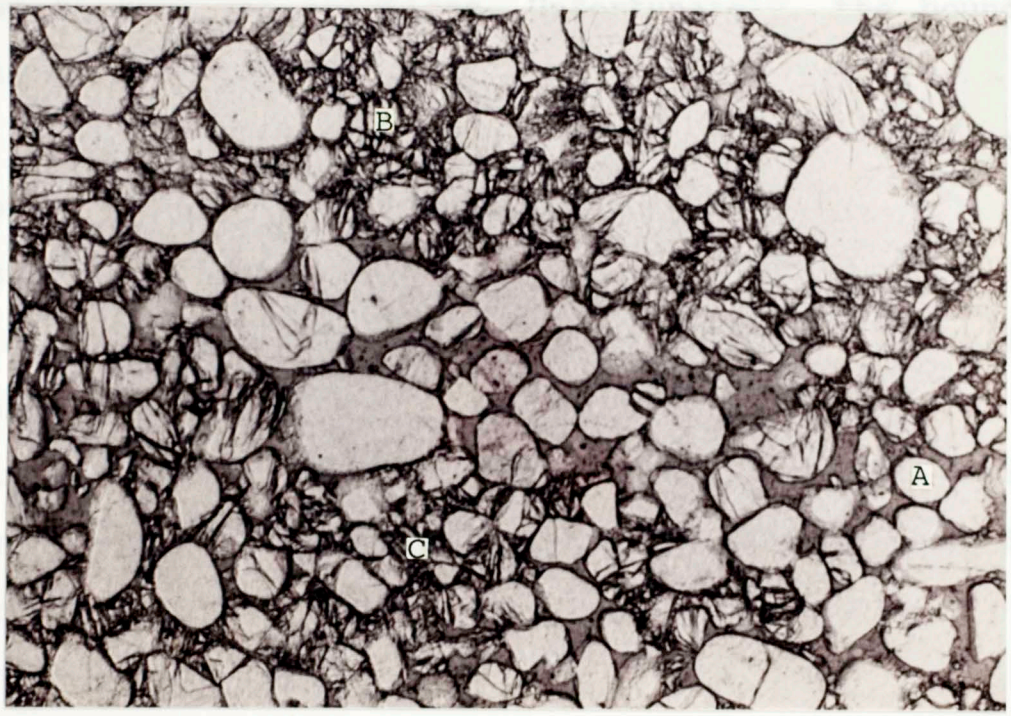

Figure 39. Photomicrograph illustrating heterogeneous distribution of strain in an indention test. Points A, B, and C are the centers of 0.5 mm diameter circles.

To gain a better understanding of physical parameters (i.e., mean pressure, shear and normal stress conditions, invariants of deviatoric stress and/or strain, etc...) that control mode 1 and mode 2 grain fracturing, it would be desirable to compare these microscopic observations to already existing theoretical solutions. Unfortunately, the boundary conditions used in most published theoretical solutions are either dissimilar to those in this study or unstated. Therefore, comparison between microscopic observations and theoretical solutions is precluded at this time. However, the finite element study by Wang and Lehnhoff (1976) does exhibit some similarities with the indention tests at the low confining pressure. Unfortunately, their results are reported in "degrees of compressive failure" which does not provide a physical basis to understand how the material deforms.

CHAPTER IV

COMPARISON OF MICROSCOPIC RESULTS TO NATURAL DEFORMATION BAND TEXTURES

There seems to be a similarity between grain scale textures in tests done here and textures in naturally formed deformation bands. In triaxial compression tests that exhibit brittle behavior grain scale deformation at first appears similar to that observed in natural deformation bands (compare Figure 14 to Figure 40). However, the difference is that the experimentally created texture (Figure 14b) is not produced until slip has occurred along the shear fracture (compare Figures 14a and 14b). Based on this observation, and the definition of a fracture, we conclude that deformation band generation is not associated with conditions that produce brittle behavior in porous sandstones. This also supports Aydin's (1978) hypothesis that deformation bands are not a discontinuity.

Recently, Scott (1989) put forth the hypothesis that deformation bands are created under conditions similar to those that produce transitional behavior in porous sandstones

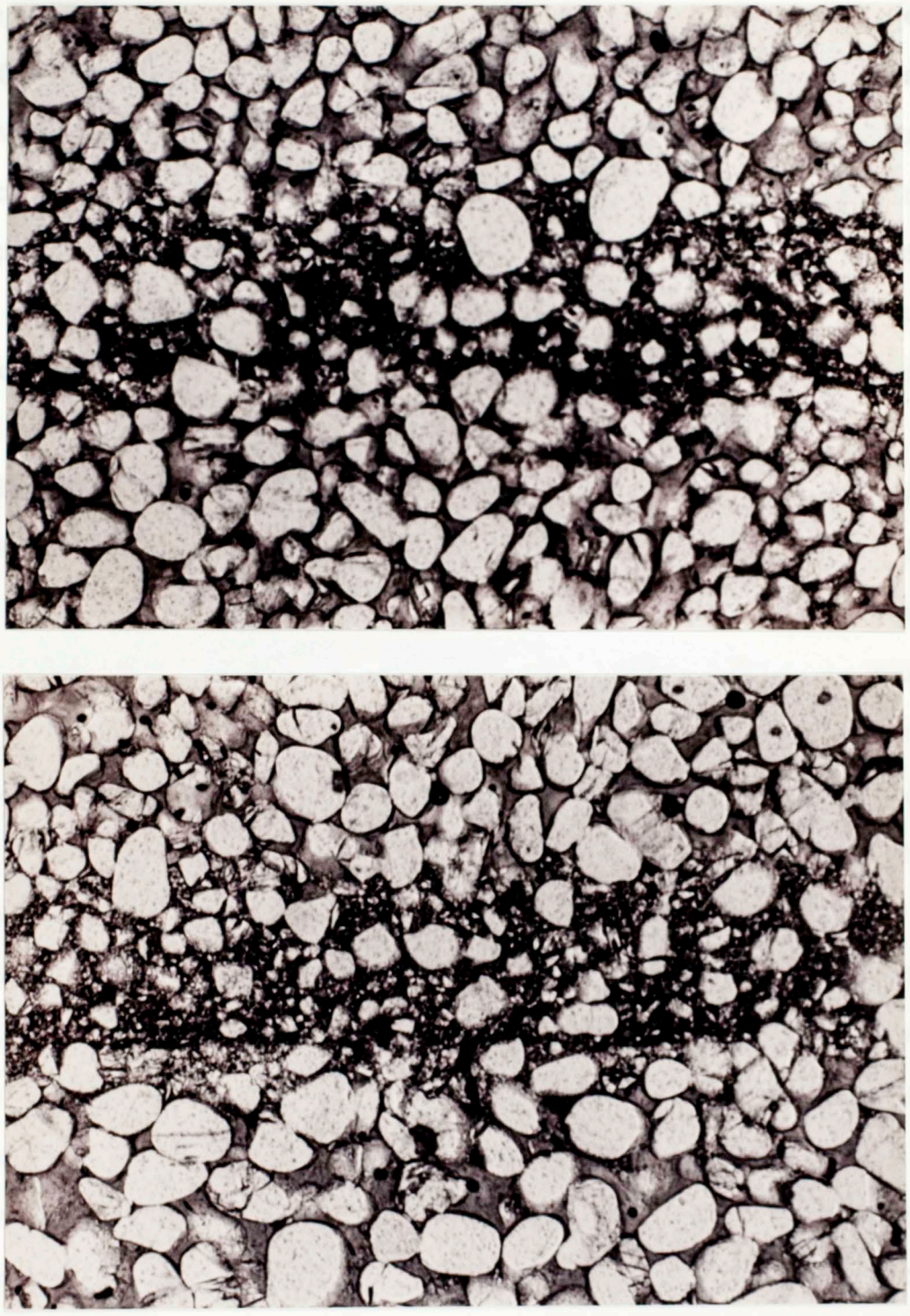

Figure 40. Photomicrographs of deformation bands in naturally deformed Oil Creek Sandstone.

in the laboratory. The evidence supporting his hypothesis comes from the macroscopic appearance of triaxial compression test samples. Comparing the microscopic texture in Oil Creek Sandstone associated with the upper boundary of transitional behavior to natural deformation bands (compare Figure 16 to Figure 40), indicates that the textures are nearly identical. Based on similarities in grain scale deformation, we might refine Scott's 1989 hypothesis to: deformation bands are created under conditions that place the sandstone at, and/or span, the boundary of the transitional and ductile domains. Because this hypothesis is based on limited data, further testing, and more detailed studies at the microscopic scale, of transitional behavior in sandstones is required to accept or alter this hypothesis. Grain scale deformation well into the ductile domain is definitely not similar to textures in deformation bands (compare Figure 17 to Figure 40).

The only similarities between grain scale deformation in indention tests and deformation bands occurs in low confining pressure tests (compare Figures 27, 29, and 31 to Figure 40). Textures developed at the boundary between deformed and undeformed regions, and within the zone of mode 2 grain fracturing, are similar to textures in natural deformation bands. In addition, the growth and development of this zone of mode 2 grain fracturing is similar that of deformation bands. That is, with continued displacement, the zone becomes wider,

the degree of sorting is reduced, and whole grains, or grains containing few microfractures, are incorporated into the zone. However, in this study, the zone of mode 2 grain fracturing is never abandoned as usually is the case with natural deformation bands. This could be attributed to an insufficient amount of displacement or an artifact of the mechanics of the indention test. Because a physically sound, theoretical solution, with the appropriate boundary conditions, does not exist for indention tests in this study, it would be premature to generate a hypothesis regarding the creation of deformation bands based of these results.

CHAPTER V

CONCLUSIONS AND RECOMMENDATIONS FOR FUTURE WORK

Conclusions

A. Triaxial Compression Tests

1) The behavior mode of Oil Creek Sandstone as a function of confining pressure does not follow the exact path established in other studies (Scott and Nielsen (1991)). Brittle behavior extends to significantly higher confining pressures than in earlier studies.

2) Stick-slip behavior exhibited in the stress-strain curves in the transitional and ductile domains appears to be related to either heterogeneous size and distribution of pores or well rounded sand grains within Oil Creek Sandstone.

3) The entire yield surface, including the cap portion, for Oil Creek Sandstone could be expected at confining pressures encountered in the shallow crust.

   a) The Hvorslev segment of the yield surface follows the trend established by Dunn et al. (1973). That is, porosity is a dominate factor controlling fracture strength.

   b) Based on microscopic observations, the hydrostatic compaction point of Oil Creek Sandstone probably occurs between 138 MPa and 145 MPa.

4) In the brittle domain, grain contact microfractures dominant and are parallel to the load axis. Slip along a fracture plane is required to produce an extreme reduction in grain size.

5) In the transitional domain, grain scale damage in Oil Creek Sandstone is divided into two categories. Category 1, associated with the lower boundary of transitional behavior, is similar to brittle behavior. That is, grain contact microfractures that parallel the load axis are dominate and there is very little change in grain size. Category 2 is associated with the upper boundary of transitional behavior. Here there are still grain-contact microfractures that are parallel to the load axis, but they are fewer in number and there is a significant increase in the percentage of small particles even in the absence of apparent slip along the cataclastic zone.

6) In the ductile domain, grain-contact microfractures again dominate, but there is no preferred orientation. In addition, there is virtually no increase in the percentage of small particles.

B. Indention Tests

1) Force-displacement records, at both confining pressures, indicate that more force is required to produce more indention. This confirms that the deformation is, in fact, constrained.

2) At the macroscopic scale, confining pressures used in this portion of the study produce distinctly different deformation patterns.

3) There are two different modes of grain fracturing that operate in all indention tests. Mode 1 grain fracturing is simply grain-contact microfractures. Mode 2 grain fracturing, on the other hand, is grain crushing which polygonizes the grain into randomly oriented, small segments.

4) Strain is heterogeneously distributed within the damaged region in all indention tests.

5) At both confining pressures, there appears to be an increase in the amount of undulose extinction in the highly compacted region when compared to the undeformed region.

6) In low confining pressure tests, with increasing amounts of indention, the zone of mode 2 grain fracturing becomes wider, there is an increase in the percentage of small particles, and unfractured or slightly fractured grains become incorporated into the zone.

7) In low confining pressure tests, grain-contact microfractures appear to follow the maximum principal stress trajectories for an elastic solution.

C. Microscopic Test Results and Natural Deformation Bands

1) Based on microscopic observations, deformation bands are created under conditions that place the sandstone at, and/or span, the boundary between transitional and ductile behavior.

   a) The texture associated with category 2 in transitional behavior is very similar to the texture of natural deformation bands in Oil Creek Sandstone.

   b) The texture associated with brittle behavior is also somewhat similar to natural deformation bands, but it is not produced until observable slip along a fracture plane has occurred. This is not the case with natural deformation bands.

   c) The texture associated with ductile behavior is not similar to natural deformation bands.

2) In low confining pressure indention tests, the texture associated with, and the development of, the zone of mode 2 grain fracturing is similar to features in natural deformation bands.

Recommendations for Future Work

A. More triaxial compression testing on high porosity, quartz sandstones is needed to constrain deformation mode as a function of confining pressure. Specifically, studying the effects of composition, grain shape, and sorting on the deformation mode.

B. Detailed microscopic study across transitional domain would 1) enlarge the data base concerning transitional behavior, and 2) test the hypothesis of where deformation bands are created.

C. Derivation of an appropriate theoretical solution for these indention tests would delineate physical parameters that control genesis of the zone of mode 2 grain fracturing.

REFERENCES CITED

Aydin, A., 1978. Small Faults Formed as Deformation Bands in Sandstone. Pure and Applied Geophysics, 116: 913-930.

Aydin, A. and Johnson, M., 1983. Analysis of Faulting in Porous Sandstones. Journal of Structural Geology, 5: 19-31.

Aydin, A. and Reches, Z., 1982. Number and Orientation of Fault Sets in the Field and in Experiments. Geology, 10: 107-112.

Bernabe, Y. and Brace, W.F., 1990. Deformation and Fracture of Berea Sandstone in Duba, A.G., Durham, W.B., Handin, J.W., and Wang, H.F., eds. The Brittle-Ductile Transition in Rocks: The Heard Volume. American Geophysical Union, Monograph 56: 91-101.

Borg, I., Friedman, M., Handin, J. and Higgs, D.V., 1960. Experimental Deformation of St. Peter Sand: A Study of Cataclastic Flow in Rock Deformation, Griggs, D., and Handin, J., eds.: Geol. Soc. America, Mem. 79: 133-191.

Byerlee, J.D., 1968. Brittle-Ductile Transition in Rocks. Journal of Geophysical Research, 73: 4741-4750.

Cook, R.A. and Stearns, D.W., 1975. Mechanisms of Sandstone Deformation: A Study of the Drape Folded Weber Sandstone in Dinosaur National Monument, Colorado and Utah in Rocky Mountain Association of Geologists--1975 Symposium on Deep Drilling Frontiers in the Central Rocky Mountains: 21-32.

Dunn, D.E., La Fountain, L.J. and Jackson, R.E., 1973. Porosity Dependence and Mechanism of Brittle Fracture in Sandstones. Journal of Geophysical Research, 78: 2403-2417.

Engelder, J.T., 1974. Cataclasis and the Generation of Fault Gouge. Geological Society of America Bulletin, 85: 1515-1522.

Freeman, D.H., 1990. Permeability Effects of Deformation Bands in Porous Sandstones, unpublished master's thesis, University of Oklahoma, 90 p.

Friedman, M., 1963. Petrofabric Analysis of Experimentally Deformed Calcite-Cemented Sandstones. The Journal of Geology, 71: 12-37.

Friedman, M.F., 1969. Structural Analysis of Fractures in Cores from Saticoy Field, Ventura County, California. Am. Assoc. Petrol. Geol. Bull., 52: 367-389.

Gallagher, J.J., Friedman, M., Handin, J. and Sowers, G.M., 1974. Experimental Studies Relating to Microfracture in Sandstone. Tectonophysics, 21: 203-247.

Griggs, D. and Handin, J., 1960. Observations on Fracture and a Hypothesis of Earthquakes in Griggs, D. and Handin, J., eds., Rock Deformation -- A Symposium: Geol. Soc. America Mem. 79: 347-373.

Handin, J., Hager, R.V., Jr., Friedman, M. and Feather, J.N., 1963. Experimental Deformation of Sedimentary Rocks under Confining Pressure: Pore Pressure Tests. Am. Assoc. Petrol. Geol. Bull., 47: 717-755.

Handin, J. and Hager, R.V., 1957. Experimental Deformation of Sedimentary Rocks under Confining Pressure: Tests at Room Temperature on Dry Samples. Am. Assoc. Petrol. Geol. Bull., 41: 1-50.

Hillman, D.M.J., 1986. A Study of Small-Scale Deformation Features Associated with the Embudo Fault Zone, North-Central New Mexico, unpublished master's thesis, University of Oklahoma, 79 p.

Hoshino, K. and Koide, H., 1970. Process of Deformation of the Sedimentary Rocks in Proc. 2nd Congr. Int. Soc. Rock Mech., Belgrade, 1: 353-359.

Jamison, W.R., 1979. Laramide Deformation of the Wingate sandstone, Colorado National Monument: A study of cataclastic flow, dissertation, Texas A & M University, 170 p.

Jamison, W.R. and Stearns, D.W., 1982. Tectonic Deformation of Wingate Sandstone, Colorado National Monument. Am. Assoc. Petrol. Geol. Bull., 66: 2584-2608.

Jones, M.E. and Addis, M.A., 1986. The Application of Stress Path and Critical State Analysis to Sediment Deformation. Journal of Structural Geology, 8: 575-580.

Lawn, B. and Wilson, R., 1975. Indentation Fracture: Principles and Applications. Journals of Materials Science, 10: 1049-1081.

Linscott, J.P., 1985. A Laboratory Study of the Effects of Shear Stress on Fracture Permeability, unpublished master's thesis, University of Oklahoma, 82 p.

Pittman, E.D., 1981. Effect of Fault-Related Granulation on Porosity and Permeability of Quartz Sandstones, Simpson Group (Ordovician), Oklahoma. Am. Assoc. Petrol. Geol. Bull., 65: 2381-2387.

Reches, Z., 1978. Analysis of Faulting in Three-Dimensional Strain Field. Tectonophysics, 47: 109-129.

Reches, Z. and Dieterich, J.H., 1983. Faulting of Rocks in Three-Dimensional Strain Fields. I. Failure of Rocks in Polyaxial, Servo-Control Experiments. Tectonophysics, 95: 111-132.

Suarez-Rivera, F.R., Cook, N.G.W., Cooper, G.A. and Zheng, Z., 1990. Indentation by Pore Collapse in Porous Rocks in Hustrulid & Johnson, eds., Rock Mechanics Contributions and Challenges -- 31st U.S. Symposium on Rock Mechanics: 671-679.

Scholz, C.H., 1968. Microfracturing and the Inelastic Deformation of Rock in Compression. Journal of Geophysical Research, 73: 1417-1432.

Scott, T.E., 1989. The Effects of Porosity on the Mechanics of Faulting in Sandstones: dissertation, University of Texas at Dallas, 191 p.

Scott, T.E. and Nielsen, K.C., 1991. The Effects of Porosity on the Brittle-Ductile Transition in Sandstones. Journal of Geophysical Research, 96: 405-414.

Spurr, A.R., 1969. A Low-Viscosity Epoxy Resin Embedding Medium for Electron Microscopy. J. Ultrastructure Research, 26: 31-43.

Stearns, D.W., 1967. Certain Aspects of Fractures in Naturally Deformed Rocks in Riecker, R.E., ed., NSF Advanced Science Seminar in Rock Mechanics, Air Force Cambridge Research Laboratories, Bedford, Mass., 97-118.

Stearns, D.W., 1968. Fracture as a Mechanism of Flow in Naturally Deformed Layered Rocks in Proceedings, Conferences on Research in Tectonics, Geol. Survey of Canada Paper 68-52: 79-96.

Stearns, D.W., 1972. Structural Interpretation of the Fractures Associated with the Bonita Fault. New Mexico Geol. Soc. Guidebook, 23: 161-164.

Stearns, D.W., Couples, G.D., Jamison, W.R. and Morse, J.D., 1981. Understanding Faulting in the Shallow Crust: Contributions of Selected Experimental and Theoretical Studies in Carter, N.L., Friedman, M., Logan, J.M., Stearns, D.W.S., eds., Mechanical behavior of crustal rocks. American Geophysical Union, Monograph 24: 215-229.

Stearns, D.W. and Friedman, M., 1972. Reservoirs in Fractured Rock in Stratigraphic Oil and Gas Fields-Classification, Exploration Methods and Case Histories: Am. Assoc. Petrol. Geol., Memoir 10: 82-106.

Stearns, D.W. and Jamison, W.R., 1977. Deformation of Sandstones over Basement Uplifts, Colorado National Monument in Rocky Mountain Association of Geologists--1977 Symposium on Exploration Frontiers of the Central and Southern Rockies: 31-39.

Swartz, J.F. and Lindsley-Griffin, N., 1990. An Improved Impregnation Technique for Studying Structure of Unlithified Cohesive Sediments in Suess, E., von Huene, R., et al., 1990. Proceedings of the Ocean Drilling Program, Scientific Results, 112: 87-91.

Underhill, J.R. and Woodcock, N.H., 1987. Faulting Mechanisms in High-Porosity Sandstones; New Red Sandstone, Arran, Scotland in Jones, M.E. and Preston, R.M.F., eds., 1987. Deformation of Sediments and Sedimentary Rocks. Geological Society Special Publication No. 29: 91-105.

Wang, J.K. and Lehnhoff, T.F., 1976. Bit Penetration into Rock-A Finite Element Study. Int. J. Rock Mech. Sci. & Geomech. Abstr., 13: 11-16.

Young, S.R., 1982. Characterization of and Parameters Controlling Small Faults in Naturally Deformed, Porous Sandstones: unpublished master's thesis, Texas A & M University, 117 p.

Zhang, J., Wong, T. and Davis, D.M., 1990a. Micromechanics of Pressure-Induced Grain Crushing in Porous Rocks. Journal of Geophysical Research, 95: 341-352.

Zhang, J., Wong, T., Yanagidani, T. and Davis, D.M., 1990b. Pressure-Induced Microcracking and Grain Crushing in Berea and Boise Sandstones: Acoustic Emission and Quantitative Microscopy Measurements. Mechanics of Materials, 9: 1-15.

Zhang, J., Wong, T., and Davis, D.M., 1990c. High Pressure Embrittlement and Shear-Enhanced Compaction of Berea Sandstone: Acoustic Emission Measurement and Microstructural Observation in Hustrulid & Johnson, eds., Rock Mechanics Contributions and Challenges -- 31st U.S. Symposium on Rock Mechanics: 653-660.

APPENDIX A

POROSITY DETERMINATION METHOD

Effective porosity is determined using a water immersion technique suggested by T.E. Scott. A sizeable chip or core of rock is tied with a piece of light weight, non-braided thread (to reduce wicking) approximately 20 cm long, leaving a 10-15 cm long tail. The sample is then placed in a beaker of de-ionized water which, in turn, is placed in a vacuum chamber. To ensure full saturation, the sample should be left under vacuum for 12 to 24 hours depending on sample permeability. Select a beaker that is large enough that the sample can be suspended without touching the sides while totally immersed in water. After the samples are fully saturated, determine the combined mass of the de-ionized water and beaker. Next, pick up the saturated sample by the thread tail, remove excess water, place the sample on the beaker bottom, and record the saturated mass (M_{sat}). Next, using the tail, suspend the sample under water without touching the beaker sides and record the suspended mass (M_{sus}). Next, dry the sample after removing the thread (without damaging the sample). To do this place the

sample in a 70°C oven for 24 hours. After the sample is dry, record the dry mass (M_{dry}). By measuring the dry mass last, any error in measurement due to loss of sand during the saturation process is reduced. Obviously, the more friable the sample is then the more care must be taken during the entire procedure. The effective porosity is determined using the following equations:

$$V_{pore} = (M_{sat} - M_{dry}) \div P_{fluid}$$

$$V_{solid} = (M_{sus} + M_{dry} - M_{sat}) \div P_{fluid}$$

$$V_{total} = V_{pore} + V_{solid} = M_{sus} \div P_{fluid}$$

$$\Phi_{eff} = V_{pore} \div V_{total} = (M_{sat} - M_{dry}) \div M_{sus}$$

where:

V = volume (cm^3)

M = Mass (g)

P = density ($g\backslash cm^3$)

Φ_{eff} = effective porosity

APPENDIX B

ROCK SAMPLE PREPARATION

The friable nature of the Oil Creek Sandstone precludes right-circular cylindrical samples being prepared in the standard manner using diamond core bits. Instead the dry rock must be manually cored. This process involves using a thin-walled PVC, or metal, pipe with an inside diameter equal to the desired diameter of the sample. For ease of coring, cut saw-tooth like notches into one end of the pipe coring tool. An aluminum or plastic cylinder, with an outside diameter slightly smaller than the inside diameter of the coring tool is used to guide the coring tool as it penetrates the rock. The guide is chuck mounted in a drill press and the coring tool is slid over the guide. Once the rock to be cored is in place and securely fastened, a cylindrical test sample is manually produced by gently rotating the coring tool back and forth while applying a slight downward pressure. The ends of the test cylinder are polished using 400 grit emery paper and a V-block to produce right-circular cylinders. The emery paper is mounted on a smooth surface using rubber cement. Set the V-

block on the emery paper and hold with one hand. Using the other hand, hold the sample against the V-block and begin to gently move the sample and V-block together in a circular motion. After one sample end is squared to the cylinder wall, turn the sample over and finish the other end in a similar fashion, grinding down to the appropriate sample length.

APPENDIX C

SAMPLE COLUMN AND SAMPLE TESTING PROCEDURES FOR TRIAXIAL TESTS

Sample Column Assembly Procedures

Step #1: Prepare the following items:

1- Right-circular cylindrical rock sample 3.91 cm (1.5") in diameter and 8.255 cm (3.25") in length.

2- 3.81 cm (1.5") diameter pieces of polyolefin shrink tubing 17.78 cm (7.0") in length.

Step #2: Clean the end plugs with a degreasing agent (e.g., Acetone).

Step #3: Place a continuous bead of Thermogrip® hot melt glue around the circumference in the middle of each end plug.

Step #4: Place the bottom end plug on a solid right-circular cylinder of metal 2.54 cm (1.0") in diameter and 5.08 cm (2.0") long. Next, assemble the rest of the sample column (i.e., rock sample-end plug).

Step #5: Slide one piece of shrink tubing over the sample column. Next, place a solid, right-circular cylinder of metal 2.54 cm (1.0") in diameter and 5.08 cm (2.0") long on top of

the sample column. Then place a weight of about 4.5 kg on top of the metal cylinder. Note: From this point on, keep the weight on top of the sample column.

Step #6: Shrink the tubing with a heat gun making sure to get a good bond between the jacket and the hot melt glue. Let cool 10-15 minutes and repeat Step #3.

Step #7: Once the hot melt glue is set, repeat Step #5 with the other piece of shrink tubing.

Step #8: Let cool 15-20 minutes, remove the weight and trim off excess polyolefin with a razor blade.

Testing Procedures

Step #1: assemble the sample column (see Figure 3 in text).

Step #2: attach the axial and circumferential extensometer to sample making sure both devices are centered.

Step #3: insert sample column into pressure vessel on top of the load cell (see Figure 4 in text) and wire in the instrumentation.

Step #4: seal pressure vessel and carefully raise confining pressure to the desired level.

Step #5: after reaching the desired confining pressure, let the loadcell equilibrate for 5 minutes.

Step #6: start the data acquisition system and then the test.

Step #7: terminate the test at 2%-3% axial shortening and then carefully remove the axial load and slowly bleed the confining pressure.

Step #8: open the pressure vessel, unhook instrumentation, remove sample column from pressure vessel, and remove the instrumentation.

Step #9: the last step is to impregnate the sample with epoxy for thin-sectioning purposes. Appendix E contains a description of the epoxy and impregnation technique.

APPENDIX D

SAMPLE COLUMN ASSEMBLY AND TESTING PROCEDURES FOR INDENTION TESTS

Sample Column Assembly Procedures

Step #1: Prepare the following items:

1- Right-circular cylindrical rock sample 10.16 cm (4.0") in diameter and 8.89 cm (3.5") in length.

2- 10.16 cm (4.0") diameter pieces of polyolefin shrink tubing 13.97 cm (5.5") in length.

1- 0.16 cm (0.063") thick neoprene rubber patch with an outside diameter of 10.16 cm (4.0") and an inside diameter of 1.59 cm (0.625"). Scuff one face of the rubber patch.

1- 0.16 cm (0.063") thick neoprene rubber patch with an outside diameter of 8.89 cm (3.5") and an inside diameter of 3 cm (1.18"). This rubber patch can be reused in other tests.

1- 0.04 cm (0.016") thick lead patch with an outside diameter of 10.16 cm (4.0").

1- #22 gage wire 20 cm (7.87") in length.

Step #2: Clean the indenter and base plate with a degreasing agent (e.g., Acetone).

Step #3: Place indenter on a countertop with the indenting face up. Slide rubber patch with larger outside diameter, scuffed face down, over indenter. Adjust rubber patch such that 2-3 mm are above the groove in the indenter.

Step #4: Seal the rubber patch at the groove in the indenter using the #22 gage wire.

Step #5: Place a continuous bead of Thermogrip® hot melt glue at the following areas:

a) the contact of the rubber and indenter (cover the wire)

b) the outside diameter of the rubber patch

c) the circumference of the base plate.

Step #6: Place a thin film of molykote® (MoS_2) on upper surface of base plate and then place lead shim on top of base plate. Trim the shim around the base plate with a razor blade.

Step #7: Slide one piece of polyolefin shrink tubing over a solid, right-circular cylinder of aluminum 10.16 cm (4.0") in diameter and 12.7 cm (5.0") long. Place the indenter-rubber patch assembly on top of the cylinder. Hold the rubber patch down on top of the cylinder with a thin-walled PVC pipe with an inside diameter of 7.62 cm (3.0"). Using a heat gun, shrink only the polyolefin that extends above the aluminum cylinder until it contacts the rubber patch. Quickly apply pressure around the outside edge of the rubber patch, using a thick-walled PVC pipe with an outside diameter of 10.16 cm (4.0"),

to bond the polyolefin and the hot melt glue.

Step #8: Let cool 1-2 minutes then remove assembly from the cylinder. Hold the jacket assembly with the indenter in your palm and place the second rubber patch around the indenter and carefully slide the sample into the jacket assembly. Note: The sample should contact the indenter first and remain in contact with the indenter.

Step #9: Slide the lead shim-base plate assembly into the jacket assembly until it contacts the sample.

Step #10: Place the entire sample assembly, with base plate down, on a solid, right-circular cylinder of steel 5.08 cm (2.0") in diameter and length. Using the thick-walled PVC pipe from Step #7, hold the jacket assembly down on the rock sample with one hand while shrinking the polyolefin around the base plate.

Step #11: Remove the PVC pipe and place an approximately 4.5 kg weight on the indenter. Finish shrinking jacket with the heat gun making sure to get a good bond between the polyolefin and the hot melt glue. Note: From this point on, always keep the weight on the indenter.

Step #12: Let cool for 10-15 minutes and then place a continuous bead of hot melt glue around the circumference, at the sample top and bottom.

Step #13: Once the glue is set, slide the second piece of polyolefin over the sample and shrink it with the heat gun

making sure to get a good bond between the polyolefin and hot melt glue.

Step #14: Let cool for 15-20 minutes. Remove the weight from the indenter and trim the excess polyolefin tubing off the bottom of the base plate with a razor blade. Wrap foam padding around the sample to keep it centered inside the pressure vessel.

Testing Procedures

Step #1: assemble sample column (see Figure 6 in text).

Step #2: insert assembled sample column (see Figure 7 in text) into pressure vessel.

Step #3: seal pressure vessel and carefully raise confining pressure to desired level and let the fluid equilibrate. At this stage of the test, the entire sample feels a uniform confining pressure.

Step #4: start the data acquisition system and then the test. As the piston-indenter assembly is advanced, the sample, underneath the indenter, is differentially loaded.

Step #5: terminate the test at the desired amount of indention and carefully remove axial load. At this point, the deformed sample is again under a uniform confining pressure.

Step #6: slowly bleed confining pressure and remove sample column from pressure vessel.

Step #7: the last step is to impregnate the sample with epoxy for thin sectioning purposes (see Appendix E).

APPENDIX E

EPOXY AND SAMPLE IMPREGNATION TECHNIQUE

Because of the large sample size and the possibility of local regions of reduced permeability due to the deformation, a low viscosity epoxy is required. Spurr (1969) developed a low viscosity epoxy whose components are available separately, or as a kit, from Ernest F. Fullam, Inc., 900 Albany Shaker Rd., Latham, N.Y., 12100. Different combinations of the four components allow for variations in viscosity, final hardness, curing time, and pot-life. In this study a low viscosity, long pot-life epoxy with an average final hardness are used. Spurr (1969) recommends using medicine dropper pipettes for dispensing the components, but Swartz and Lindsley-Griffin (1990) found that syringes are just as effective and easier to clean. They also recommend that the prepared epoxy be stored in an air-tight container to prevent the epoxy from absorbing moisture. By storing the container in a freezer, the pot-life can be extended for several months.

Even though the impregnation technique is fairly straightforward, the procedural steps for each test type are

different.

Prepare the following items:

Triaxial compression tests:

two, 0.04 cm (0.016") thick lead shims 3.91 cm (1.5") in diameter with numerous small .159 cm (0.063") diameter holes drilled in the shim

heavy duty aluminum foil

epoxy.

Indention Tests:

one piece of 10.16 cm (4.0") diameter polyolefin shrink tubing 10 cm (3.937") in length

modeling clay

epoxy.

<u>Procedures for Triaxial Tests</u>

Step #1: Clean the jacketed sample column to remove any excess confining fluid.

Step #2: Very carefully remove one end plug leaving approximately 0.343 cm (0.135") of the jacket remaining above the sample.

Step #3: Place one shim on top of the sample (i.e., in place of the plug). Using a heat gun, carefully heat the jacket above the sample until it curls over the lead shim. Note: This will reduce sample loss during the vacuum impregnation stage.

Step #4: Repeat steps 2 and 3 on the other end of the sample.

Step #5: Using the aluminum foil, make an epoxy reservoir,

around the sample.

Procedures for Indention Tests

Step #1: Clean the jacketed sample to remove any excess confining fluid.

Step #2: Very carefully remove the indenter-rubber seal assembly by cutting the rubber seal just above the polyolefin jacket.

Step #3: Remove inside rubber patch being very careful not to disturb the deformed region.

Step #4: Place polyolefin shrink tubing over the sample leaving 5-8 cm above the top. Using a heat gun, carefully shrink the polyolefin around the sample until it curls over the top of the sample. Note: This will restrict the amount of epoxy that can go between the sample and the reservoir.

Step #5: Use modeling clay to seal the epoxy reservoir at the bottom where it contacts the outside jacket.

Procedures for Triaxial and Indention Tests

Step #1: Place the sample-reservoir assembly in a vacuum chamber (preferably one with a transparent top) and carefully fill half the reservoir with epoxy. Seal the vacuum chamber and draw a vacuum. The next steps are dependent on the permeability of the sample and the type of vacuum pump. Even though this epoxy has a low viscosity, it still has a tendency to boil in high permeability samples depending on the rate at which the vacuum pump removes air from the chamber. Therefore,

air must be periodically let back into the vacuum chamber to prevent boiling. Usually after three or four cycles of drawing a vacuum and letting air back into the chamber, the vacuum pump can be left on. To ensure complete impregnation (dependent on the permeability), the sample should be under vacuum for about 12 hours.

Step #2: Remove sample-reservoir assembly from vacuum chamber and decant any excess epoxy leaving a thin layer of epoxy on top of the sample.

Step #3: Cure the epoxy by placing the sample-reservoir assembly in a 70^{0}C oven for 24 hours.

Step #4: In high porosity sandstones, the cut slab selected for thin sectioning is again impregnated prior to thin sectioning.

APPENDIX F

MICROFRACTURE HISTOGRAM DATA

Microscopic analysis of grain-contact microfractures was performed on the low confining pressure indention test indented to 3.18 mm. Microfracture histograms (located after this section) representing the frequency (vertical axis) and orientation (horizontal axis) of grain-contact microfractures in a 2.5 mm by 2 mm area of the thin section were prepared. Histograms that do not contain data either occur within the highly compacted region or do not contain any microfractures (i.e., undeformed region). Histogram locations are given by the abscissa-ordinate coordinates (in mm) above and to the left of each histogram. The abscissa is parallel to the bottom of the indenter and the ordinate is parallel to the axis of symmetry. The origin of this coordinate system (i.e., 0,0) is at the bottom of the indenter on the axis of symmetry. That is, the abscissa values increase towards the edge of the indenter and the ordinate values increase towards the bottom of the sample away from indenter bottom. The orientation cells are divided into positive and negative values where a negative

(positive) value indicates a counterclockwise (clockwise) measurement from the axis of symmetry.

0,0

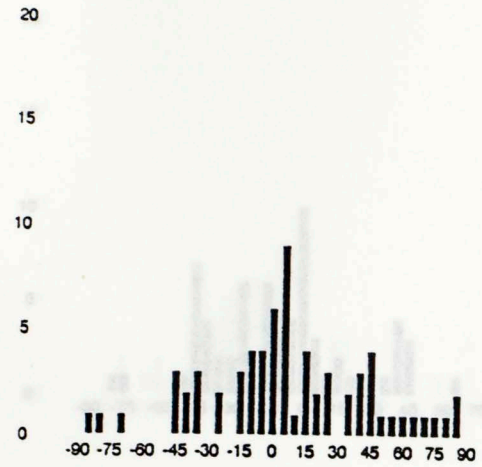

2.5,0

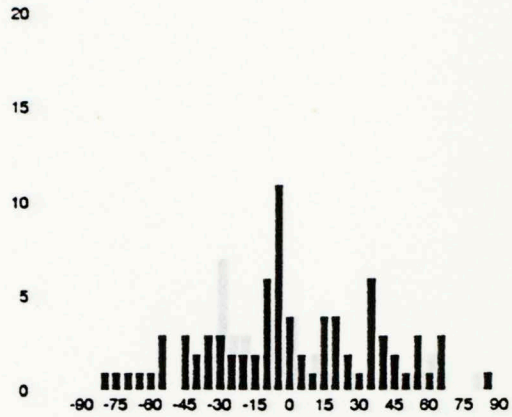

0,2

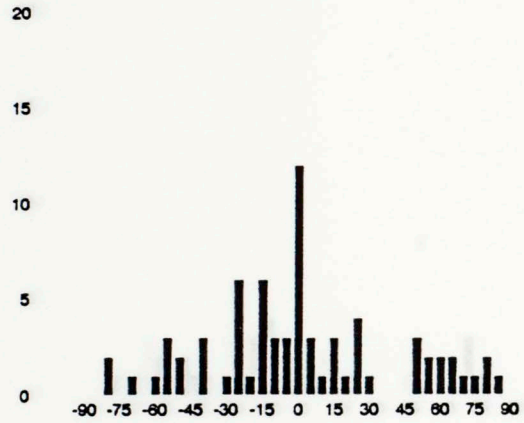

2.5,2

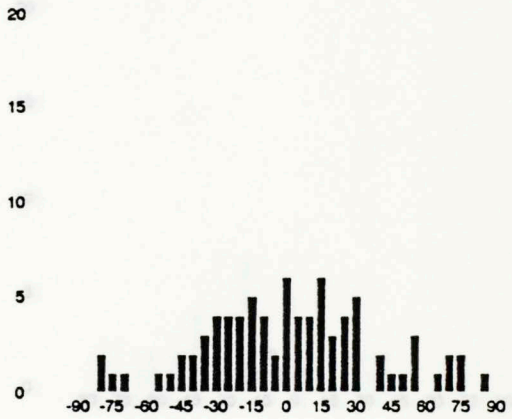

0,4

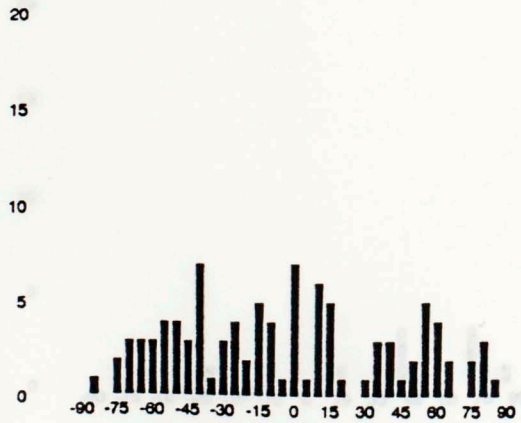

2.5,4

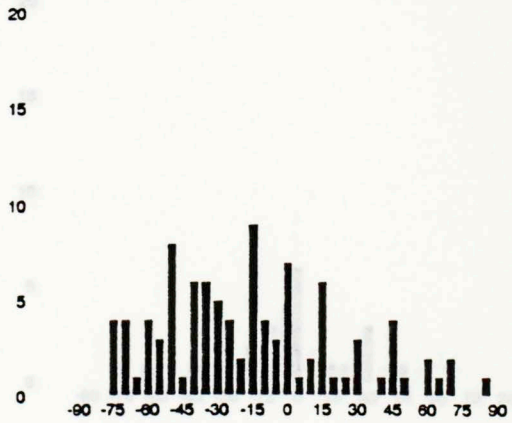

0,6

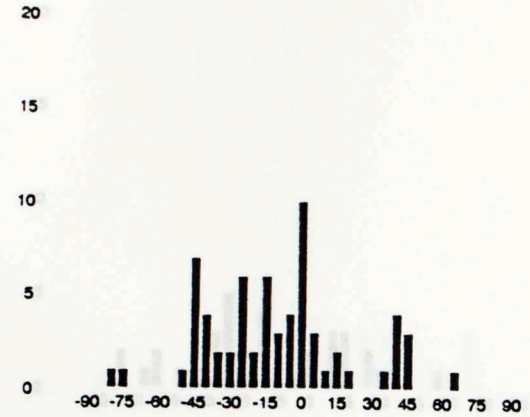

2.5,6

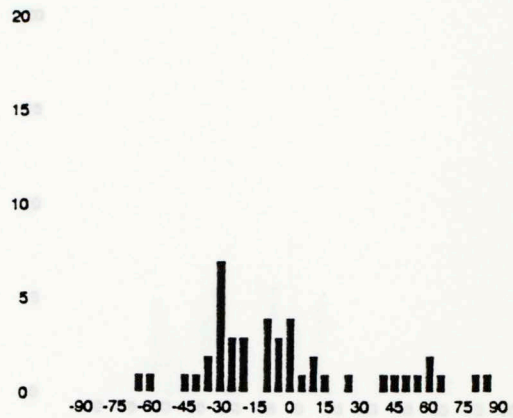

0,8

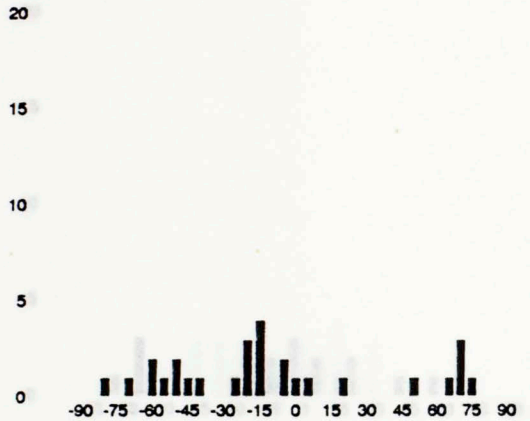

2.5,8

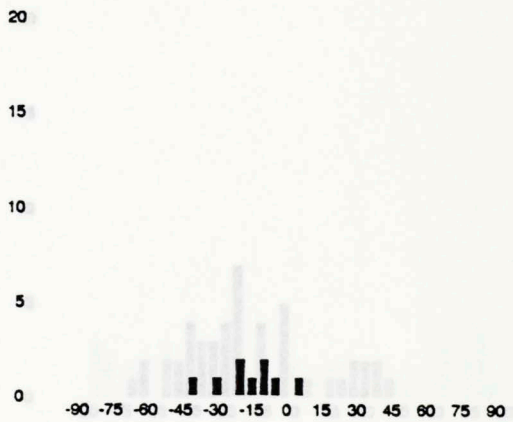

0,10

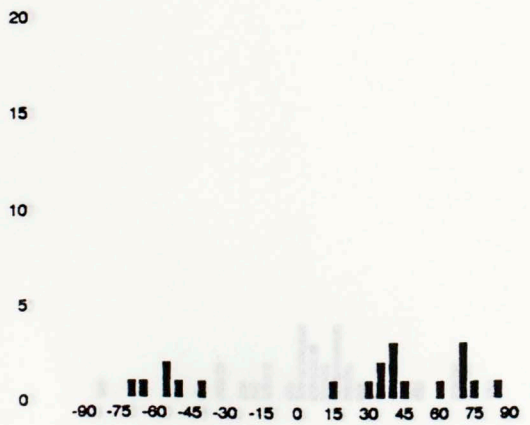

2.5,10

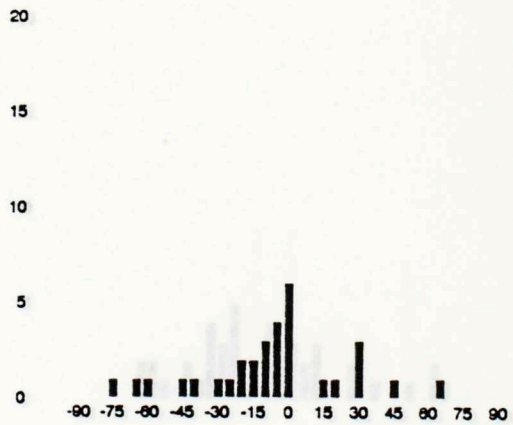

0,12

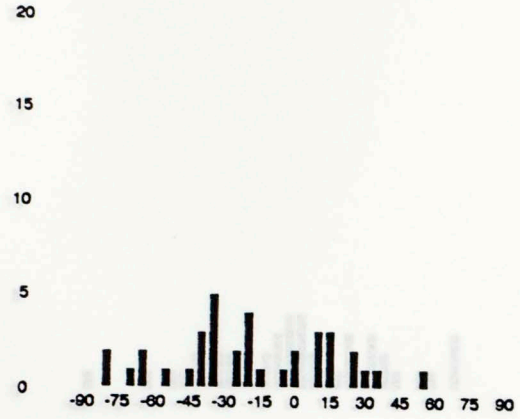

2.5,12

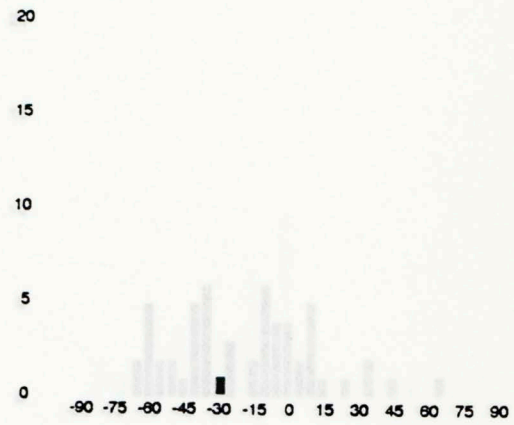

0,14

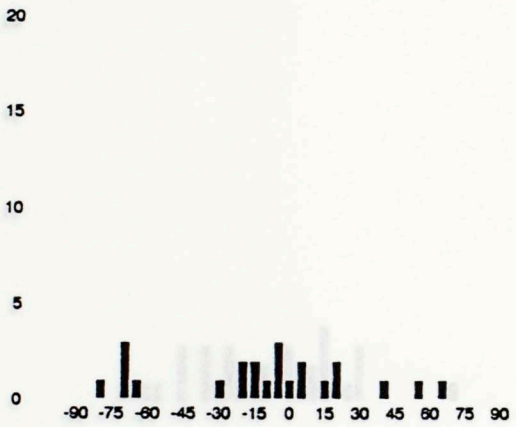

2.5,14

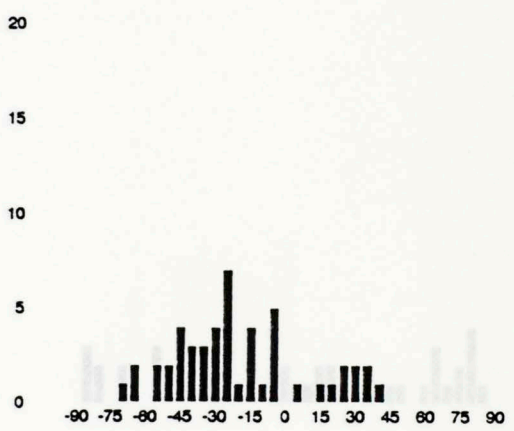

0,16

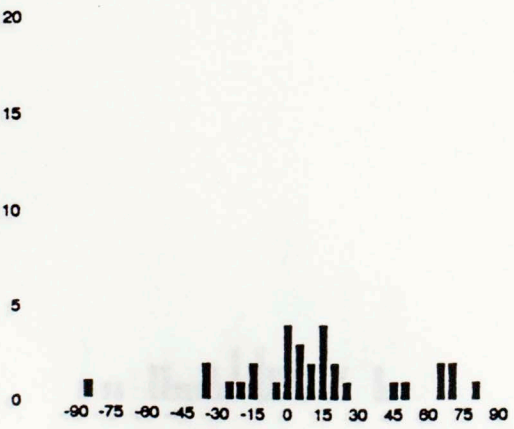

2.5,16

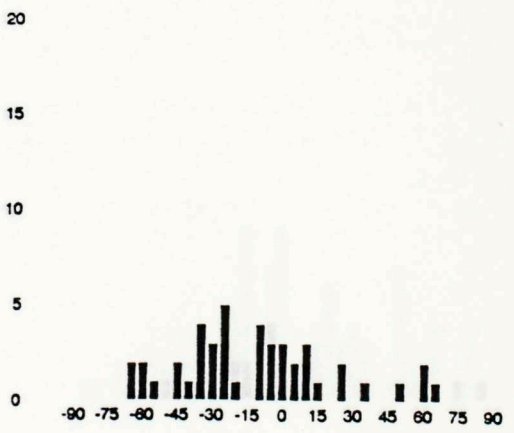

0,18

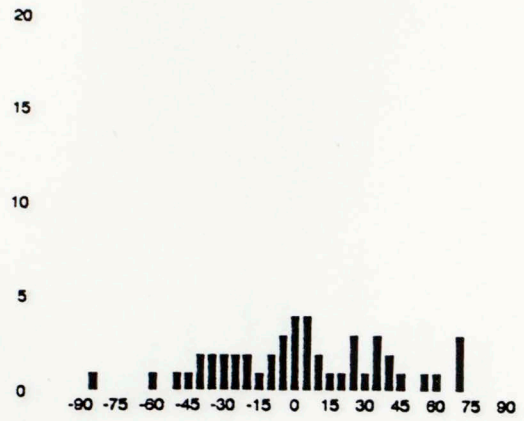

2.5,16

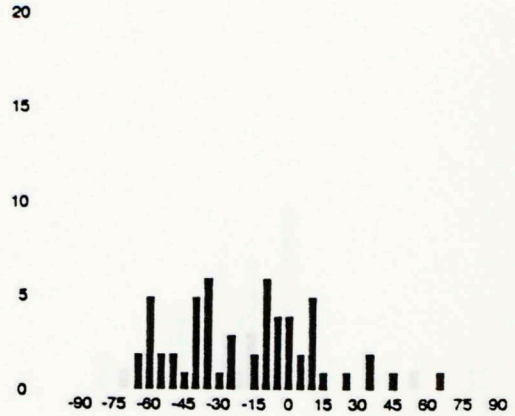

0,20

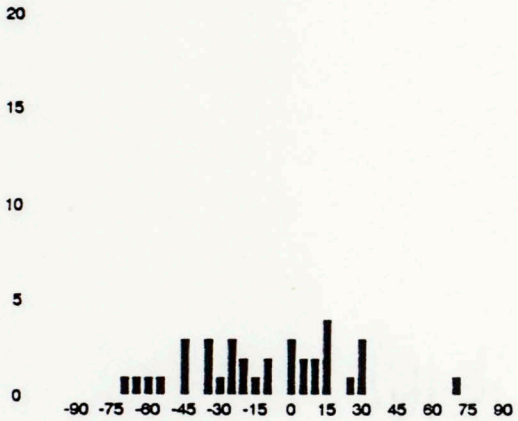

2.5,20

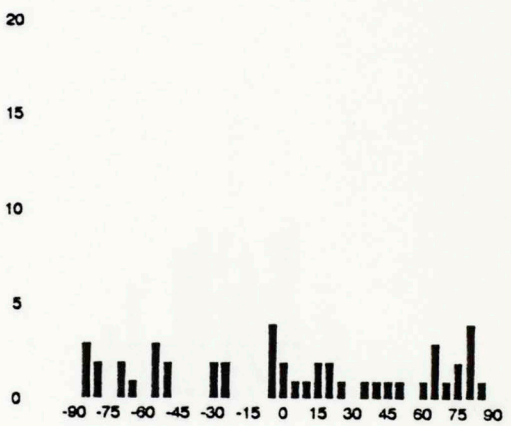

0,22

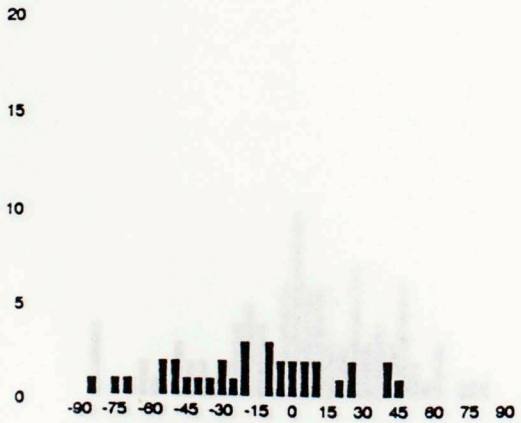

2.5,22

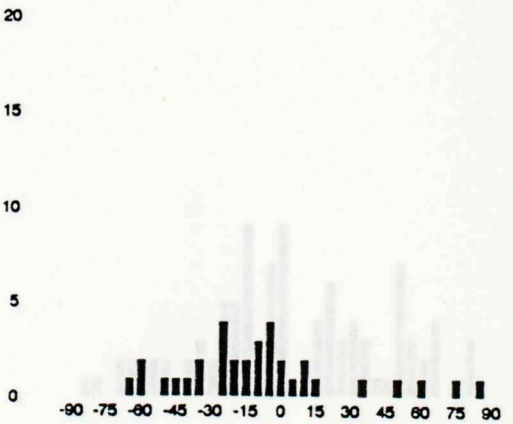

0,24

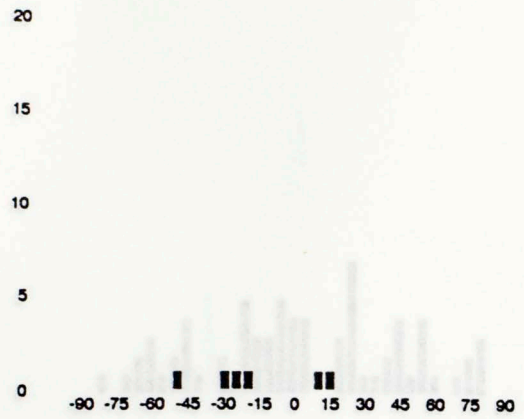

2.5,24

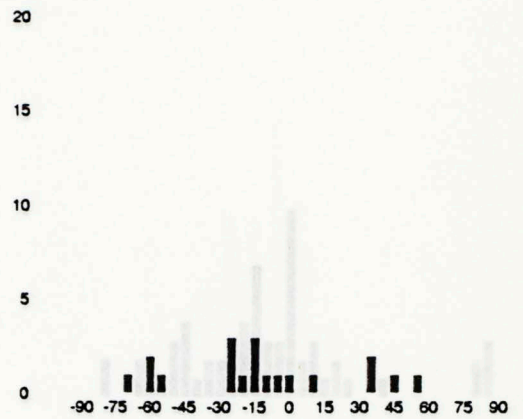

0,26

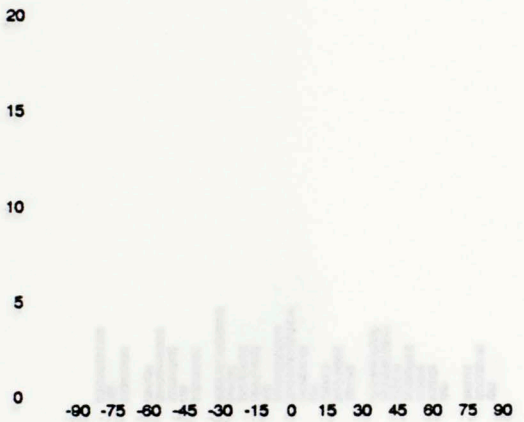

2.5,26

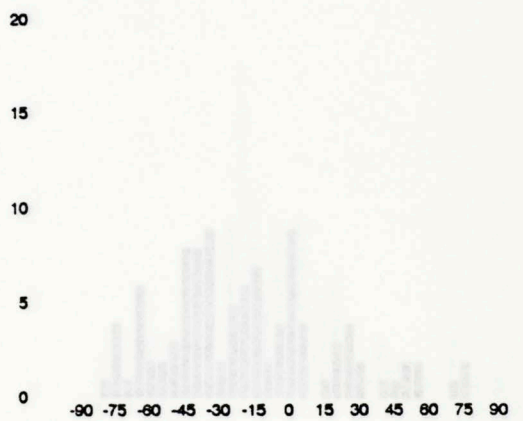

5,0

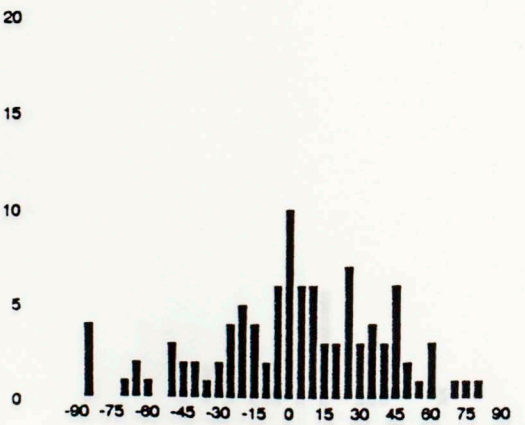

7.5,0

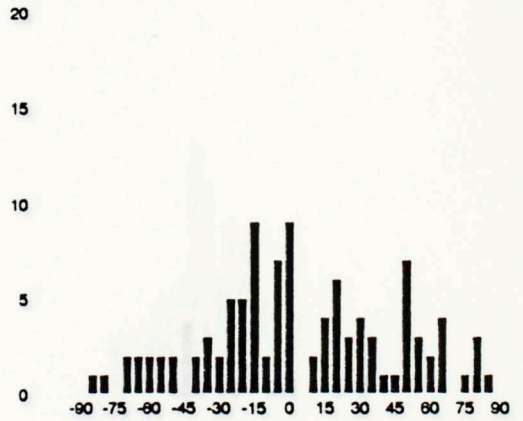

5,2

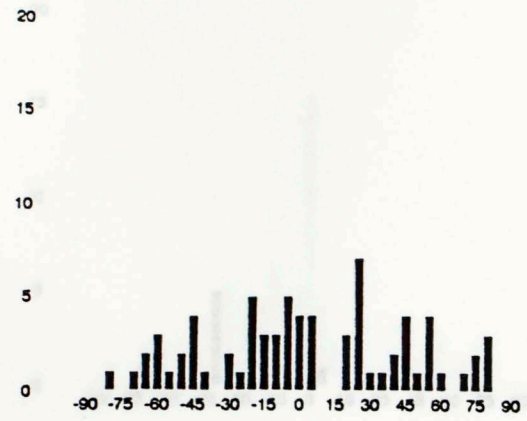

7.5,2

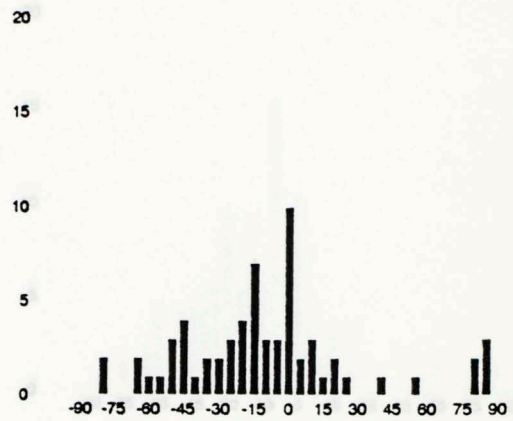

5,4

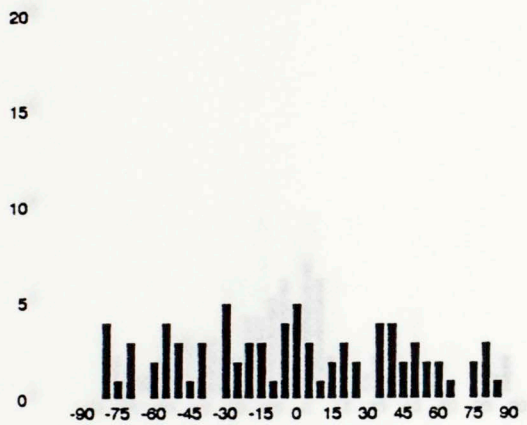

7.5,4

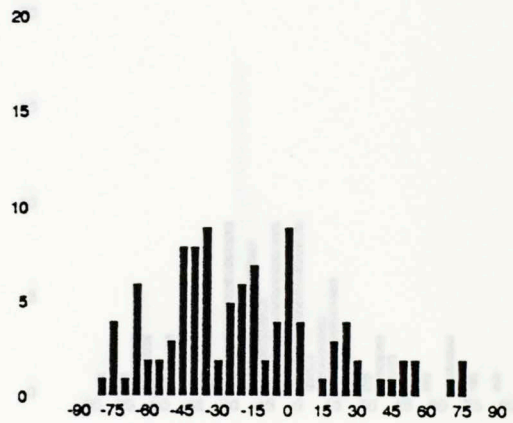

5,6

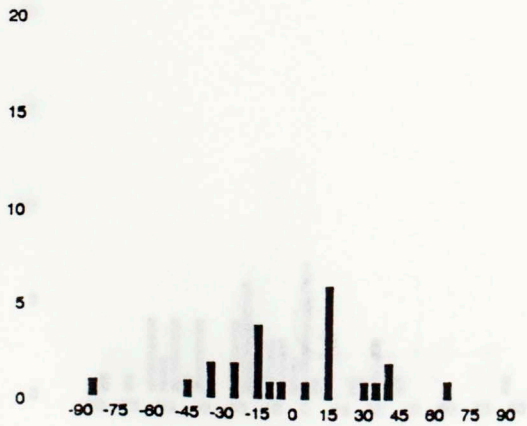

7.5,6

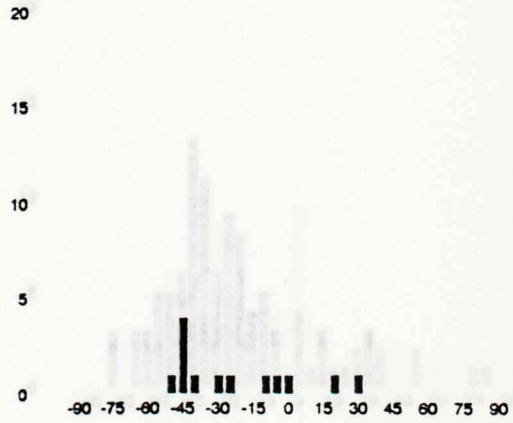

5,8

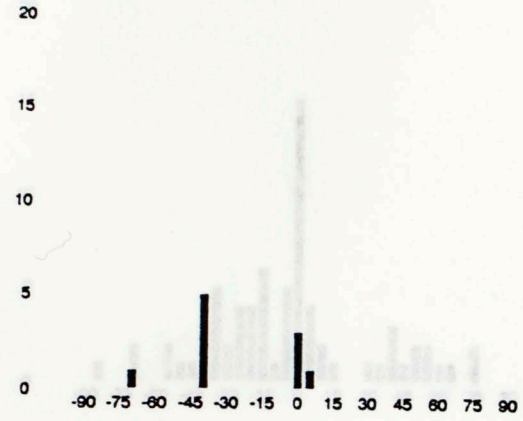

7.5,8

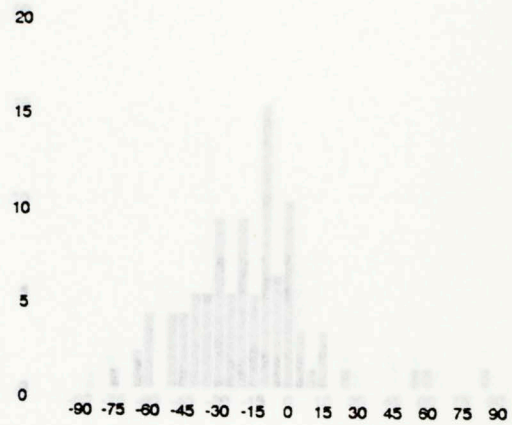

5,10

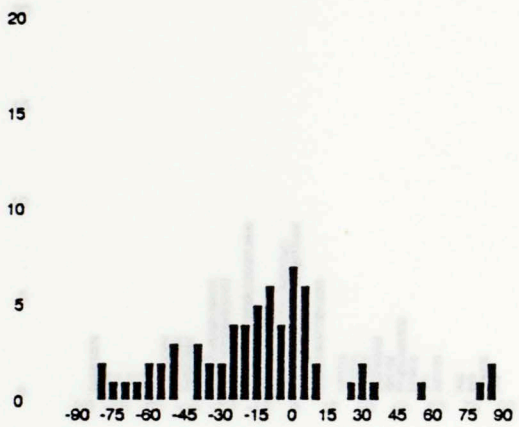

7.5,10

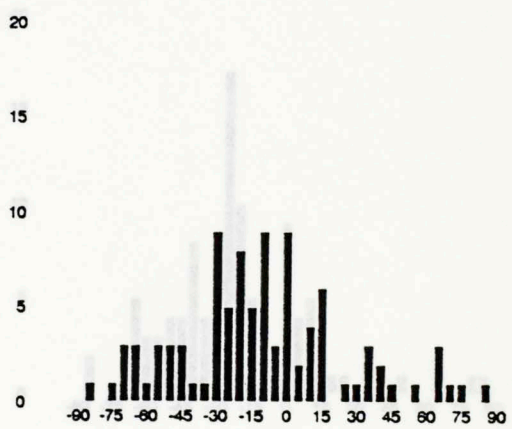

5,12

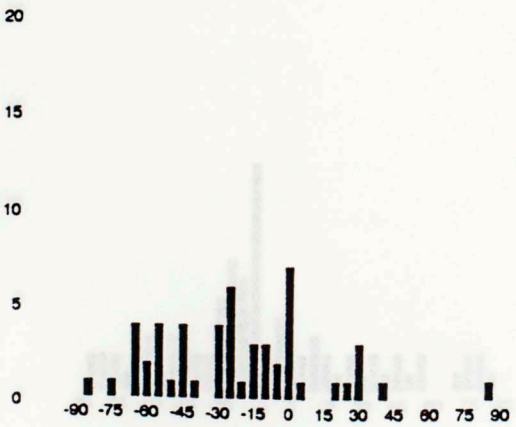

7.5,12

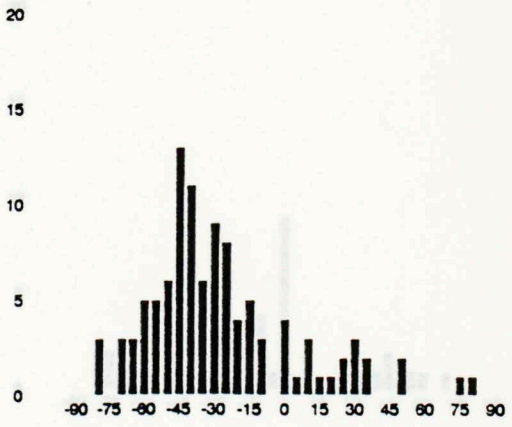

5,14

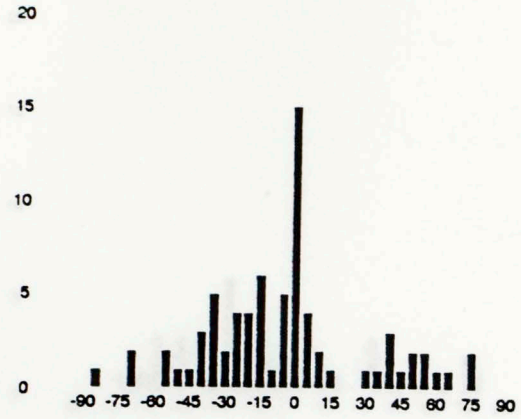

7.5,14

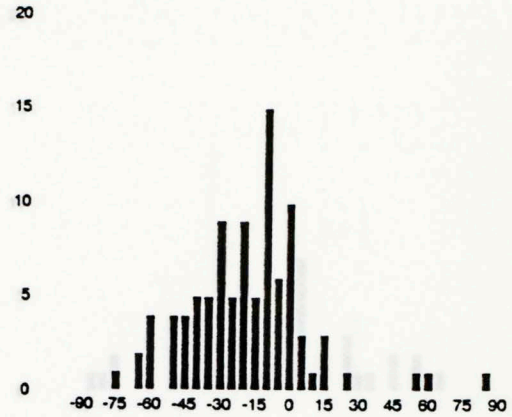

5,16

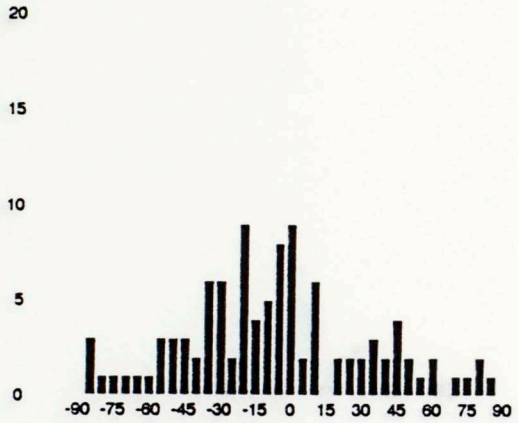

7.5,16

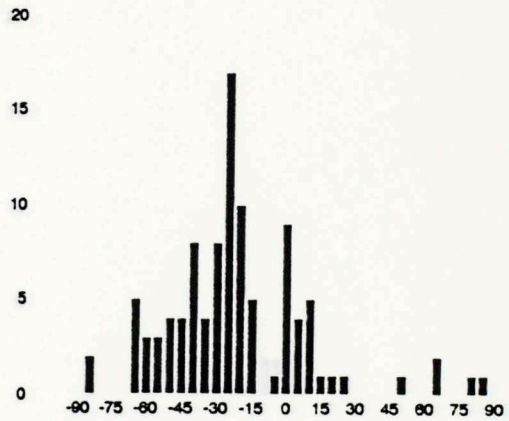

5,18

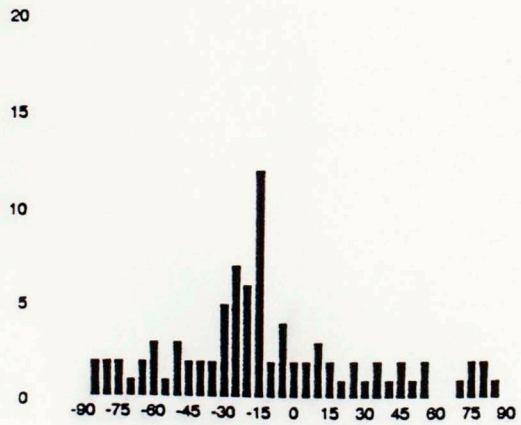

7.5,18

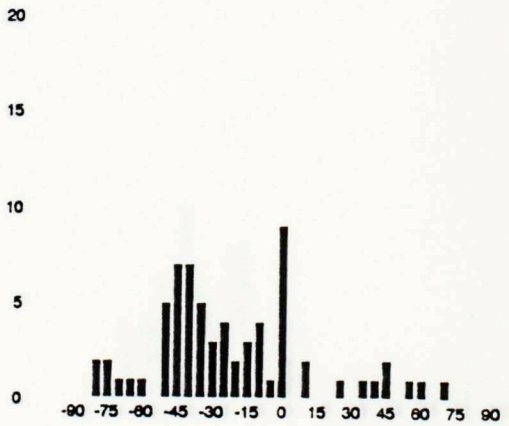

5,20

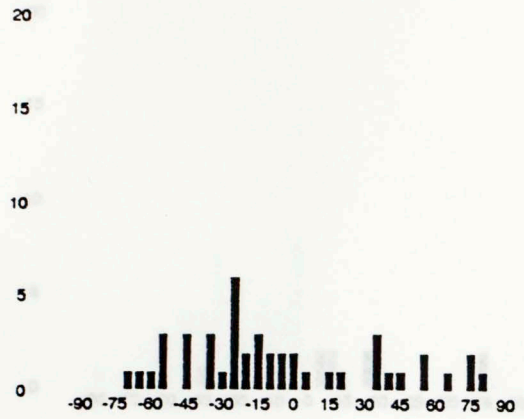

7.5,20

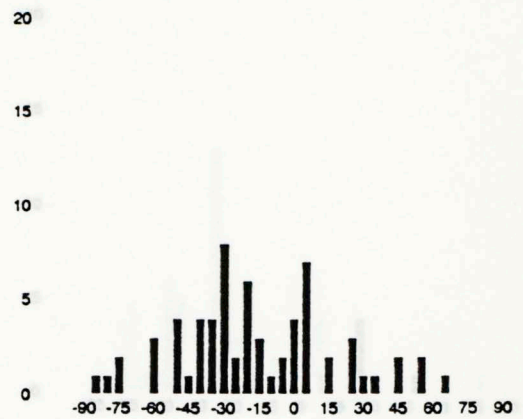

5,22

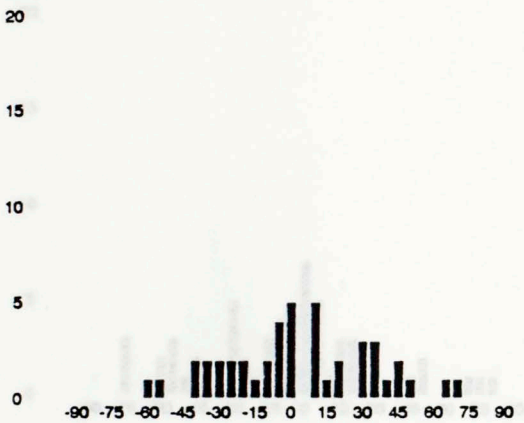

7.5,22

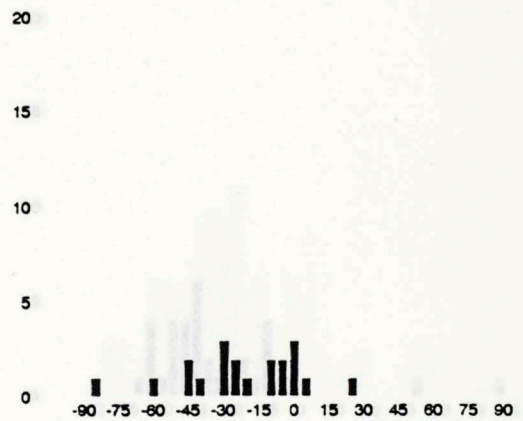

5,24

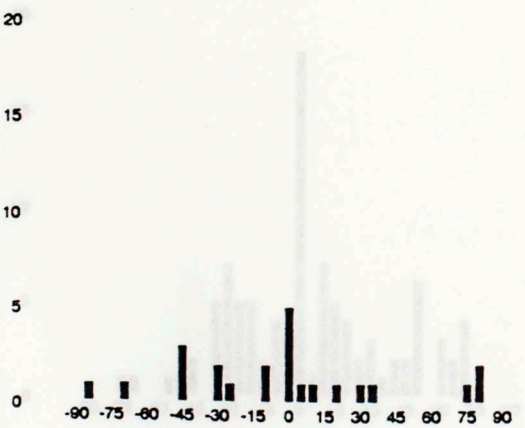

7.5,24

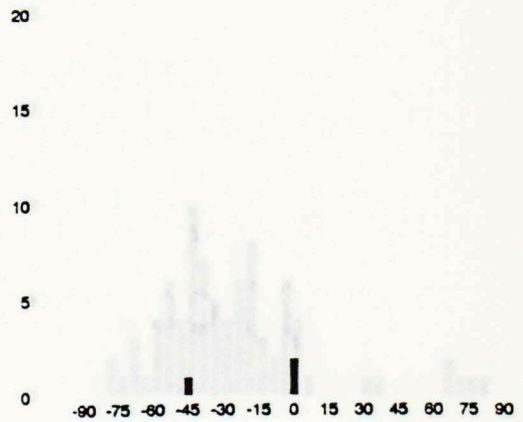

5,26

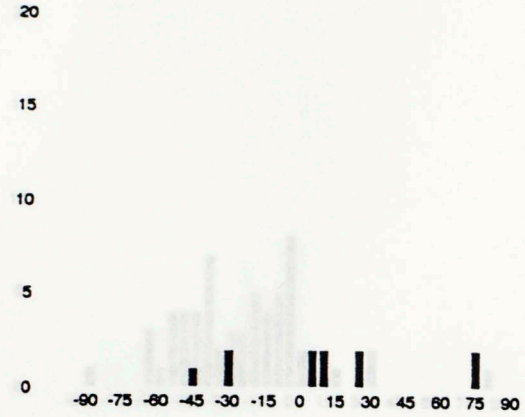

7.5,26

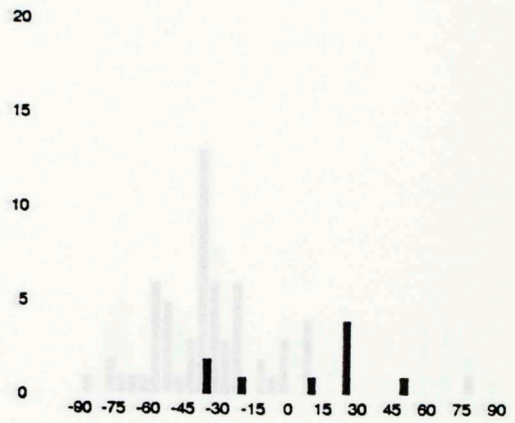

10,0

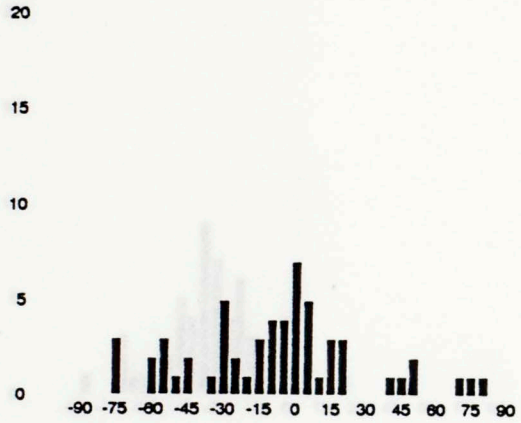

12.5,0

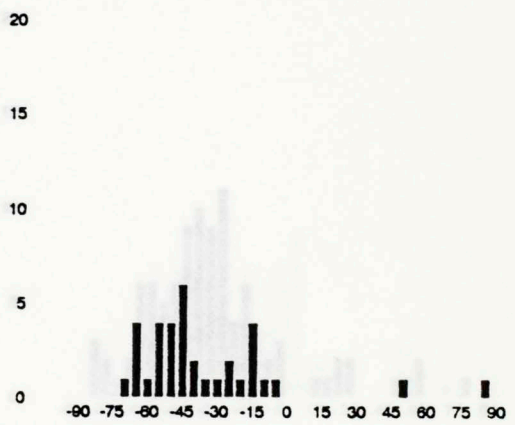

10,2

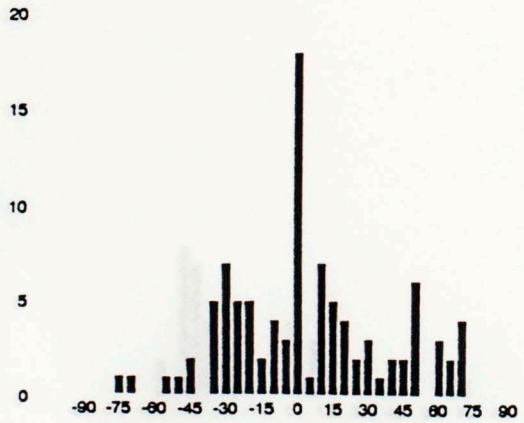

12.5,2

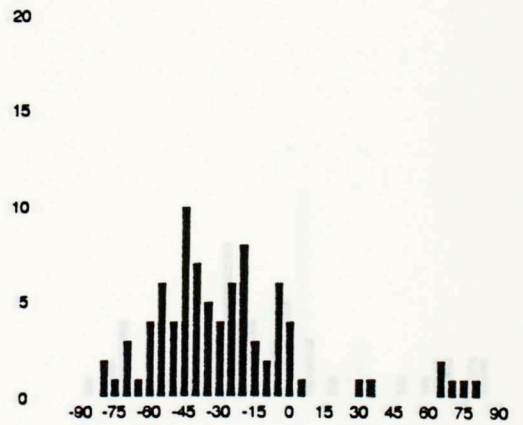

10,4

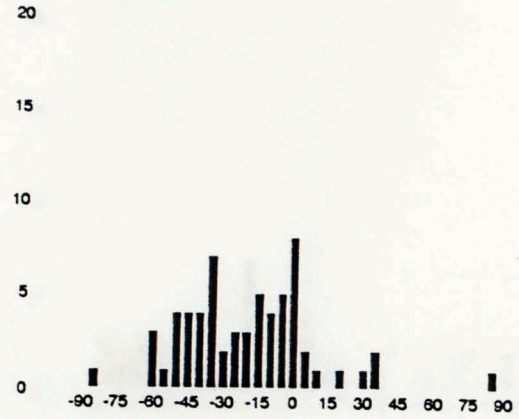

12.5,4

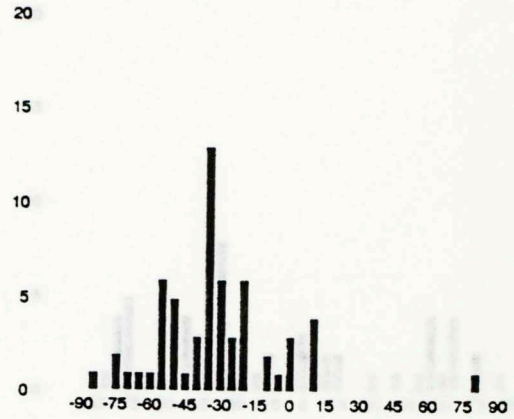

10,6

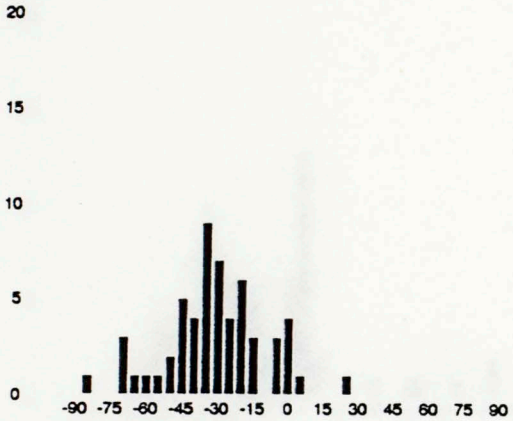

12.5,6

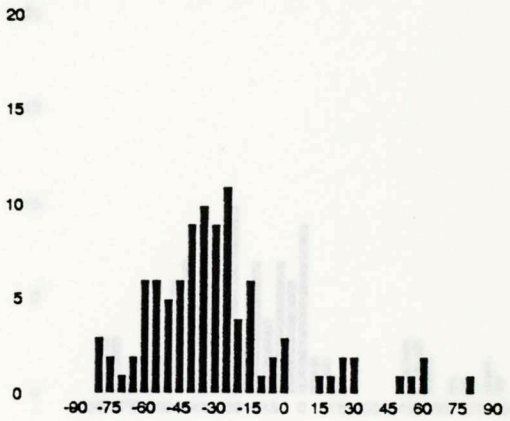

10,8

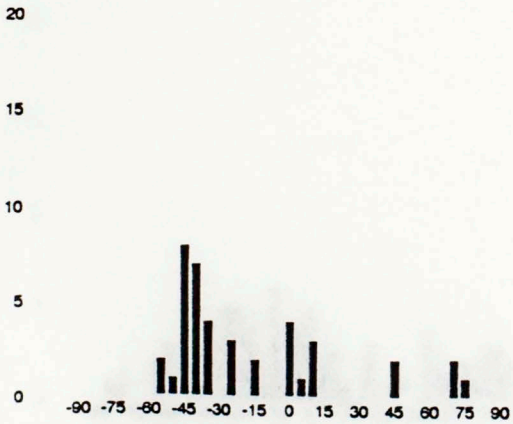

12.5,8

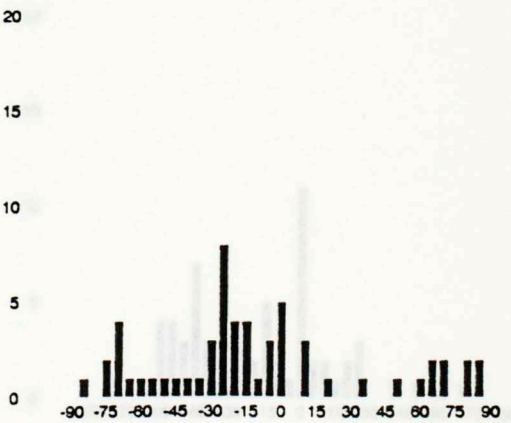

10,10

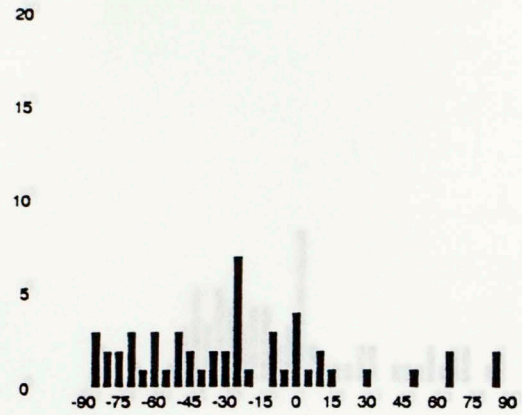

12.5,10

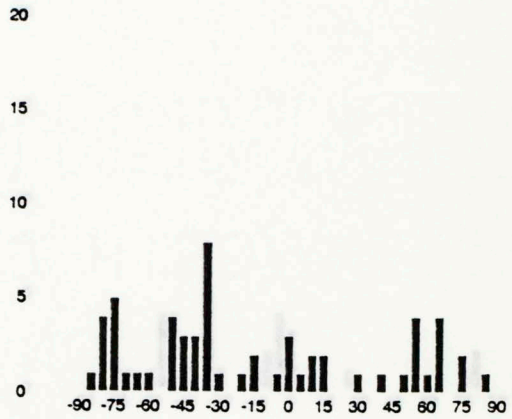

10,12

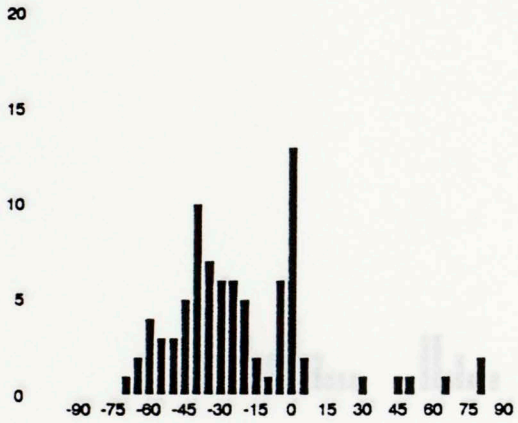

12.5,12

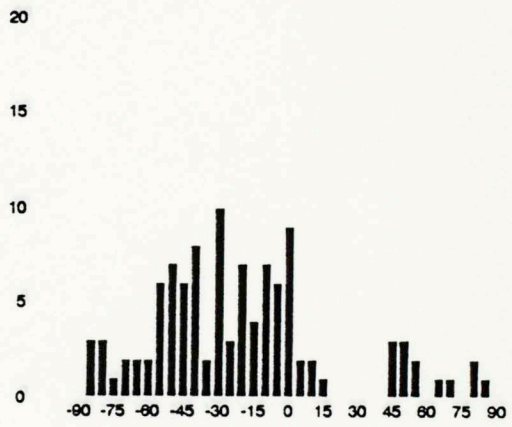

10,14

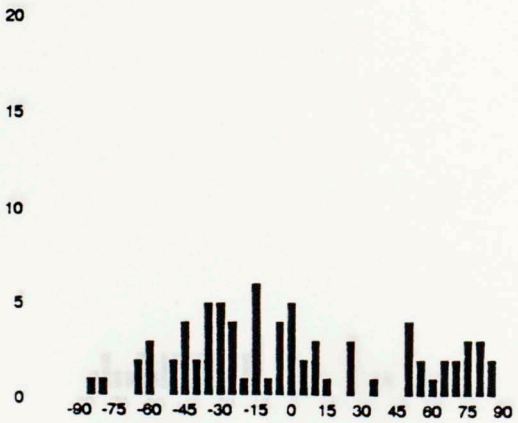

12.5,14

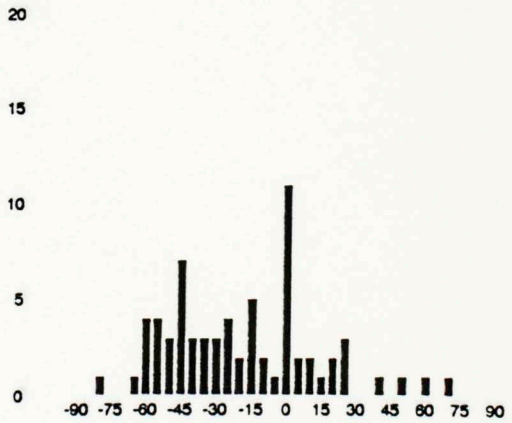

10,16

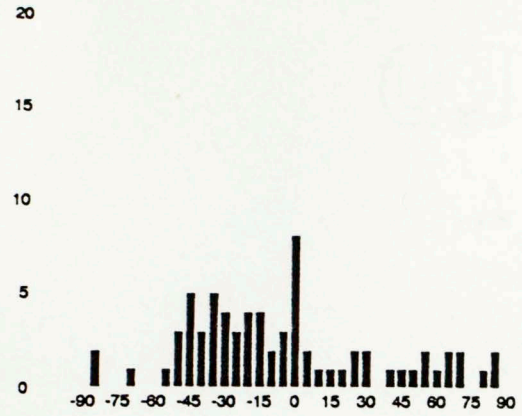

12.5,16

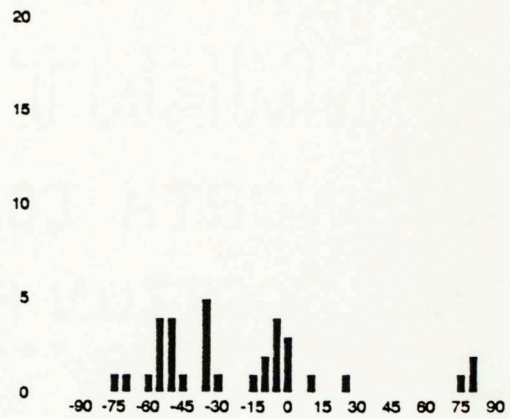

10,18

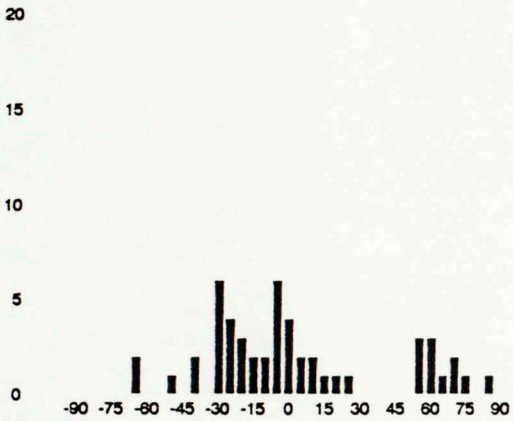

12.5,18

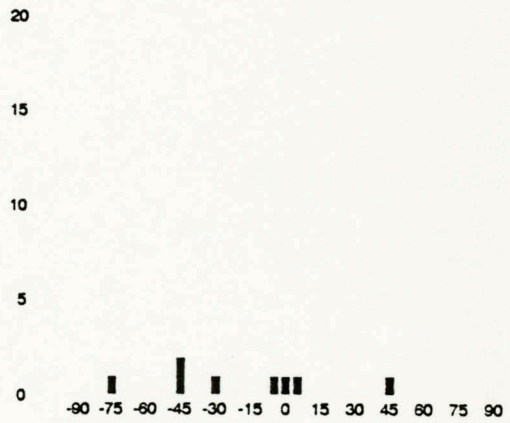

10,20

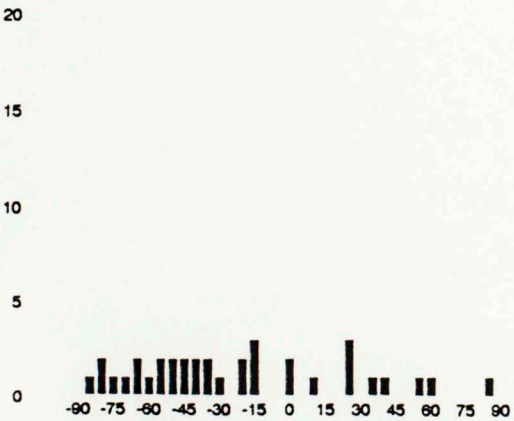

12.5,20